A STUDY OF GaAs, InP, and InGaAs GROWN BY ORGANOMETALLIC VAPOR PHASE EPITAXY

Fred R. Bacher

B.S. Worcester Polytechnic Institute, 1977
M.E.S. Oregon Graduate Center, 1984

A dissertation submitted to the faculty of the Oregon Graduate Center in partial fulfillment of the requirements for the degree

Doctor of Philosophy

in

Applied Physics

June, 1987

The dissertation "A Study of GaAs, InP, and InGaAs grown by organometallic vapor phase epitaxy" by Fred R. Bacher has been examined and approved by the following Examination Committee:

J. S. Blakemore, Thesis Advisor and Professor

Wallace B. Leigh, Assistant Professor

Nicholas G. Eror, Professor

Jack S. Sachitano, Adjunct Assistant Professor (Tektronix, Inc.)

ACKNOWLEDGEMENTS

The author is indebted to the following persons for their contributions to this dissertation. Foremost are John Blakemore and Wallace Leigh, whose advice and assistance were invaluable throughout. Especially Dr. Leigh, who taught me so much about crystal growth.

This work relied heavily on financial support from Tektronix, Inc. I am especially grateful for the ongoing commitment of Harry Anderton and Jack Sachitano.

George Howard ably performed many of the crystal growths, and contributed numerous useful suggestions.

A final note of gratitude is sounded to my wife, Corinne, who was a constant source of guidance and wisdom.

TABLE OF CONTENTS

LIST OF FIGURES

LIST OF TABLES

ABSTRACT

Presented here are the growth and characterization results of a study of the semiconductors GaAs, InP, and InGaAs. The methyl-based organometallic sources trimethylindium and trimethylgallium were used in an atmospheric pressure organometallic vapor phase epitaxy (OMVPE) reactor. Evaluation of this growth technique was conducted with an eye toward optical applications, particularly lasers and photodetectors. The OGC OMVPE system is described here, including the parameters used for growing 150+ epilayers. GaAs and InP epilayers were obtained with 300 K Hall mobilities of 6480 and 4820 cm^2/Vs, and photoluminescence (PL) peak full width at half maximum values of 12 and 10 meV respectively at 77 K.

While some optoelectronic devices require p-type InP and InGaAs, little use has been made of magnesium as a dopant. A study of Mg-doped InP is reported here. Mg offers an attractive alternative to zinc for abrupt junctions because of its low diffusivity. PL peaks seen at 1.0 and 1.3 eV from InP:Mg at 77 K suggest several Mg incorporation mechanisms beyond the simple Mg_{In} substitutional acceptor.

The growth of InGaAs epilayers of various compositions is discussed. An empirical study documents the extent in the present system of the parasitic reaction which depletes trimethylindium prior to the growth zone. InGaAs epilayers grown lattice-matched to InP are described. For these, Hall mobilities of 9000 and 26,500 cm^2/Vs at 300

K and 77 K respectively were achieved.

The optical absorption coefficient was measured over a broad energy range for $In_{1-x}Ga_xAs$ with compositions between x = 0.45 and x = 0.51, at 10, 77, and 300 K. The absorption coefficient rises abruptly to 6000 cm^{-1} just above the bandgap, and increases gradually to 30,000 cm^{-1} at 1.5 eV. Motivation for this work was provided by the scarcity of published optical absorption data for InGaAs.

An intrinsic InGaAs defect was found by PL at 77 K, giving emission near 0.7 eV. A variety of methods were used to characterize this defect, and these results are presented.

CHAPTER I

INTRODUCTION

The motivation for this work was to study the growth and material properties of InGaAs. Organometallic vapor phase epitaxy (OMVPE) is an established technique for GaAs, and so the first efforts here were to reproduce results seen in other labs and to characterize the equipment. InP epilayers were required as a prelude to OMVPE InGaAs/InP growth because InP buffer layers provide a very good surface for the ternary growth. OMVPE was used to grow thin layers of InP/InP, InP:Mg/InP, GaAs/GaAs, InGaAs/GaAs, and InGaAs/InP. These and other III-V compounds are of intense interest to those working on high speed electronic devices and optical communications networks. Characterization of these layers was performed using photoluminescence (PL) and Hall mobility, both of which give an indication of material purity and crystal perfection. These methods are commonly used to compare different samples, materials, and growth techniques.

The OMVPE technique, described in detail in Chapter II, is desirable because of its versatility. Multilayer structures with a variety of compounds can be grown with relative ease. It is the established manufacturing technique for GaAs photocathodes. Based on its reproducibility and efficiency in growing high quality GaAs layers, it is becoming a popular method for producers of optoelectronic devices. Since the propagation loss in optical communication fibers is mini-

mized at ~ 1.55 μm wavelengths, indium-containing materials are more desirable than GaAs for some applications. Solid mixtures of the four elements In, Ga, As, P in single crystal form have the energy bandgaps depicted in Fig. 1. Indium is added to GaAs to obtain response below the GaAs bandgap. Phosphorus-containing compounds are generally more easily grown by OMVPE than molecular beam epitaxy (MBE), although hybrid combinations of the two methods are being developed to retain some of the advantages of each [1]. A major disadvantage of OMVPE is that the growth process depends on chemistry and fluid dynamics that are difficult to understand. So the focus of this report is to examine the utility of OMVPE for growth of InGaAs, with GaAs and InP growth as necessary preliminaries.

Many useful semiconductor devices require doped regions or pn junctions. A long term goal of this research was to build devices with n and p doped epilayers. While p-type InP is investigated here, n-type doping and p-type InGaAs must wait for a later study. The p-type dopant used for part of this work was magnesium, in contrast to the more commonly used zinc. Magnesium has the advantage of a low diffusivity, which can be important when abrupt junctions or interfaces are desired [2]. At OGC, eight Mg-doped InP layers have been grown and studied. The few reports of InP:Mg grown by any method are cited and compared to the results herein. New incorporation mechanisms are postulated for Mg in InP.

As a part of the InGaAs/InP growth characerization, an unexpected deep level defect was observed in PL data and extensively analyzed.

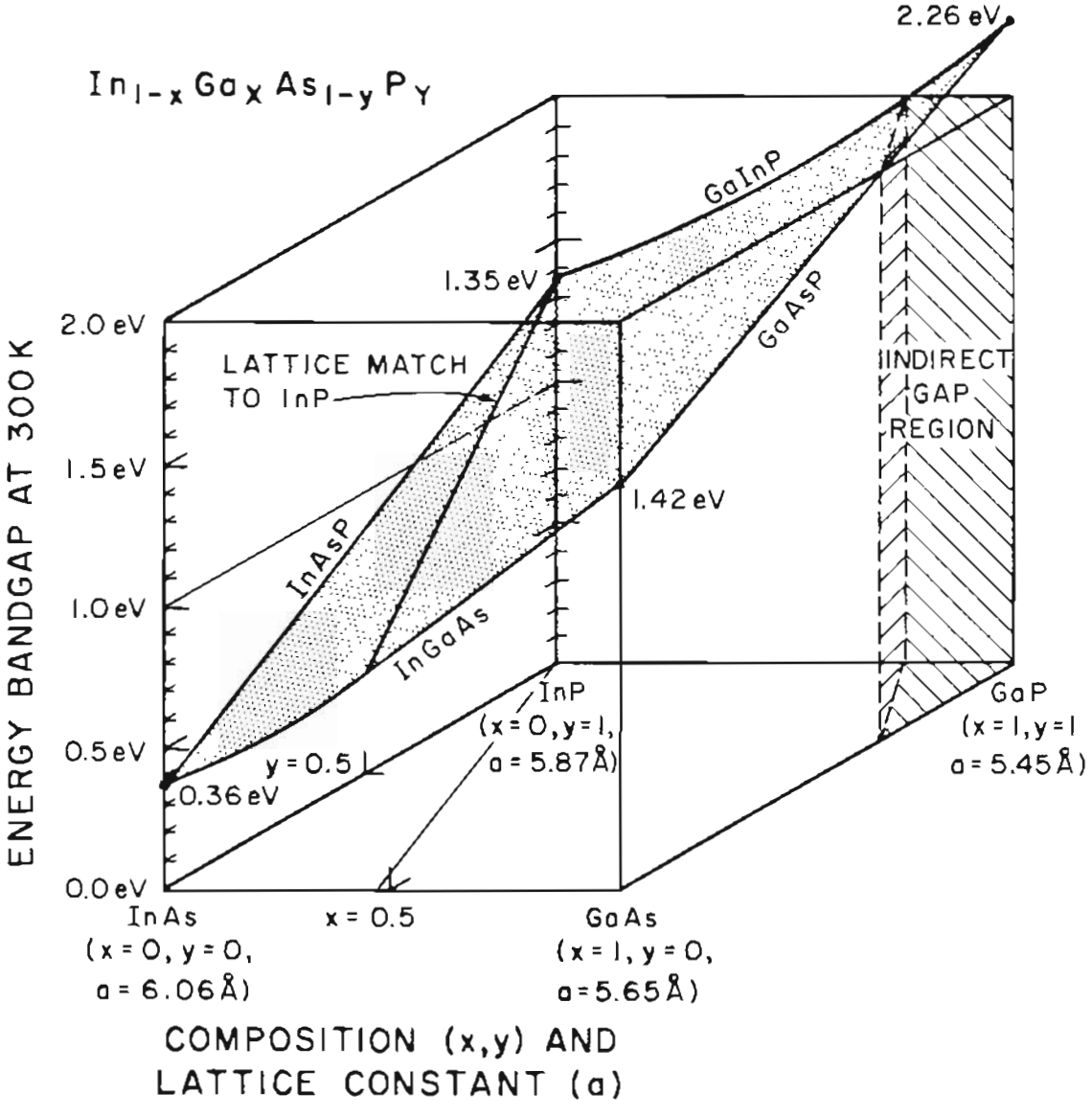

FIG. 1. InGaAsP Bandgap at 300 K.

Accurate absorption coefficient data were obtained as a function of temperature and composition of InGaAs over a wide energy range. These data are compared to the several published reports for material grown by liquid phase epitaxy (LPE).

Chapter III and the appendixes report on the various experimental techniques used for epilayer characterization. The theory behind each measurement is discussed when appropriate. The results and discussion of the crystals grown in this study are presented in Chapters IV through VI. Topics reported on include: PL of GaAs and InP substrates; PL and Hall mobility of GaAs and InP undoped epilayers; PL of InP:Mg; and PL, Hall mobility, absorption coefficient, Auger electron spectroscopy (AES), and secondary ion mass spectrometry (SIMS), of $In_{1-x}Ga_xAs$ ternary layers.

CHAPTER II

CRYSTAL GROWTH METHOD

Within the family of vapor phase epitaxial crystal growth techniques, organometallic vapor phase epitaxy (OMVPE) is an important method both for industry and research [3]. OMVPE is the elevated temperature growth of single crystal layers on a substrate with nearly the same lattice constant, using organometallic compounds and hydrides for source materials. Interestingly, growth can also occur on substrates with lattice constants quite dissimilar to the desired layer [4].

This chapter will outline the lattice-matched growth method as applied to GaAs, InP, and InGaAs. For further information on OMVPE and its history, the reader is referred to two recent reviews [5,6]. Other growth processes that are related yet distinct, namely low pressure OMVPE [7], chloride/hydride VPE [8], adduct OMVPE [9], vapor levitation epitaxy [10], and laser-induced chemical vapor deposition [11], will not be further discussed here.

InP and InGaAs were among the first materials to be grown by Manasevit in the early OMVPE investigations [12,13], dating to 1973. The increased use of this technique can be seen in the proceedings of three International Conferences on OMVPE: in 1981 [14], 1984 [15], and in 1986 [4]. The early attempts to grow InGaAs on GaAs

[16-19], or on InP [20-25], using triethylindium (TEIn) by atmospheric pressure OMVPE met with problems due to the parasitic reaction in the vapor zone of TEIn and PH_3. More consistent success growing the indium-containing compounds has been reported with the use of trimethylindium (TMIn) [26-32]. The effort at OGC was aimed particularly at reproducing the growth methods of Stringfellow [33-39] and Bass [41-43] and their co-workers, using TMIn and TMGa.

The pyrolytic reaction producing InP is:

$$(CH_3)_3In + PH_3 \longrightarrow InP + 3CH_4.$$

The reaction for InGaAs is:

$$x(CH_3)_3Ga + (1-x)(CH_3)_3In + AsH_3 \longrightarrow In_{1-x}Ga_xAs + 3CH_4.$$

Growth can take place over a wide temperature range, although optimum temperatures have been reported [42]. For some applications, minimizing the growth temperature is desirable [26]. In this study, growth temperatures ranged from 600°C to 700°C for In-containing compounds.

The reactions given above are poorly understood [5], and are inefficient due to several mechanisms. First, there is a significant evaporation of phosphorous from InP at elevated temperatures. The vapor pressure of P_2 over InP is in excess of 10^{-4} T at 650°C [44]. Consequently, an overpressure of the phosphorous-containing reagent as compared to the indium-containing reagent must be maintained. $[PH_3]$/[TMIn] ratios up to 100:1 are used. Arsenic loss from InGaAs or GaAs is not as bad, but an overpressure must still be maintained. Second, there is a loss of TMIn prior to the growth zone due to reaction with PH_3. While less severe than the corresponding loss of TEIn, it does mean

that an excess quantity of TMIn must be introduced into the reactor. Third, polycrystalline material growth can occur on the hot susceptor or contaminated areas of the substrate. Fourth, the cracking efficiency of both the group III alkyls and group V hydrides in the hot zone near the substrate is less than 100% for the typical OMVPE reactor.

Magnesium was used for p-type doping. The organometallic compound bis(cyclopentadienyl)magnesium (Cp_2Mg) was introduced into the reactor, and by the reaction

$$(C_5H_5)_2Mg \longrightarrow Mg + 2C_5H_5,$$

Mg was available at the surface of the epilayer for incorporation as growth proceeded. Since Cp_2Mg and TMIn are solids at room temperature (melting points 176 °C and 88.4 °C respectively), H_2 was passed over their solids to obtain vapor mixtures.

No attempt was made in this study to accurately determine the vapor pressure of the organometallics; the published values of Ludowise [5] were used instead. TMGa is a liquid at room temperature (boils at -15.8 °C), and was added to the gas stream by bubbling H_2 through a TMGa vessel. When $In_{1-x}Ga_xAs$ was grown, the composition was varied by adjusting the temperature of the TMGa bath.

Published growth conditions for InP and $In_{0.53}Ga_{0.47}As$ grown by the method used here are shown in Table I and Table II, which also give the typical conditions at OGC for comparison. (The specific growth conditions for various samples are given in later

TABLE I. Comparison of Atmospheric Pressure OMVPE Growth Conditions for InP Using TMIn.

Lab	TMIn source	PH_3 source (10% in H_2)	Carrier gas flow[a] (l/min.)	$\frac{[PH_3]}{[TMIn]}$	Temp. (°C)	GROWTH rate (μm/min.)	GROWTH effic.[b]	Best n (cm^{-3})
RSRE[c] 1983 [40]	Alfa 60 °C [$0.5\text{-}2\times10^{-4}$]	Air Prod. [$0.3\text{-}4\times10^{-3}$]	5 (H_2 & He) 40 mm dia.	10-30	750	0.042-0.13	3700	2×10^{15}
RSRE[c] 1984 [41,42]	Alfa 60°C [10^{-4}]	Air Prod. [2.4×10^{-3}]	7.5 40 mm dia.	24	638	0.033	1000	8×10^{14}
Cornell[c] 1985 [27]	12.2 °C [7.43×10^{-5}]	[3.19×10^{-3}]	5	43	650	...	...	...
France Telecom 1983 [30]		...	4 H_2 8 N_2 65 mm dia.	...	650	0.06	...	8×10^{14}
Fr. Tele.[c] 1984 [28]	Alfa 25 °C	Matheson [$2.5\text{-}25\times10^{-3}$]	50% N_2 50% H_2	...	650	0.033	...	...
Plessey 1984 [31]	Alfa [4×10^{-5}]	Air Prod. [3.7×10^{-3}]	4 4 cm^2	93	600	0.03	4200	2×10^{16}
British Telecom 1985 [32]		...	...	...	650	0.08	...	...
U. of Utah[d] 1983 [34-6]	17 °C [2.28×10^{-4}]	[0.015]	2 2x5 cm	66	625	0.083	4500	...
OGC[d] 1987	Alfa [9.25×10^{-5}]	Phoenix Research [7.43×10^{-3}]	4 2.4x4 cm	80	600	0.03	2000	7×10^{15}

[a] H_2 gas unless otherwise noted. Growth tube cross-section noted.

[b] Growth efficiency = (growth rate)/(TMIn molar flow), in μm/mole, assuming the vapor pressure of TMIn given in Ludowise [5].

[c] InP (100) substrates were etched in bromine-methanol, then baked in the reactor at over 650 °C for at least 10 prior to growth.

[d] InP (100) substrates were etched in H_2SO_4:H_2O_2:H_2O, but experienced no pre-bake.

TABLE II. Comparison of Atmospheric Pressure OMVPE Growth Conditions for InGaAs Using TMIn and TMGa.

Lab	TMIn source	TMGa source	AsH_3 source	H_2 flow (l/min.)	[V]/[III]	[TMIn]/[TMGa]	Temp. (°C)	GROWTH rate (μm/min.)	GROWTH effic. (μm/mole)	Best n (cm^{-3})
RSRE 1986 [42]	Queen Mary Coll. 60 °C [10^{-4}]	Alfa -9 °C [4.95×10^{-5}]	Phoenix Res. [1.2×10^{-3}]	7.5	80	2.02	660	...	...	4×10^{14}
HP, 1984 [26]	17.3 °C [3.48×10^{-5}]	-12 °C [2.3×10^{-5}]	[0.01]	13.5	173 (18)	1.52	540 (640)	...	...	2×10^{15}
Cornell 1985 [27]	[7.43×10^{-5}] 12.2 °C	-14 °C [3.8×10^{-5}]	[1.6×10^{-3}]	5	14.3	1.95	650	...	...	2×10^{15}
Fr. Tele. 1983 [28]	Alfa 25 °C	Alfa	Air Liquide [0.01]	50% N_2 50% H_2	...	...	650	0.06	...	...
Bell Labs, 1986 [29]		...	...	5	...	...	625	...	...	2×10^{15}
Plessey 1984 [31]	Alfa [4×10^{-5}]	Alfa [2.3×10^{-5}]	Air Prod [3.7×10^{-3}]	4.4	59	1.74	600	0.06	5300	9×10^{15}
British Telecom 1985 [32]		...	5% in H_2	...	...	...	650	0.13	...	...
U. of Utah:										
1983 [37-8]	10 °C	-12 °C	...	...	80	...	530	...	20,000	...
1984 [33]	10 °C	-11.5 °C	...	2	31	...	650	0.05	6800	5×10^{15}
OGC 1986	Alfa [9.25×10^{-5}]	Alfa [4.5×10^{-5}]	Phoenix Res.	4	80	2.07	600	0.057	2600	3×10^{15}

chapters along with results.) Major variables which are not represented in the tables are source material purity and interior reactor surface cleanliness, which have a large impact on the ability to grow defect-free epilayers.

What follows is a description of the OGC reactor. The reactor geometry and apparatus design were based on a compilation of published reports. It was built by Crystal Specialties, Inc. in 1985. The reactor produced material acceptable for this study, but was not optimized for growth rate, growth efficiency, two-dimensional uniformity, or interface abruptness.

The general layout of the reactor is shown in Fig. 2. (See Appendix E for an equipment list.) Arsine, phosphine, and hydrogen were contained in gas cabinets (shown in the top view only). When each of these cylinders was changed, the individual line was evacuated to remove any room air introduced during the change. The toxic lines could be individually purged with nitrogen prior to opening to room air. The four cabinets, reactor vacuum seal, and glove box were exhausted through a single blower to outside air, 24 hours/day. All hydrogen and toxic gas regulator bodies, and the growth tube itself were vented through an activated charcoal barrel to the outside air. All gas tubing was 1/4 inch O.D. 316 S.S., either welded or joined by VCR fittings. O-rings were used only to seal glassware: thermocouple tube, reactor tube, and reactor exhaust oil trap. Plated VCR gaskets were used throughout. Valves contained teflon seal

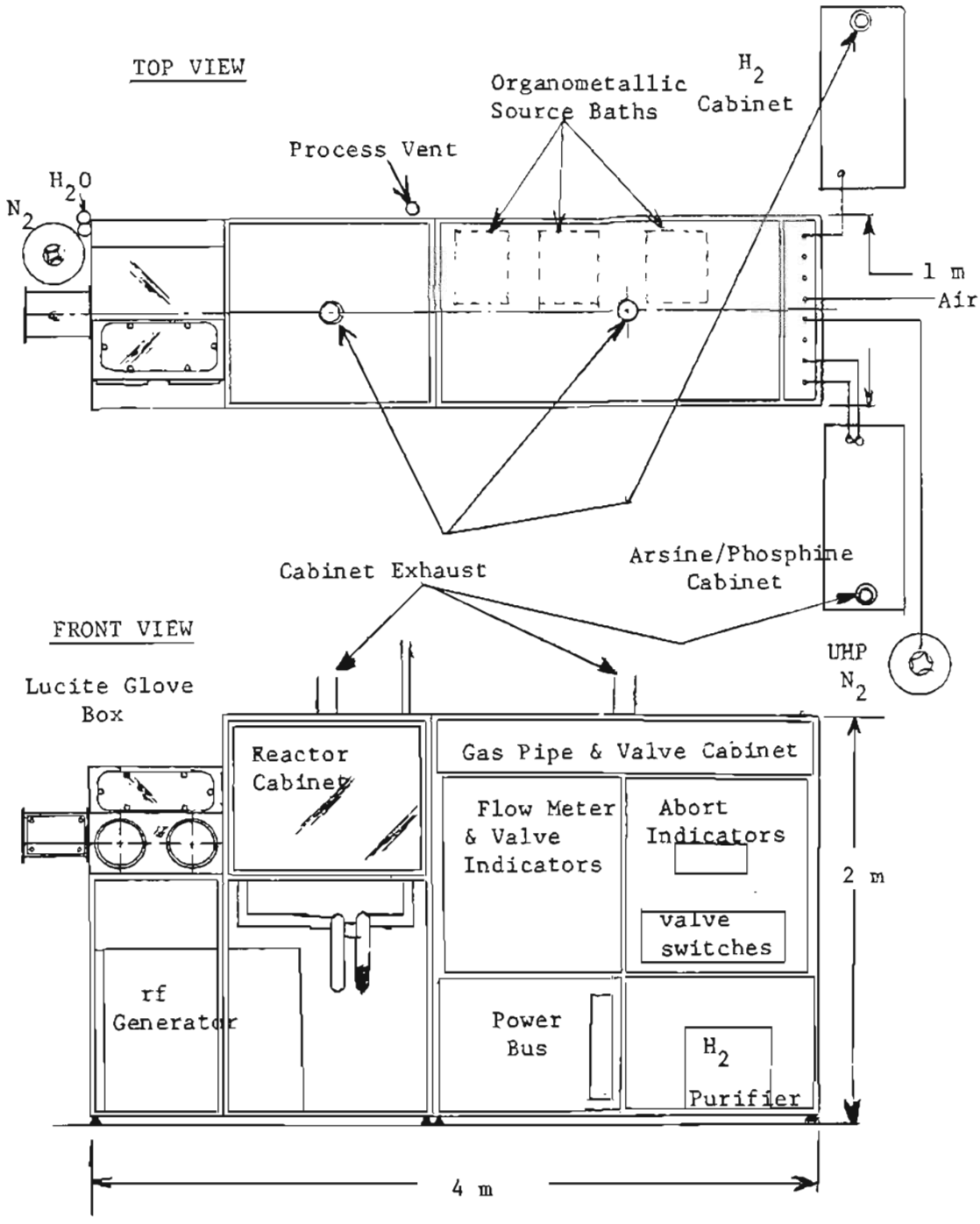

FIG. 2. OMVPE Reactor General Layout.

gaskets.

Prior to installation, all gas line components were degreased with hot trichloroethylene and hot acetone, followed by cold rinses with acetone and methanol. The assembled system was helium leak checked to 10^{-8} T. The two gas cylinder cabinets were built by OGC, using double-wall flammable-liquid cabinets. All regulators and vacuum ports were inside the cabinets, and process gases flowed through bulkheads and connecting tubing to the reactor. Gas flow in Fig. 2 is right to left. The glove box was employed for loading and unloading reactor tube components or substrates. This box was purged with low purity N_2 for at least 10 minutes before opening the reactor load/unload door.

The programmable process sequencer supplied with the reactor was not used in this study because it provided no control over flow rates; all valve switching was done manually.

A schematic of the gas pipe and valve cabinet is given in Fig. 3. Gas flow is left to right in this figure. Heat tape was wrapped around the organometallic source lines from within 40 cm of the source output valve to the 3-way valve manifold leading into the reactor tube, maintaining the tubing at about 40 °C at all times. This was done to prevent plating or condensation of the organometallics in the tubing prior to the reactor tube. Details of the reactor cabinet are shown in Fig. 4. The rf coil and bake-out oven could be positioned along the reactor tube as desired. The bake-out oven was used occasionally to convert white phosphorus to red, and to otherwise clean the reactor tube components.

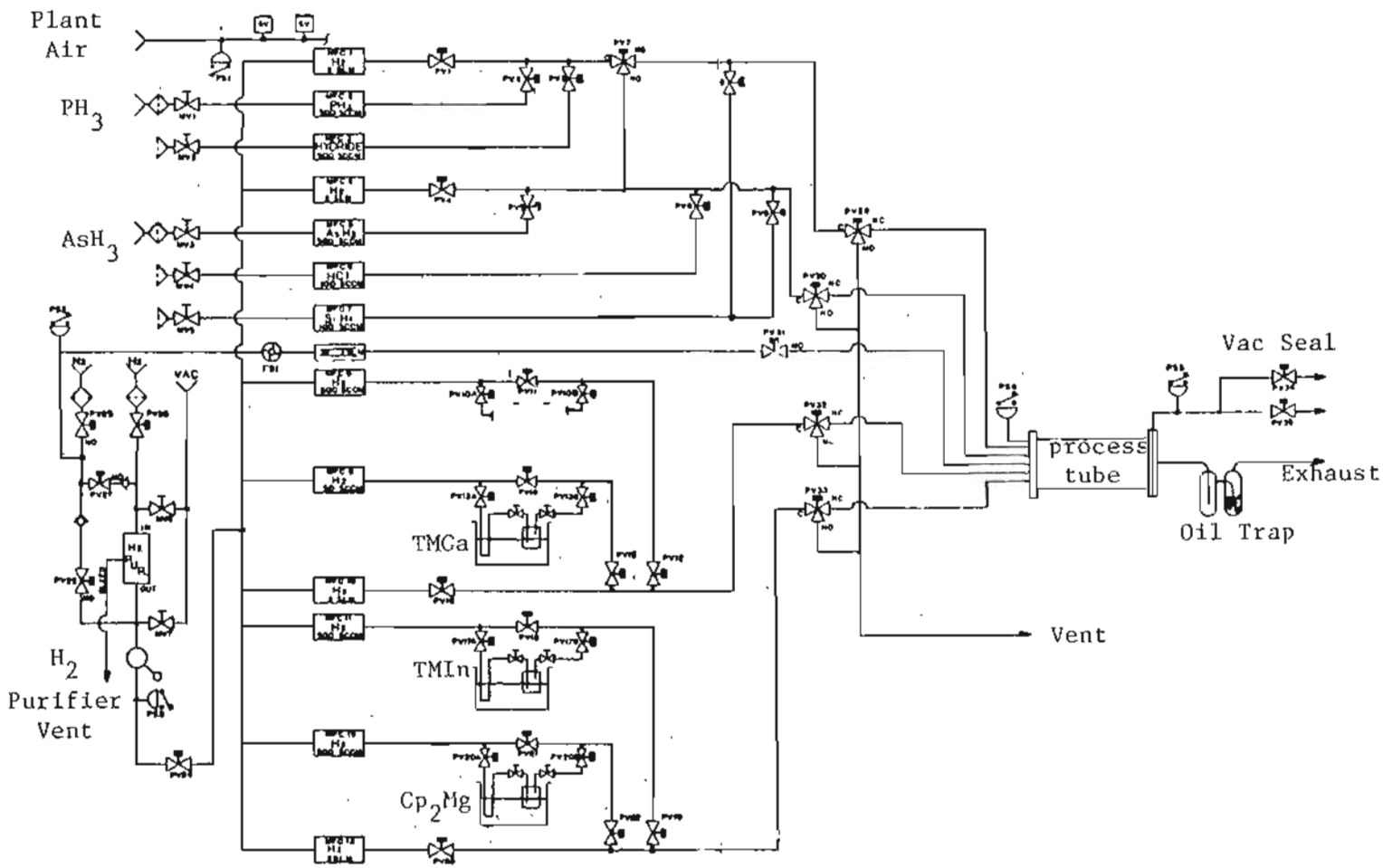

FIG. 3. OMVPE Reactor Gas Schematic.

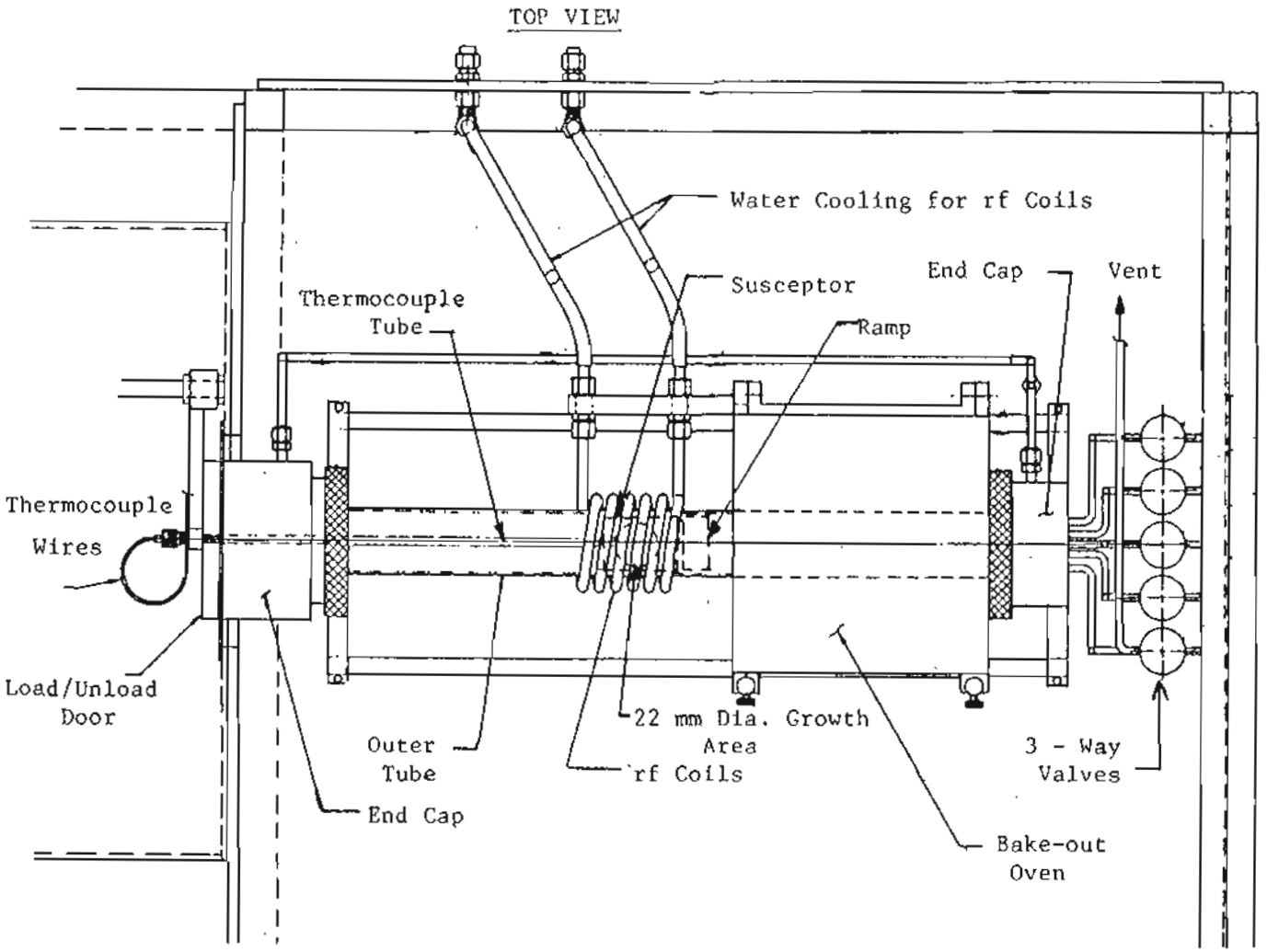

FIG. 4. QMVPE Reactor Cabinet.

The reactor tube itself is detailed in Fig. 5. The purpose of the quartz ramp in front of the susceptor was to reduce turbulence. The susceptor was SiC-coated graphite (2.4 × 0.6 cm front cross section), and held substrates at a 10° angle. A 5 mm diameter quartz tube containing a thermocouple was fitted in a hole in the rear of the susceptor. The growth temperatures were measured solely with this thermocouple, which was Pt vs. Pt with 13% Rh in an inconel sheath (ungrounded). Approximately 100 cc/min. of H_2 were kept flowing through the reactor whenever possible to sweep away contaminants. 1000 to 3000 liters of H_2 were purged through the system after long shutdowns during which no H_2 flow could be maintained.

Substrates were etched just prior to growth at 40 °C in a 5:1:1 solution of H_2SO_4:H_2O_2:H_2O for two to four minutes. The samples were then rinsed until a clean water break was obtained. Talc-free latex gloves were worn, sample edges were held with teflon tweezers, and the etch or rinse was done in a teflon beaker dedicated to the purpose. The quartz insert and ramp were cleaned prior to each growth in aqua regia, and rinsed in water followed by acetone and methanol. Every five to ten growths, the susceptor was cleaned in aqua regia and baked for 30 minutes in H_2 at 900 °C. GaAs substrates were baked at 800 °C for 5 minutes in 10^{-3} atm of AsH_3 just prior to growth. When InGaAs was grown on InP, a two minute gap was kept between the end of PH_3 flow and start of AsH_3 flow during which 1 1/min. of H_2 flushed out the remaining PH_3. This was to prevent InGaAsP growth.

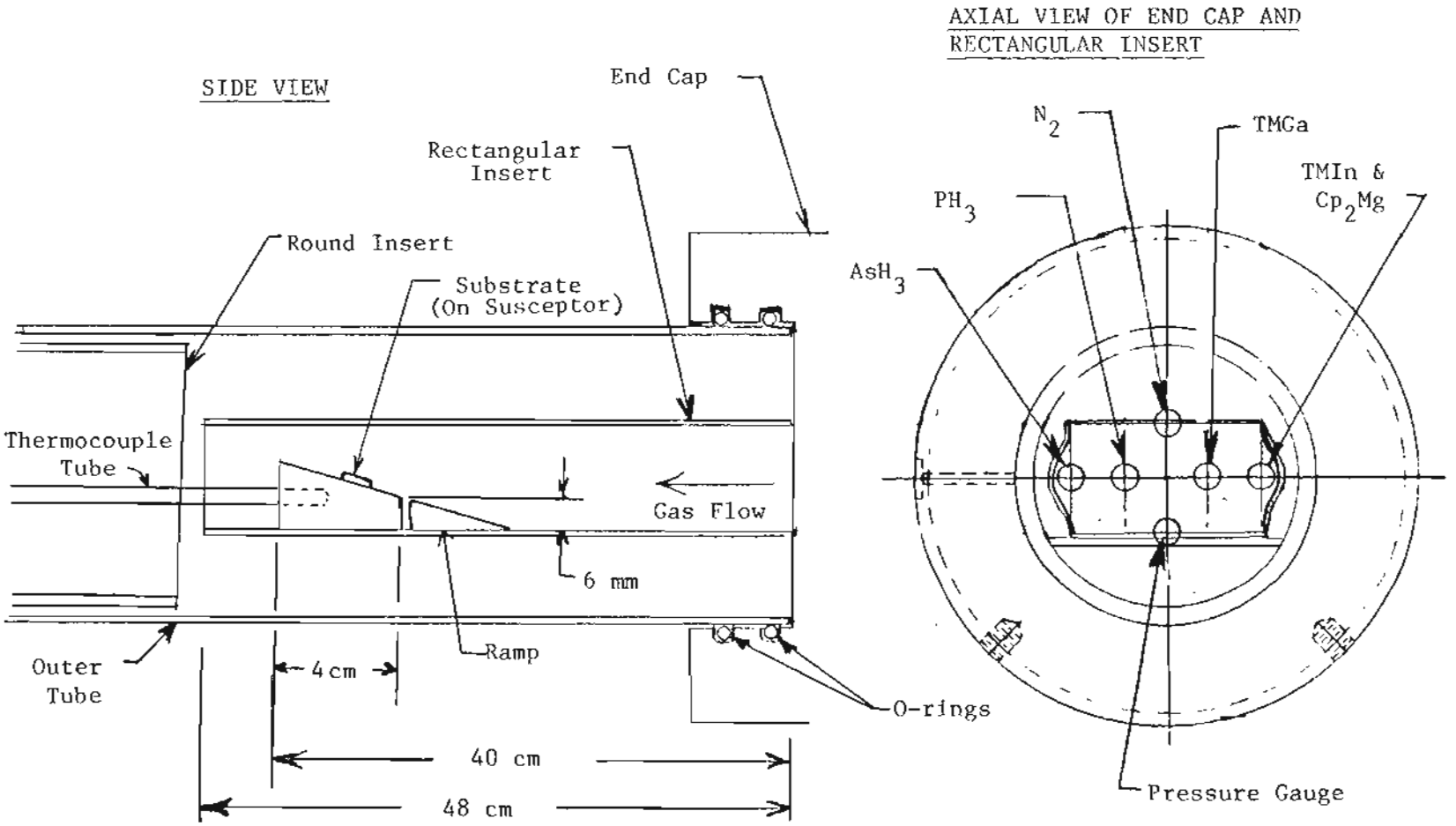

FIG. 5. OMVPE Reactor Tube.

Numbering of samples was sequential by epilayer material. GaAs 1 was grown 10/17/85, while GaAs 62 was grown 9/15/86. InP 1 was grown 3/30/86 and InP 47 1/16/87. InGaAs 1 was grown 4/25/86, while InGaAs 69 was grown 2/2/87. Growth times ranged from 30 to 120 minutes, and the resulting epilayer thicknesses were 1 to 6 microns.

CHAPTER III

CHARACTERIZATION TECHNIQUES

A. Photoluminescence (PL)

Photoluminescence spectra were taken on nearly all epilayers and substrates for the purpose of establishing relative purity and defect levels. A good general discussion of the theory and measurement of PL has eluded the author, but some theoretical background is in reference [45], and good information in regard to the quaternary alloys InGaAsP is in reference [46]. For the following description, refer to the experimental setup in Fig. 6.

An argon ion laser provided radiation of above bandgap energy (514.5 μm) at up to 20 W/cm^2. (Power level calibration data was provided by the manufacturer in 1981 and was occasionally checked by OGC personnel afterward.) The laser was focused, unfiltered, on the surface of the sample by a f = 120 mm, 42 mm diameter lens. The same surface point was at the focus of a large diameter (30 mm), short focal length (10 mm) lens. The same was mounted, using rubber cement, on the low temperature pad of a MMR cryostat.

In order to obviate the need for precise location of the monochromator with respect to the sample and to match more closely the focal length of the monochromator, a third lens (f = 32 mm, diameter = 34 mm) was used to focus the light onto the entrance slit of the monochromator. A filter was introduced into the collimated portion of

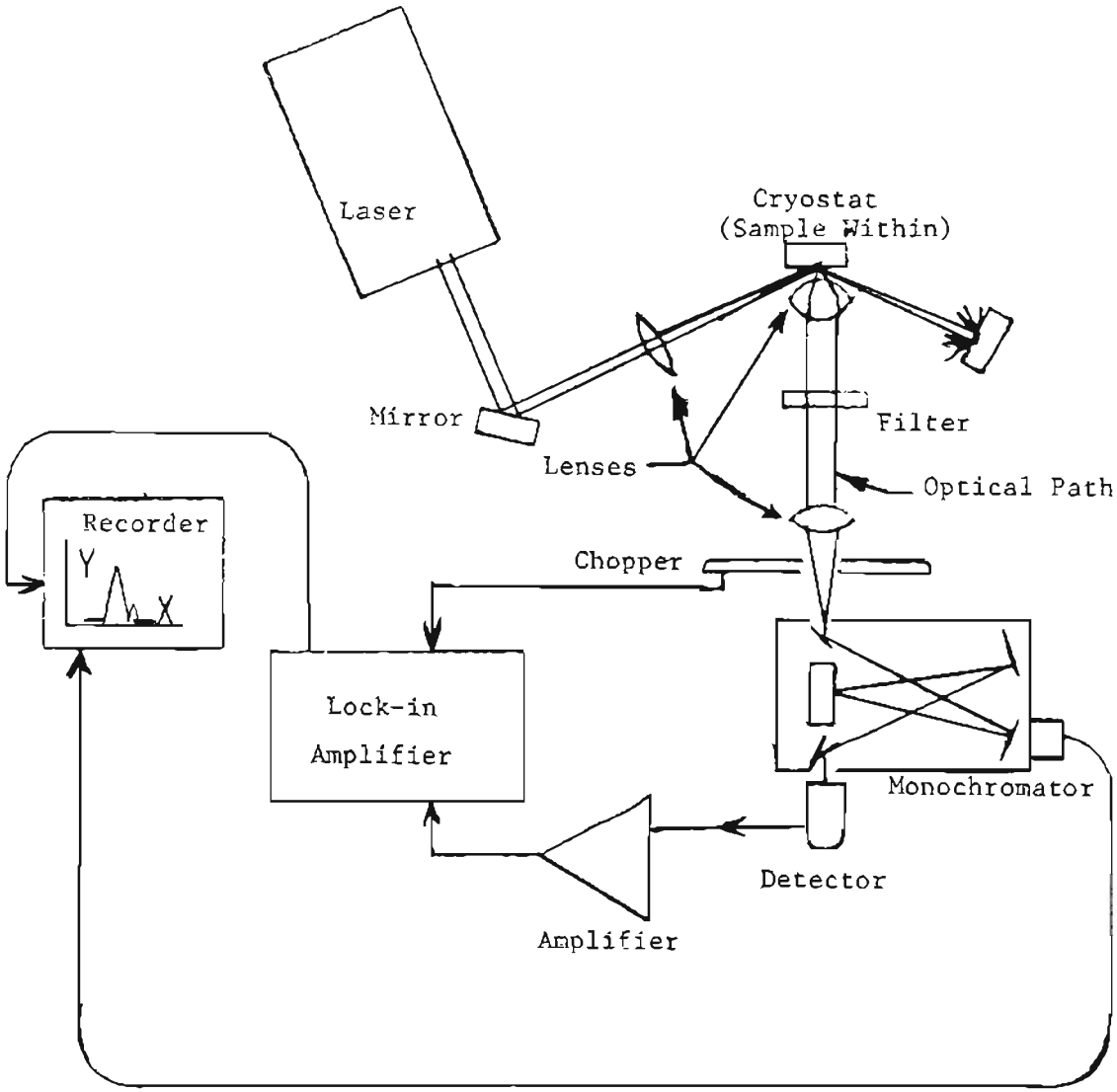

FIG. 6. Schematic of Photoluminescence Apparatus.

the light path to remove laser emission and to prevent lower order wavelengths from passing through the monochromator. Slit width was minimized to obtain good energy resolution (dispersion was 6 nm/mm slit width), but light throughput dropped off rapidly with decreasing slit width, as can be seen in Fig. 7. Input and output slits were always set to the same width.

The monochromator wavelength indicator was calibrated using both the Ar^+ ion laser (514.5, 496.5, and 488 nm lines) and a He-Ne laser (632.8 nm). No selective absorption was observed by the windows or lenses used in this study. The detector was positioned as close as possible to the output slit, with no optics in between. The signal was amplified and fed to an X-Y recorder by a conventional lock-in detection system. Detector response curves are given in Fig. 8. (The light source was the Oriel lamp as used for absorption measurements.) The (uncooled) PbS detector was used for all PL data since it had a better response than the cooled Ge detector beyond 1500 nm.

The monochromator was fitted with a gas inlet to purge water vapor with clean N_2. The well known atmospheric H_2O absorption peak at 1375 nm [47] was observed as can be seen in the inset of Fig. 8. Since this absorption did not affect the PL studied here, N_2 was not typically used. The larger absorption drop at 1410 nm was obtained only with the PbS detector and was therefore assumed to be characteristic of this detector. The detector response curve was used to correct relative peak heights in some of the PL data; whether or not this was done is noted in the text with each figure. An equipment list for PL

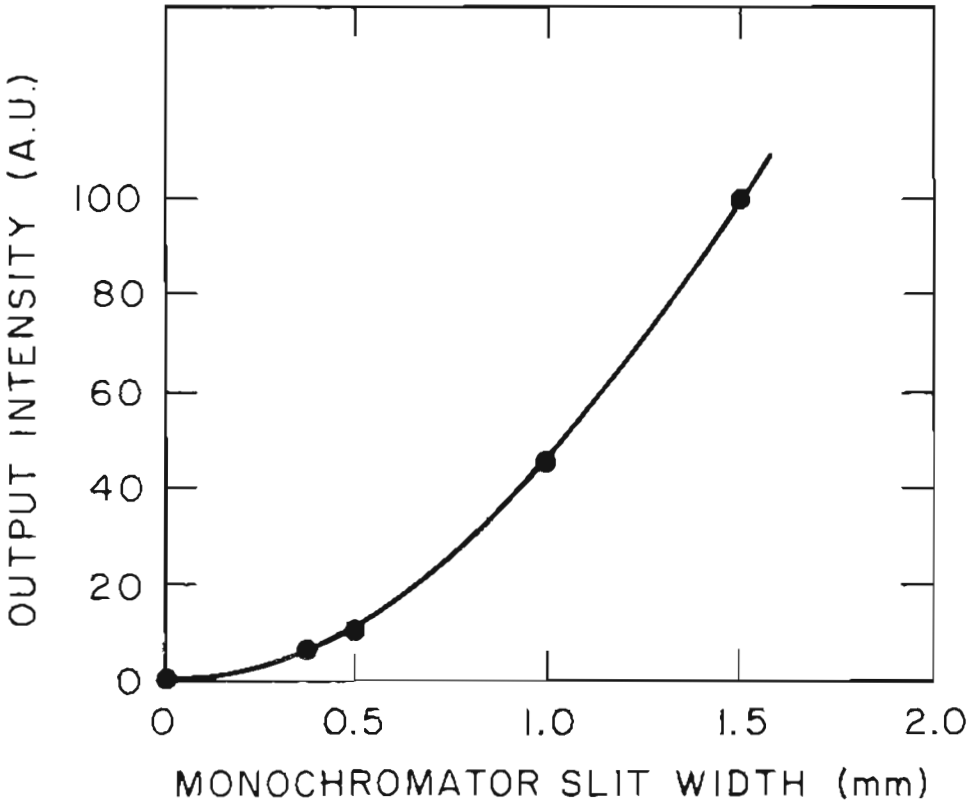

FIG. 7. Light Output for Various Monochromator Slit Widths.

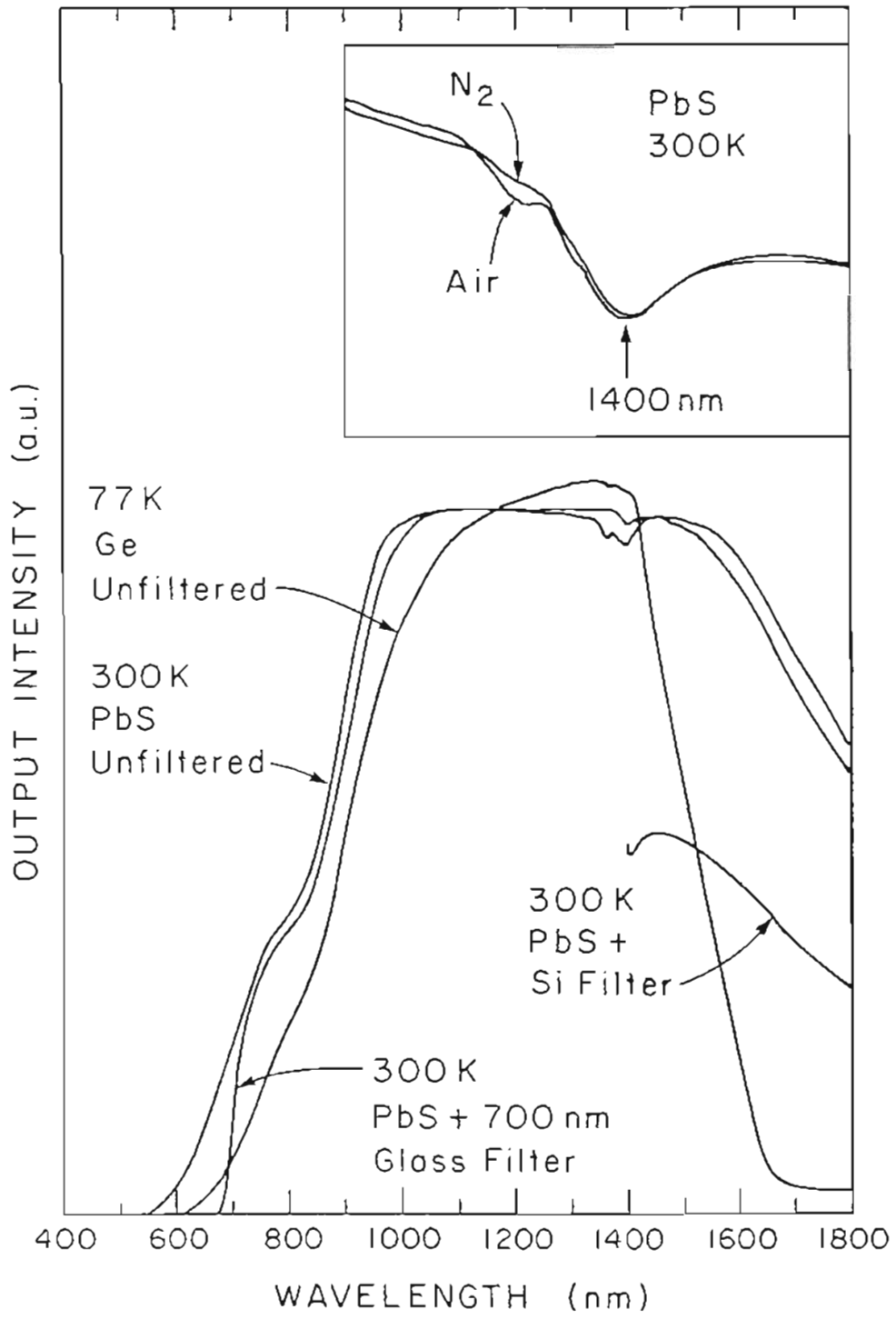

FIG. 8. Optical Detector and Filter Spectral Response.

measurements is given in Appendix E.

When determination of impurity concentrations was attempted using photoluminescence data, a simple comparison was made to literature values [46,48-50]. The presence of impurities broadens the width of the impurity transition peaks in PL. This can be seen in Fig. 9, which is a compilation of least squares fits to the above referenced data. (Raw data are in Appendix C.) Peak widths are given throughout this report as full width at half maximum (FWHM).

Data from [46] are used in Chapter IV to estimate N_A-N_D for InP:Mg samples. It is obvious from the data in Fig. 9 that considerable uncertainty--perhaps a factor of two--exists in the determination of carrier concentrations by this method. This method is valid only for doping levels in excess of 10^{16} cm^{-3}. A method has also been claimed to determine compensation ratios from PL [51], but that was not attempted in this study.

Photoluminescence was not always easily seen, and several methods were employed to increase the signal-to-noise ratio. One step that was important in early measurements was to direct scattered laser beam light away from the detector. As indicated in Fig. 6, the laser beam was directed obliquely toward the sample, thus the specular reflections from the sample face and cryostat window were unable to enter the monochromator. Secondly, although a Si filter is desirable for order sorting at wavelengths greater than 1200 nm, a glass filter was occasionally substituted for looking at weak emissions in this range (because the Si filter transmission is only about 50%). Third, the monochromator slits were opened as wide as possible (consistent with reasonable

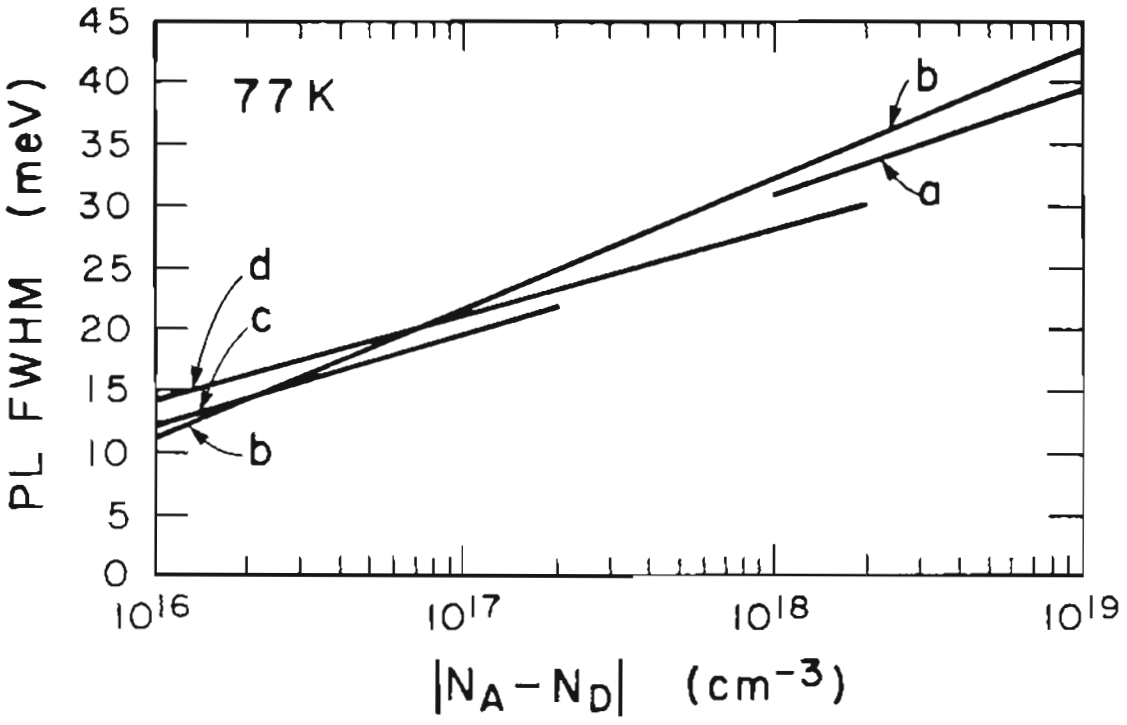

FIG. 9. PL FWHM for Various Doping Concentrations. a) LPE InGaAs:Zn [48], b) LPE InGaAsP:Zn [46], c) VPE InP [49], d) LPE InP:Zn [50].

energy resolution). Fourth, PL emission was greatly enhanced when the laser was focused on the edge of the epilayer as opposed to its surface. An example is shown in Fig. 10: PL results from InGaAs 62 with all parameters constant except for location of the incident laser beam. Variations this large were never observed along the surface of any samples. It is presumed that laser light entering the edge excites a larger thickness of the InGaAs layer. (This enhancement was seldom needed, and all data reported in subsequent

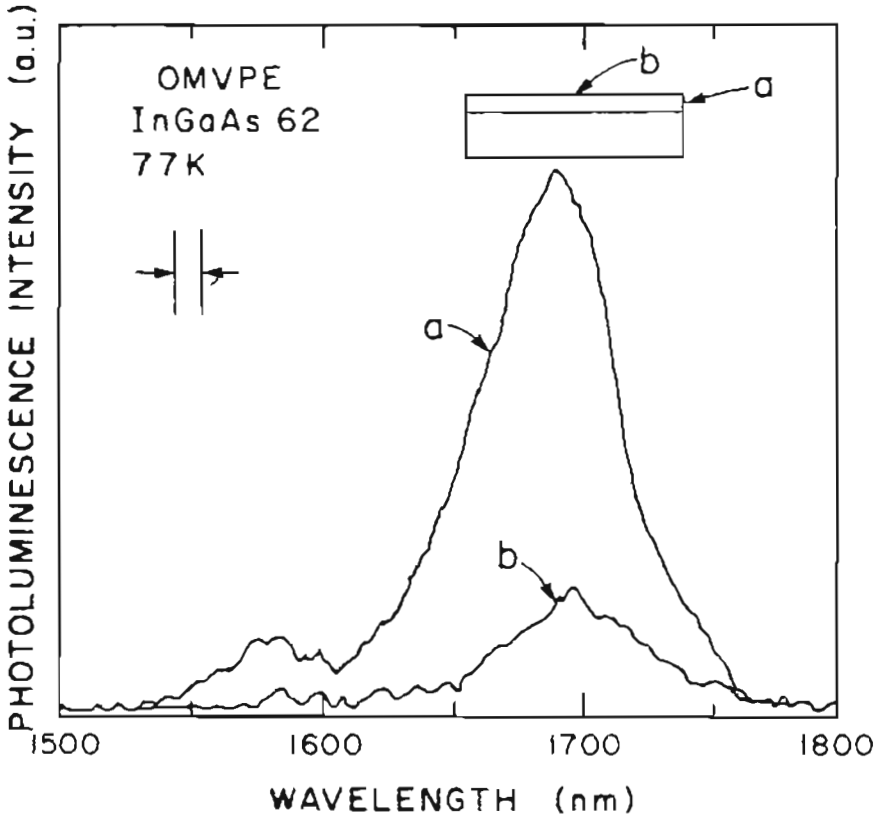

FIG. 10. PL for OMVPE InGaAs. a) edge-focused laser input, b) surface-focused laser input.

chapters were generated with the laser striking the surface near the center of the sample.)

When estimates of peak energy or FWHM were made from PL data, the accuracy was assumed to be limited by the monochromator resolution. This resolution is shown in each figure containing PL spectra as the spacing of two vertical lines.

B. Hall Mobility

Measurements of the sheet resistance and Hall effect were made by the van der Pauw technique [52]. (All formulae in this section are from this reference.) Ohmic contacts were made by the method given in Appendix A, and were placed in the corners of samples that had been cleaved into 3-4 mm squares. For inhomogeneous samples, the epilayer was cut with a diamond scribe midway between the contacts to form a cloverleaf (see Fig. 11). The normal configuration (without scribe lines) was used for all data reported herein.

These measurements give the low field response of the majority carriers (Hall mobility), information about compensation (when the data cover a suitable temperature range), as well as the resistivity and net carrier concentration (given the epilayer thickness, d). The quantity that is measured is the voltage between the contacts A, B, C, and D in Fig. 11 when a known current is injected into the sample. For resistivity, a current I is passed through points A and B while a voltage V is measured across C and D. Then the resistivity $\rho = \pi dR/\ln 2$ where $R = V/I$. In practice, this measurement is repeated for all four edges with current of both polarities and the resulting eight resistances are averaged to obtain R. Any lack of symmetry in the placement of contacts is corrected by including a factor, F, in the calculation. F depends on the resistances R and R_s obtained from adjacent sample edges as:

$$F \simeq 1 - \left(\frac{R - R_s}{R + R_s}\right)^2 \frac{\ln 2}{2} - \left(\frac{R - R_s}{R + R_s}\right)^4 \left[\frac{(\ln 2)^2}{4} - \frac{(\ln 2)^3}{12}\right] .$$

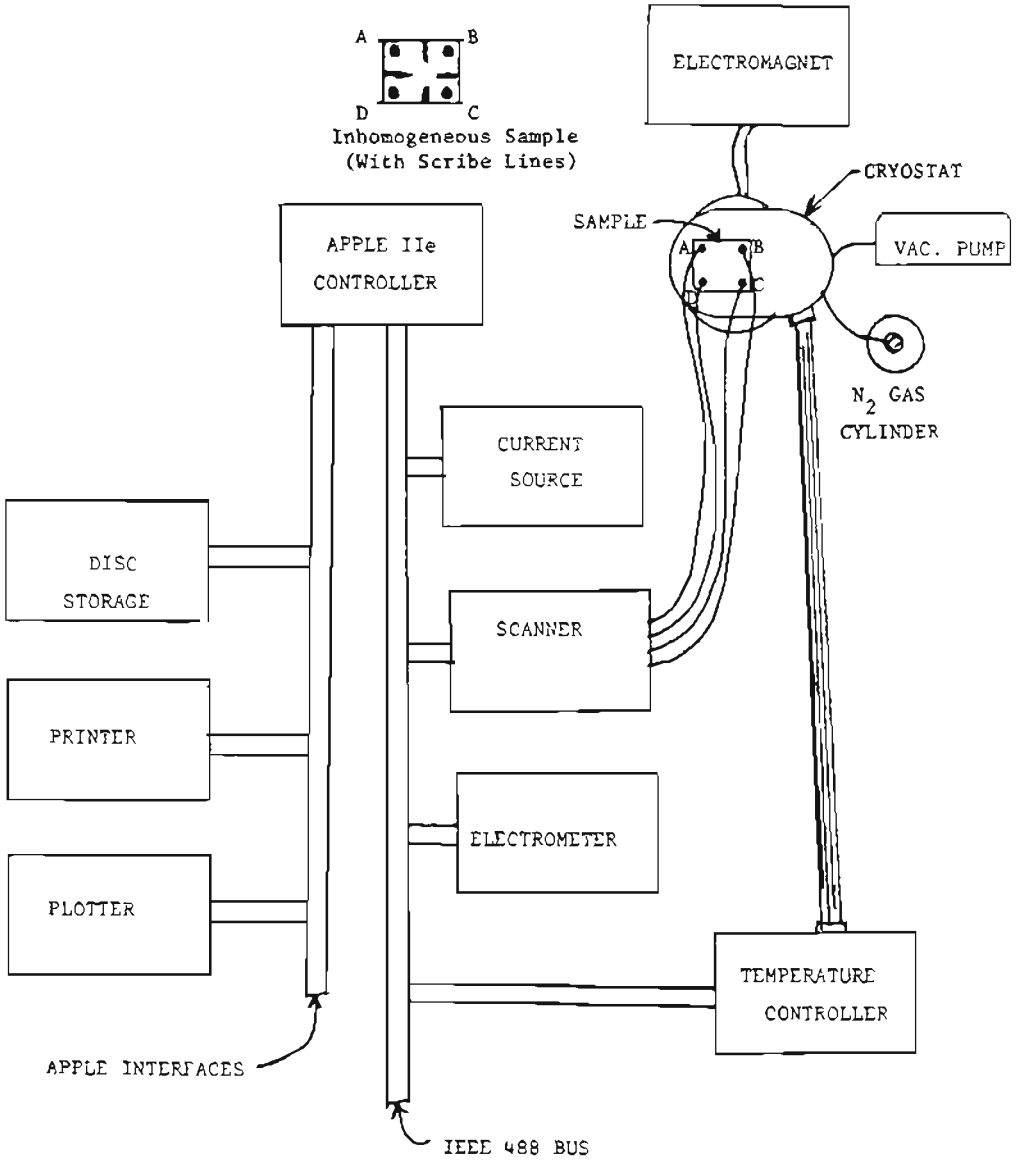

FIG. 11. Schematic of Hall Mobility Measurement Apparatus.

For nearly symmetrical contacts, F ≃ 1. Including possible asymmetries, $\rho = \pi dRF/\ln 2$.

Calculation of the Hall mobility μ_H requires ρ, and a further resistivity measurement in the presence of a known magnetic induction, b, perpendicular to the sample. The voltage v is measured diagonally across the sample from B to D (or A to C) with current i injected through A and C (or B and D). Now r = v/i, and with current polarity reversed there are then four r values. Each is to be subtracted from its corresponding value when the magnetic field is zero, to give four Δr values. (The polarity of Δr indicates p-type or n-type conductivity.) From the resultant $\overline{\Delta r}$ (the average of the absolute values of these four differences), $\mu_H = d\,\overline{\Delta r}/b\rho$. Note that since $\rho \propto d$, μ_H does not depend on d. Carrier concentration can then be calculated, assuming conductivity by one type of carrier dominates. If the Hall factor, r_H, is known for the material, magnetic induction, and temperature used, then $n = r_H/e\mu_H\rho$.

These formulae were incorporated in a program (see Appendix F) which controlled a semi-automated Hall mobility measurement system. Shown schematically in Fig. 11, this system was set up as described in the Keithley application note #501, omitting the unity gain amplifiers. (The equipment list is in Appendix E.) The computer monitored the sample temperature--or set a particular value--via the MMR temperature controller. From any starting temperature, the sample temperature stabilized after a 10 °C increase in 30 s. It took 50 s after a 50 °C increase. The Hall factor was assumed to be unity for InP and InGaAs. For GaAs, values were used from [53]. (A recent report estimated the

Hall factor for InP [54].)

All measurements were made in the dark. Current values were chosen within the particular sample's ohmic conduction regime such that the voltage drop was in the range 10-100 mV. The actual current was usually not measured (except for some early samples) because it was found to have no deviation from the programmed value. Calibration of the magnet control setting was performed for both field polarities (see Fig. 12), although only one magnetization polarity was used. To see how the field magnitude might affect the data, the magnetoresistance of GaAs 27 was tested. The resistance changed 2% with a 3000 Gauss induction change. Mobility changed 0.3% with the same induction change. Since this was a small effect, no further study was done of magnetic effects. For 5000 Gauss and 10,000 Gauss data the control was set to 4.0 and 9.0 respectively. (See Fig. 12.)

Corroborative data were sought to confirm the accuracy of the Hall mobility apparatus. These data are summarized in Table III. The recent OGC data agree with other independent measurements to within 10% over a broad range of temperatures, sample thicknesses, and mobilities, for both p-type and n-type materials. This is quite good agreement for parameters which range over several orders of magnitude.

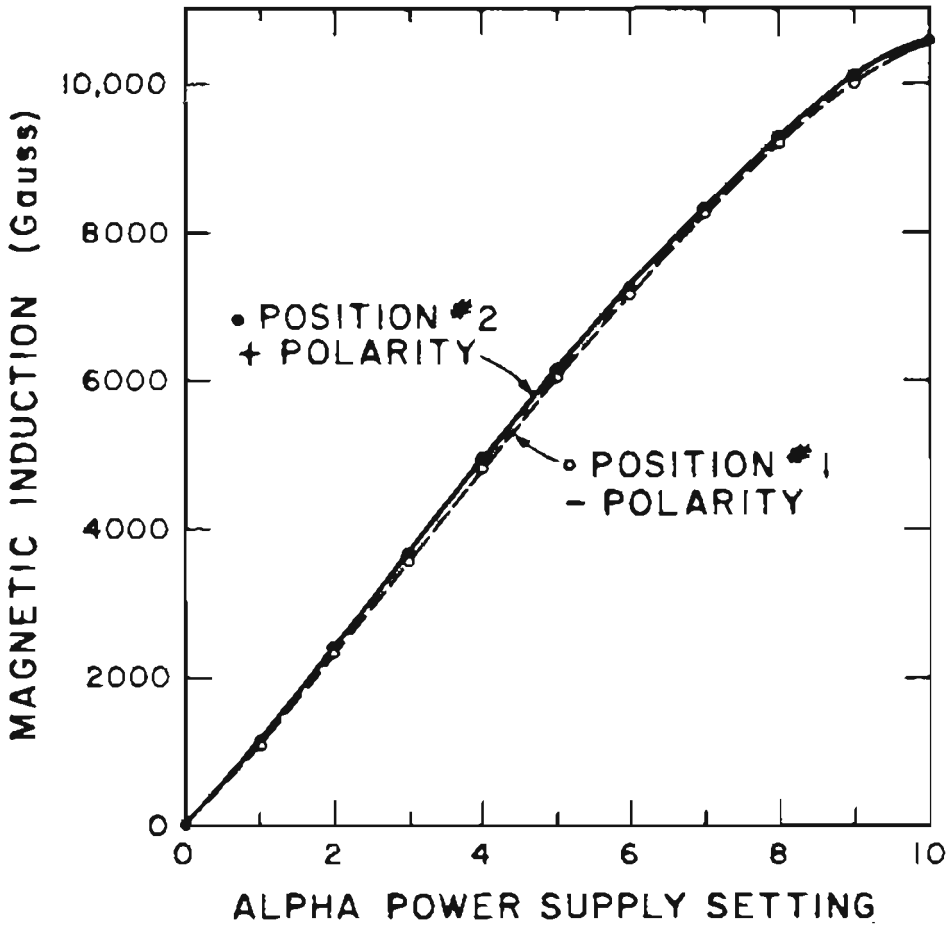

FIG. 12. Electromagnet Power Supply Calibration.

TABLE III. Comparison of OGC Hall Mobility Results with Other Labs.

Sample identity	Data source	Test date	Temp. (K)	ρ (Ωcm)	μ_H (cm^2/Vs)	n or p (cm^{-3})
Laser Diode Lot #A.0809	OGC	1/79	300	0.018	112	3×10^{18}
GaAs:Zn (111) t = 500 μm	OGC	6/86	292	0.0202	128	2.7×10^{18}
OGC GaAs55 n-type (100)	UET	10/86	77	0.0733	88,700	9.6×10^{14}
t = 1 μm	OGC	9/86	79.5	0.0816	86,100	9.1×10^{14}
Tektronix #7 B-doped (100)	Tek	7/86	300	0.0267	10.3	2.3×10^{19}
polysilicon t = 0.4 μm	OGC	3/86	292	0.0267	11.2	2.5×10^{19}

C. Auger Electron Spectroscopy (AES)

Auger analysis was undertaken on one InGaAs sample to verify the relative amounts of indium and gallium. (Optical absorption and photoluminescence had predicted that this sample was nearly lattice-matched.) The AES work was performed in January, 1987, at Charles Evans & Associates for the sample InGaAs 65. A 10 kV primary beam of 10-20 microns diameter was used. The beam current was approximately 1 μA, and the sputtering rate was 100 Å/min.

A comparative "standard" ternary sample was also analyzed at the Evans laboratories, under the same conditions. This was the InGaAs sample OSU 1-29-7-86, grown by molecular beam epitaxy and obtained from Professor J. R. Arthur of Oregon State University. The bandgap of this "standard" was measured at OGC by photoluminescence at 77 K and 300 K. These data are presented in Fig. 13. The peak heights have been corrected for detector response with wavelength. The 77 K peak is centered at 0.789 eV and the 300 K peak is centered at 0.736 eV. (As will be seen in Chapter VI, the PL results for InGaAs 65 were ambiguous.) Using the relations for $E_g(x)$ of $In_{1-x}Ga_xAs$ given in [55], namely $E_{g(300\ K)}(x) = (0.35 + 0.61x + 0.46x^2)$, and $E_{g(77\ K)}(x) = (0.41 + 0.57x + 0.53x^2)$ eV, the composition parameter x for this sample is x = 0.47, i.e. lattice-matched to InP. (At 300 K, the precise value for a lattice match is x = 0.468 [56]; lattice-matching for a given sample can only occur at one temperature because the coefficients of thermal expansion are different for InGaAs and InP.) Alternative relations have been proposed for $E_g(x)$ at room temperature [57,58] and at 2 K [59], as well

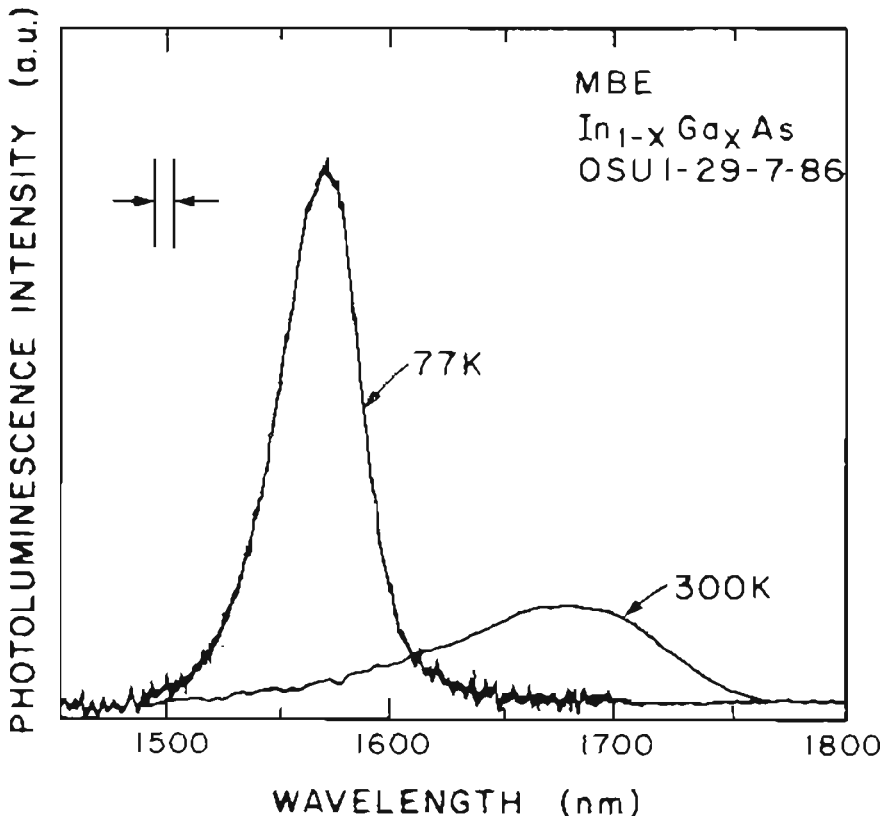

FIG. 13. PL Spectrum for $In_{0.53}Ga_{0.47}As$ "Standard".

as a relation for $E_g(T)$ [56].

The value x = 0.47 for the MBE "standard" sample was used to calibrate the atomic percent data derived from the AES raw intensity data of that sample. The result is given in Fig. 14, which shows 50% As content, 23.5% Ga content, and 26.5% In content uniformly throughout the top 4000 Å of the layer. That compositional scaling derived from PL/AES analysis of the MBE sample was then used to interpret the AES data for OMVPE sample InGaAs 65, as reported in Chapter VI.

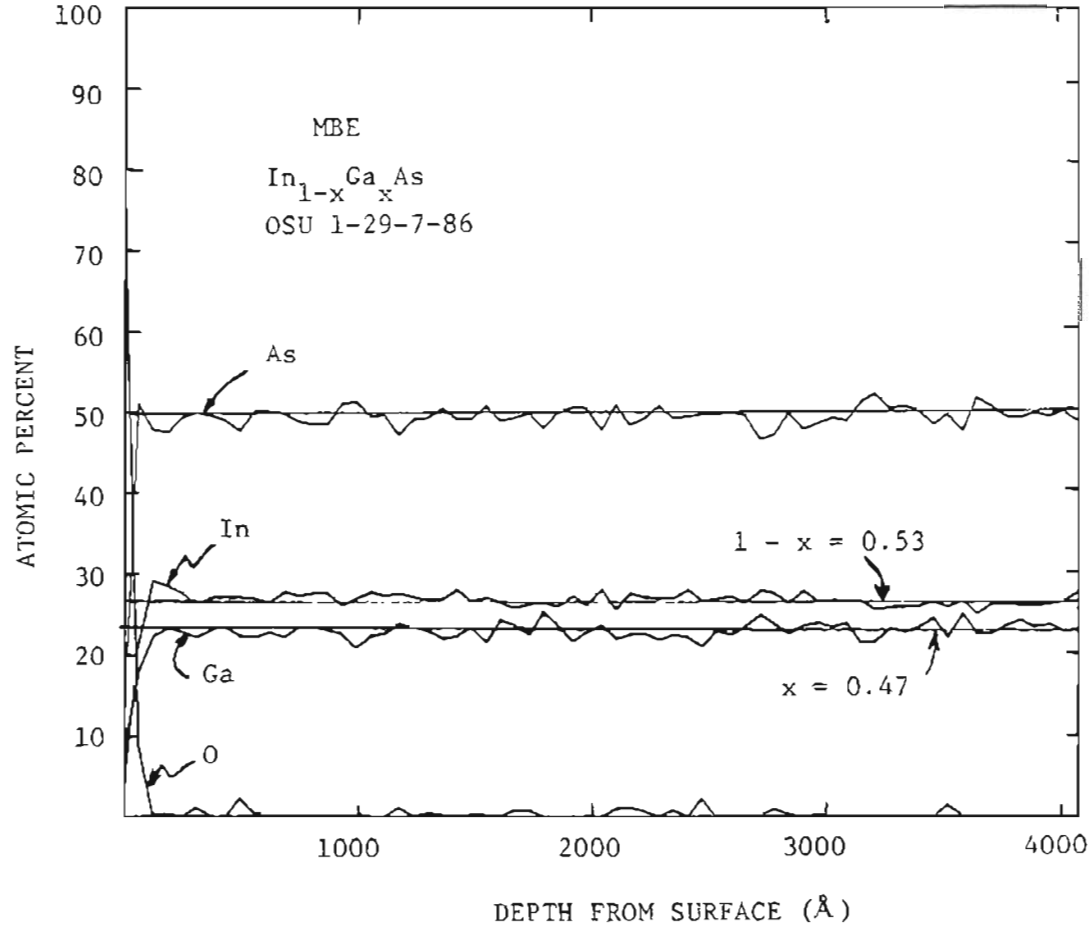

FIG. 14. AES Profile for $In_{0.53}Ga_{0.47}As$ "Standard".

D. Secondary Ion Mass Spectrometry (SIMS)

The SIMS technique, using Cs^+ ion bombardment and negative sputtered ion mass spectrometry, was employed by Charles Evans & Associates to measure O, C, S, Si, Cl, and Ag distributions in InGaAs/InP. SIMS with O^+ ion bombardment and positive sputtered ion spectrometry was used to measure Fe, Mg, Hg, Na, W, Cu, Ni, Cr, and Al distributions. SIMS with Cs^+ ion bombardment and positive sputtered ion spectrometry was used to measure the Zn (as $ZnCs^+$) distributions. Arsenic was also monitored to locate the interface between the epilayer and the substrate.

Appendix D contains the processed data, plotted semi-logarithmically as "concentration" versus depth. The right-hand axis of each processed data plot is labeled "secondary ion counts," and the As data are referenced to this scale. With the exception of Ag, the conversion of ion current to concentration was based on analyses of ion implant standards in GaAs, and should be accurate to a factor of two in a GaAs matrix. For InGaAs the uncertainty is unknown and probably much larger. The quantitative Ag data were obtained by estimating a sensitivity factor from the relative electron affinities of Ag and As. The accuracy for Ag should be within about an order of magnitude.

S, Si, Cu, Zn, and Hg, were monitored using at least two isotopes per element to check for possible molecular ion interferences. If they were not in the correct isotopic ratio when measured, there must have been an interference at one or all of the isotopes of that element. The profile which yields the lowest concentration after this comparison

will be closer to the actual concentration. The Hg data are unreliable because no ion implant standard was available, and isotopes of In-Ga-As are near those of Hg. Thus the Hg data probably track the ternary rather than Hg!

The SIMS data are used only for comparison purposes in Chapter VI, and no conclusions are drawn from them regarding the absolute concentrations of expected or unexpected contaminants.

E. Optical Absorption

Optical absorption coefficient data for InGaAs (α) were sought for two reasons. First, they were used to estimate the bandgap of ternary samples. Also, knowledge of α helps predict the performance of photodetectors and other optoelectronic devices.

While InP does not strongly absorb light in the wavelengths of interest for InGaAs, the absorption is large enough for a substrate of 400 microns thickness that removal of the InP substrate is desirable to improve the signal-to-noise ratio. For substrates used in this study, intensity reductions of up to a 2:1 factor were observed for 1500 nm light passing through the substrate. Several methods for removing the substrates were tried.

The substrates on some samples were mechanically thinned by polishing, but this proved destructive. Since HCl etches InP but not InGaAs, substrates could be selectively etched, which meant that an etch fixture was needed to support the ternary. Several ways of mounting samples to a glass slide using wax are depicted in Fig. 15. While all these methods could be made to work, there was difficulty in controlling the process, because the wax solidified very quickly when removed from the heat, and would not always completely seal all edges. Also, when hot, the wax had an extremely low surface tension, and would flow between the InGaAs layer and the glass, ruining the sample. Despite such difficulties, several early samples were etched this way, and yielded some data. After the InP substrate was entirely etched away, free-standing samples were attached by their edges to a glass

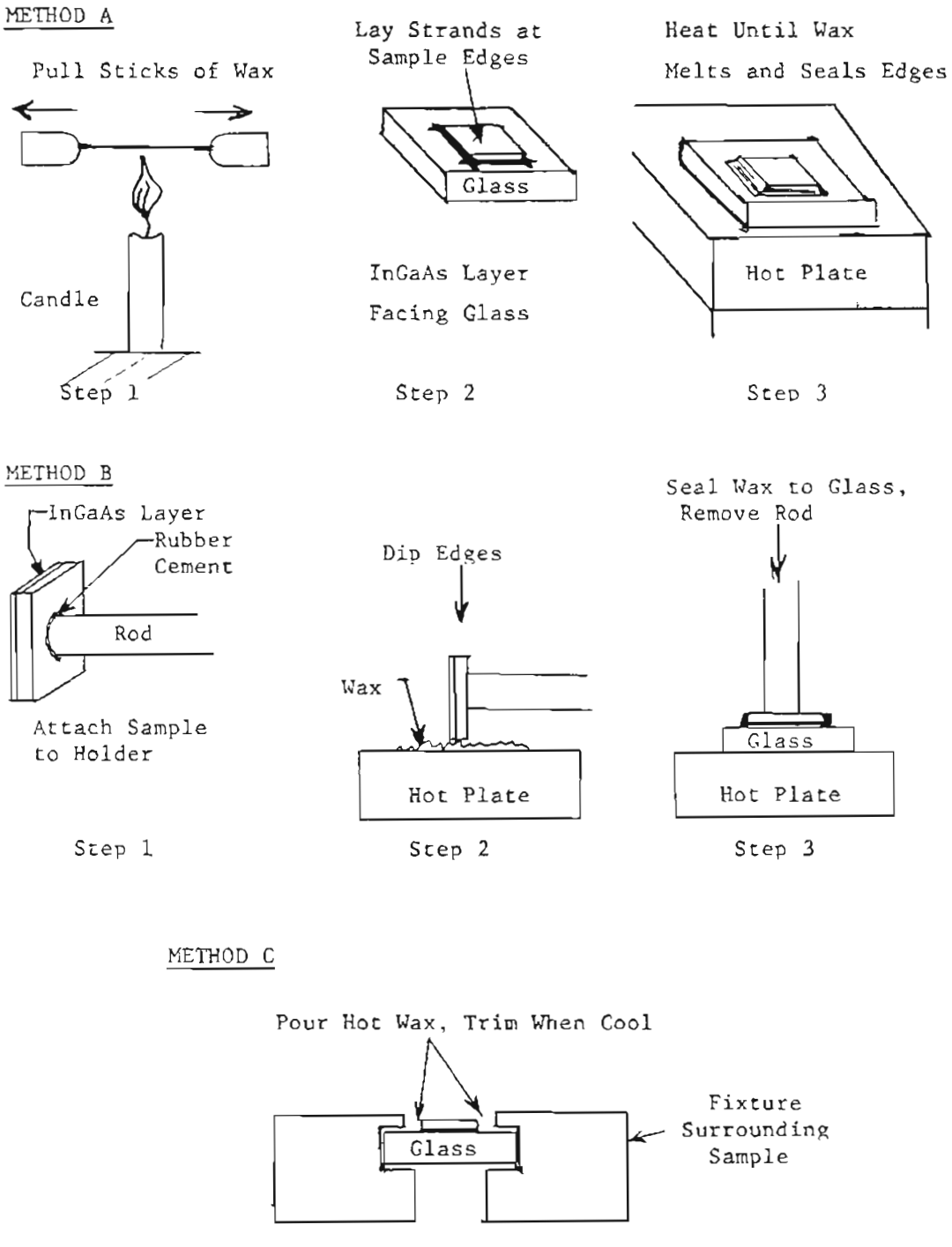

FIG. 15. Methods of Mounting Epilayers for Substrate Etching.

slide with GE #7031 varnish. However, this mounting scheme was not ideal because strain in the epilayer could cause cleavage and curling of the sample. In addition, if the InP was only partially etched, it was difficult to quantify scattering and reflection losses at the InP exit face.

The most successful sample preparation method developed involved sealing the InGaAs layer to a glass slide by means of a transparent epoxy. While the epoxy was not immune from attack by HCl, the thin layer sealing the epilayer to the glass was not attacked. So for the data presented here, unless noted otherwise, samples were prepared by epoxying to a small glass slide (6 x 10 mm), etching in 38% HCl for 1-2 hours at room temperature to fully remove the substrate, rinsing, and mounting in the cryostat with GE #7031 varnish as shown in the inset of Fig. 16.

Figure 16 also shows the optical apparatus. (See Appendix E for an equipment list.) The cryotip of the Displex refrigerator is depicted in the inset. The stability of the lamp was quite adequate for the short (about 5 min.) measurement time; it drifted no more than 1% per hour after a two hour warmup. The accuracy of the temperature measurement was $\pm$ 1 °C. As in PL, a Si filter and glass filter were employed for the 1300-1800 nm and 800-1300 nm ranges respectively. Transmission was checked on each sample at 1300 nm to ensure that consistent data were obtained using each filter. The reference aperture and sample aperture were alternately positioned within the beam such that the intensity was maximized through each. The light from

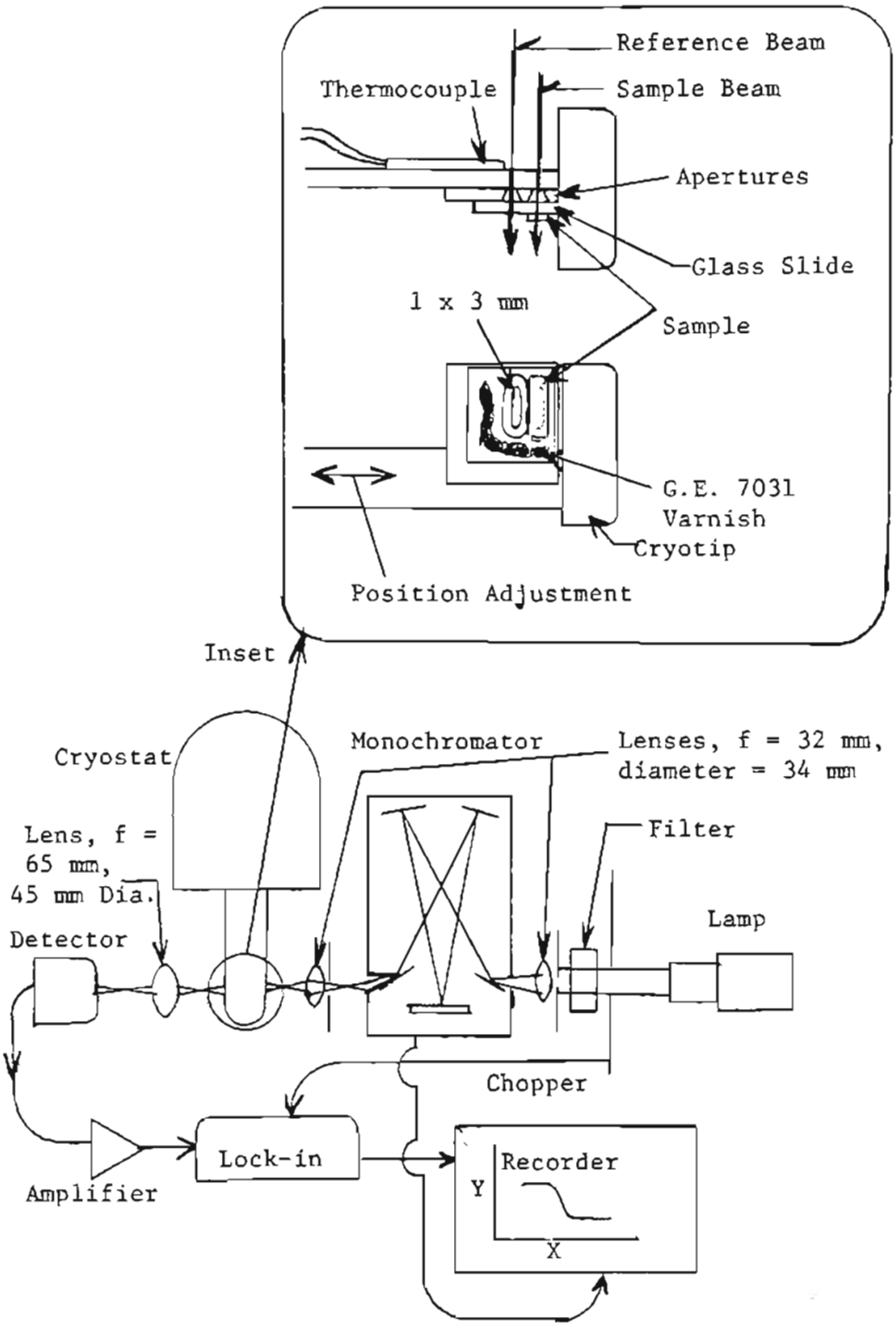

FIG. 16. Optical Absorption Apparatus.

the monochromator was imaged onto either aperture, and was in turn imaged onto an (uncooled) PbS detector. Since the two apertures were not identical in area, a scaling factor (the ratio of intensities through both apertures when open) was measured and applied to the raw transmission data. Transmission data (T) were extracted graphically at various discrete energies from the X-Y plots of intensity versus wavelength. The resolution of the monochromator was 3 nm for all measurements (0.5 mm slits).

To convert T data to absorption coefficient, knowledge of the refractive indexes of both the epoxy and InGaAs was necessary. Only two studies of InGaAs refractive index are known to the author [60,61]. The data from these, valid at 300 K, are reproduced in Fig. 17. Data from Burkhard et al [61] are used for energies above 1.2 eV, and those of Chandra et al [60] are used for energies below 0.76 eV. In the range between those energies, a smooth curve was interpolated. For calculations at 77 K and 10 K, these data were shifted to higher energy by 40 meV and 60 meV, respectively, to correspond with the variation of bandgap with temperature. (These data were measured on LPE material with the composition parameter $x = 0.47$; no estimate of variation of refractive index with changing x was attempted here.)

The index of the epoxy, n_e, was measured by comparing the transmission of 1300 nm light through a layer of epoxy sandwiched between two glass slides to the transmission through the same two slides with no epoxy. A similar measurement was made with one of the glass slides replaced by an InP substrate. A schematic of each is given in Fig 18.

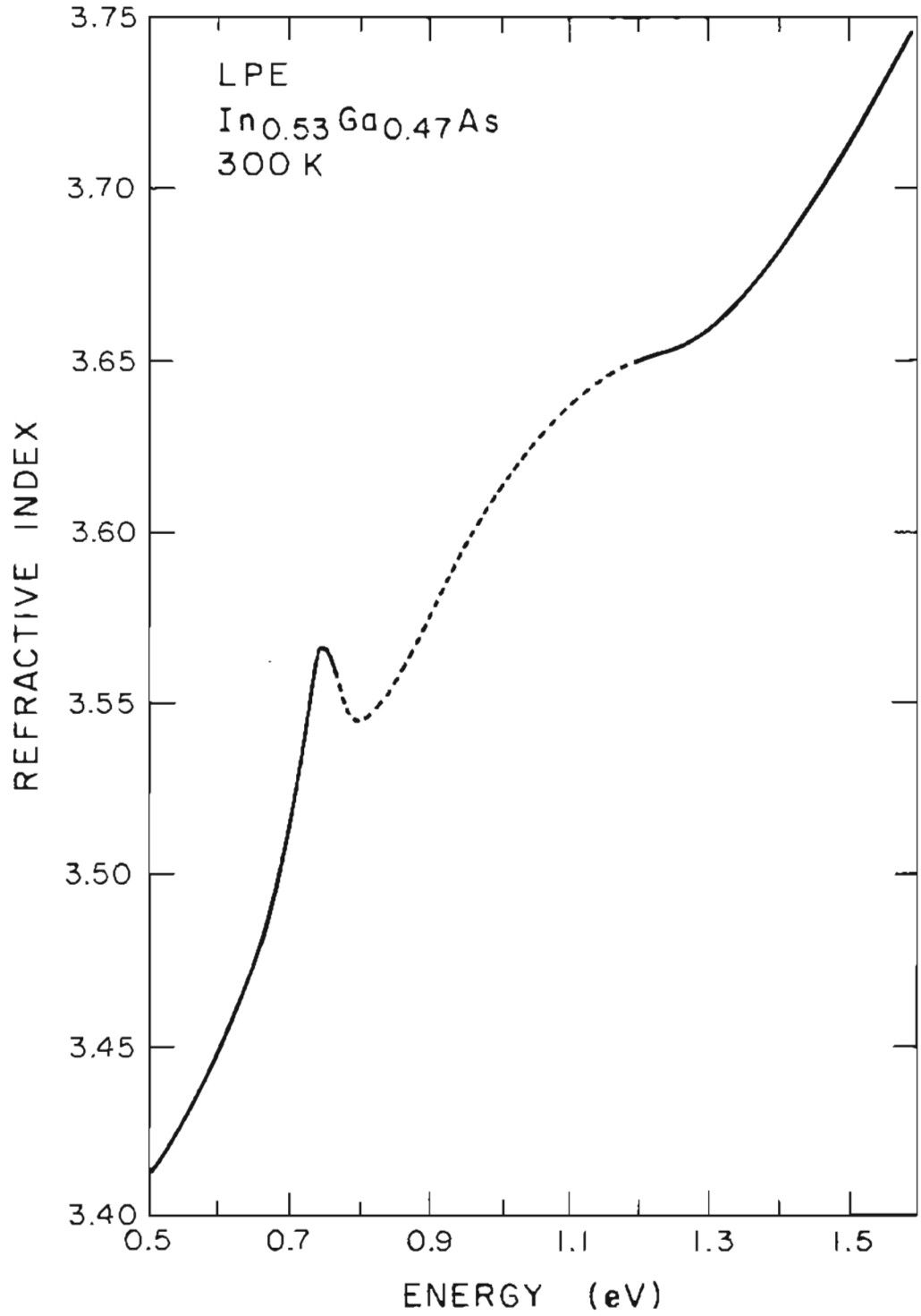

FIG. 17. InGaAs Refractive Index. Solid line below 0.76 eV is data from [60], above 1.2 eV is data from [61]. Broken line is an interpolation estimate.

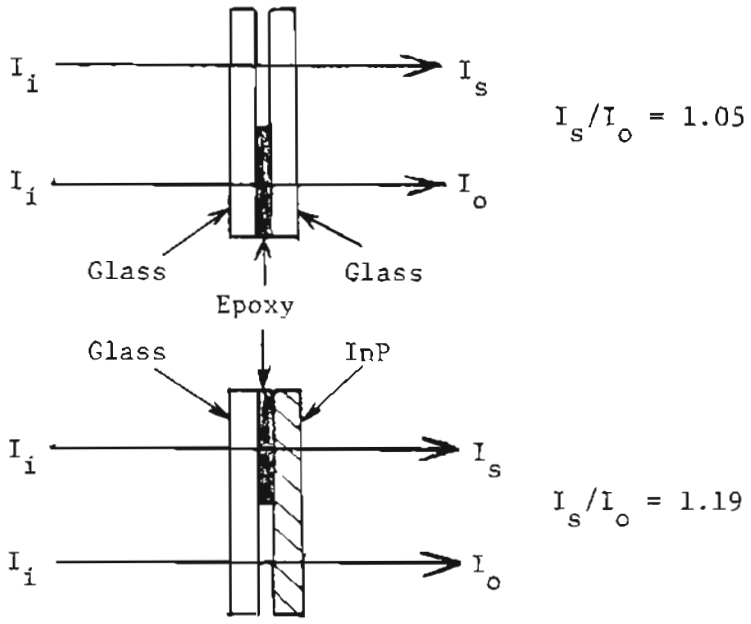

FIG. 18. Schematic for Epoxy Refractive Index Measurement.

In the first case, the ratio of intensity through the epoxy to that through the air gap was 1.05:1. Assuming that the reflectivity of each air-to-glass interface is 0.04 (i.e. a glass with $n_g = 1.5$), the reflectivity of the epoxy-to-glass interface, R_{eg} can be estimated from

$$1.05 = (1 - R_{eg})^2/(1 - 0.04)^2;$$

so that

$$R_{eg} \simeq 0.16 = (1.5 - n_e)^2/(1.5 + n_e)^2.$$

This implies that $n_e \simeq 1.2$.

In the second case, the measured intensity ratio was 1.19:1. Assuming an InP refactive index of 3.21 [61], which gives an InP-to-air reflectivity of 0.276, a slightly different expression results:

$$1.19 = \frac{(1 - R_{eg})(1 - R_{es})}{(1 - 0.04)(1 - 0.276)} \quad ,$$

where $R_{eg} = (1.5 - n_e)^2/(1.5 + n_e)^2$ and $R_{es} = (3.21 - n_e)^2/(3.21 + n_e)^2$. This expression is well satisfied if $n_e = 1.3$.

Based on these two measurements, the refractive index of the epoxy was assumed to be $n_e = 1.3$ for all temperatures. No spectral dependence of this refractive index was observed in the wavelengths of interest. The refractive index of the glass slides was assumed to be 1.5 for all temperatures.

The values of proportional error, all independent and symmetrical with regard to sign, for the various parts of the absorption coefficient measurement are given in Table IV. Combining these errors by the method of least squares gives a simplified estimate of the total

TABLE IV. Proportional Error Estimates for Optical Absorption.

parameter	proportional error (ϵ)
n_e	0.04
$n(\lambda)$	0.004
t	0.05
T	0.005
λ	0.005
S	0.005
n_g (glass)	0.004

error [62], equal to $\pm$ 6.5%. The measurement of sample thickness contains the largest contributing error; the thickness measurement technique is given in Appendix B.

To calculate the absorption coefficient (α), a formula was used from Moss [45] for transmission (T) of an absorbing layer with coherent addition of multiply-reflected components:

$$T = \frac{(1 - R_{vt})(1 - R_{et})[1 + k^2(\lambda)/n^2(\lambda)]}{S(1 - 0.04)\{[\exp(\alpha t/2) - \sqrt{R_{vt}R_{et}}\exp(-\alpha t/2)]^2 + 4\sqrt{R_{vt}R_{et}}\sin^2(\delta + \psi)\}}.$$

Here, R_{vt} = reflectivity of vacuum-to-InGaAs interface

$= [1 - n(\lambda)]^2/[1 + n(\lambda)]^2$,

$n(\lambda)$ = $In_{0.53}Ga_{0.47}As$ index of refraction, which is temperature dependent as noted above,

R_{et} = reflectivity of epoxy-to-InGaAs interface

$= [1.3 - n(\lambda)]^2/[1.3 + n(\lambda)]^2$,

$k(\lambda)$ = imaginary part of the complex refractive index, i.e. $N = n(\lambda) + ik(\lambda)$, which is temperature dependent,

S = scaling factor from transmission measurement,

λ = light wavelength,

$\delta = (2\pi t/\lambda)n(\lambda)\cos\phi$,

ϕ = angle of incidence = 0°, so $\cos\phi = 1$,

t = sample thickness,

$\psi = \arctan[2k(\lambda)/n^2(\lambda) + k^2(\lambda) - 1)]$, and finally

α = the InGaAs absorption coefficient = $4\pi k(\lambda)/\lambda$, i.e. what we are trying to measure.

This formula was derived from the Fresnel formulae for reflection and transmission coefficients at each interface, and a linear superposition of the amplitudes of reflected and transmitted electric vectors in a plane parallel plate (see e.g. [63]). Interference effects were significant in the data for thin, highly relective samples. An example of the raw data is given in Fig. 19. The intensity of light through the reference aperture (top) and sample aperture (bottom) is shown in the figure, with interference peaks on the left.

Note that even for quite large values of α, $k^2 \ll n^2$. For example, if $\lambda = 1\ \mu m$ (where $\alpha \simeq 4.6 \times 10^4\ cm^{-1}$ and $n \simeq 3.65$ at 300 K), then $k^2 = 0.134$ while $n^2 = 13.3$, two orders of magnitude larger. Note further that since $k < n$, the argument of the arctangent will always be less than unity. The series expansion $\arctan(z) = z - z^3/3 + z^5/5 -$ etc. [64] then holds, and we can safely assume:

$$\arctan[2k(\lambda)/n^2(\lambda) - 1)] \simeq 2k(\lambda)/(n^2(\lambda) - 1).$$

For example, if $\lambda = 1378$ nm, $\alpha \simeq 10^4\ cm^{-1}$, and $n = 3.58$, then $n^2 = 12.8$ and $k^2 = 0.012$. In this case, $2k/(n^2 - 1) = 0.0185798$, while $\arctan[2k/(n^2 - 1)] = 0.0185777$. Finally, note that $\cos 2z = 1 - \sin^2 z$, so our formula can be simplified to:

$$T = \frac{(1 - R_{vt})(1 - R_{et})}{0.96S\left[e^{\alpha t} + R_{vt}R_{et}e^{-\alpha t} - 2\sqrt{R_{vt}R_{et}}\cos\left(\frac{4\pi nt}{\lambda} + \frac{\alpha\lambda}{\pi(n^2 - 1)}\right)\right]}.$$

Since this formula could not be solved uniquely for α in terms of T and λ, a computer program was written which allowed for trials of α iteratively matched to measured T values to three significant digits.

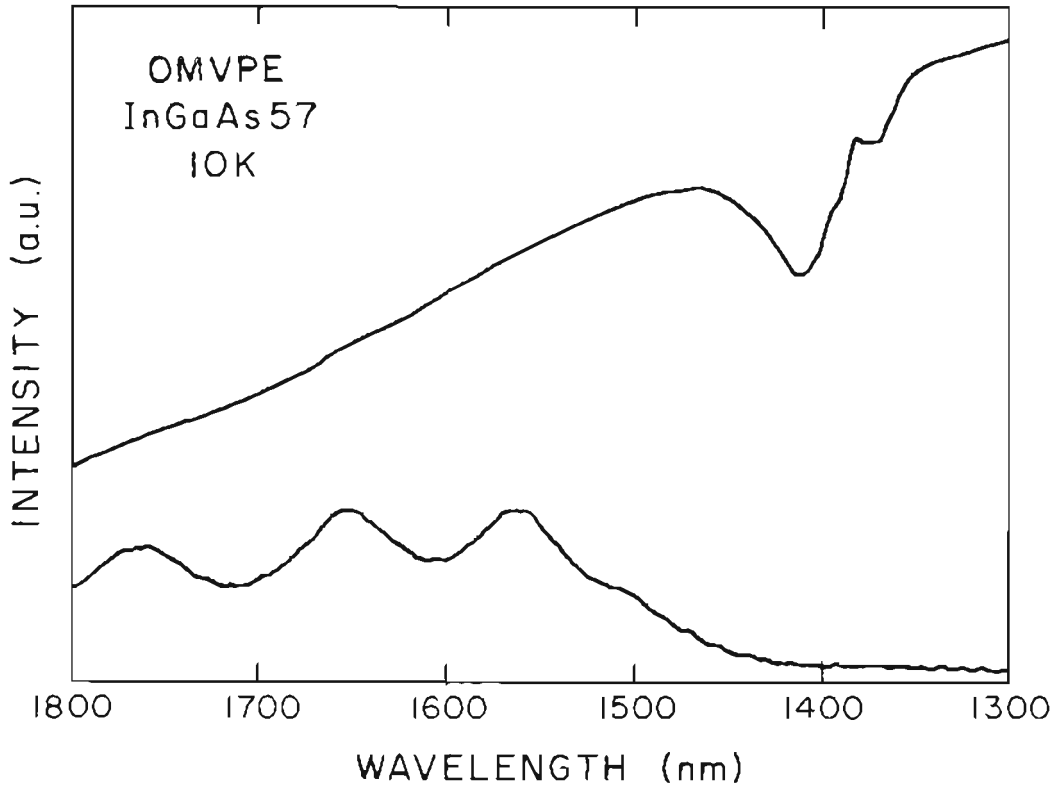

FIG. 19. Raw Transmission Data for Optical Absorption. Top curve, light through reference aperture; bottom curve, light through sample aperture.

This program is given in Appendix F.

The author has despaired in his search for an accurate method of determining bandgaps from absorption data. There are a variety of methods in the literature, including taking the "midpoint" in the rise of %T [65]. Some authors ignore exciton effects and extrapolate α^2 versus $h\nu$ to zero, and ascribe the resultant energy to the bandgap [25,66,67]. Others include the exciton effects, and fit Elliot's theory [68] to their data [59,69]. A number of assumptions are required, and so a variety of "bandgaps" can be fitted to the data. For this study, I decided not to take time for the computation involved in accurately fitting absorption data to Elliott's theory, choosing instead a graphical technique.

The bandgap of samples in this study was assumed to be somewhat higher in energy than the energy at which the absorption begins to fall off rapidly. This point was typically found by extrapolating two straight lines fitted to above-bandgap and below-bandgap absorption to their intersection at the "knee". When experimental technique improved and the below-bandgap absorption was nearly a vertical line, the bandgap was assumed to be 5 meV higher in energy than this point. (The appearance of strong exciton peaks would have made bandgap determination easier.) The accuracy of this method is estimated at $\pm$ 5 meV.

CHAPTER IV

SUBSTRATE AND UNDOPED EPILAYER CHARACTERIZATION RESULTS

A. GaAs and InP Substrates

The effect of substrate impurities and defects on OMVPE epilayers is a fascinating and useful topic of research [70], but is beyond the scope of this study. However, PL characterization of the substrates used here was useful as a benchmark for comparison to epilayer results. This section presents the substrate PL data. Table V lists the substrates along with information provided by the manufacturer. SIMS analysis was done for the semi-insulating InP:Fe substrate; these data are discussed in conjunction with InGaAs analysis in Chapter VI.

PL spectra at 77 K are presented in three figures: Fig. 20, GaAs substrates; Fig. 21, n-type InP substrates; and Fig. 22, p-type InP substrates. Weak PL was observed for some substrates at 300 K. No PL was observed for the semi-insulating InP substrate. For these three figures, no peak height correction for detector spectral response was employed.

Detection of PL proved more difficult for GaAs than for InP. Casey and Buehler [71] reported that InP is 100 times more efficient as a luminescent emitter because the surface recombination velocity is 100 times smaller than that of GaAs. The luminescence from the semi-insulating GaAs substrate in Fig. 20 is near the limit of reliable detection for this PL system. The 31 meV shift of luminescence to lower energy in the Zn-doped GaAs substrate corresponds to the well known binding

TABLE V. Substrates and OMVPE Growth Numbering.

Material & Orientation[a]	Manufacturer & Wafer #	Resistivity (Ω cm)	n or p (cm^{-3})	OGC usage[b]
GaAs (100) $\pm$ 0.25°	Spectrum Tech. 13252	10^7	...	GaAs 10-29, 31-62 InGaAs 2, 4-11
GaAs:Zn (100) $\xrightarrow{2°}$ (110)	Crystal Spec. E2652	0.0025	10^{18}	GaAs 2-9, 30 InGaAs 3
InP:Fe (100) $\xrightarrow{2°}$ (110)	ICI Americas R1163	10^6	...	InP 37, 39-47 InGaAs 50-6, 65-7
InP (100)	Atomergic H1667	0.20	10^{16}	InP 19-26, 32-4 InGaAs 20-3
InP:S (100)	Atomergic H1668	0.001	10^{18}	InP 17-8 InGaAs 3-7, 24, 31-6
InP:S (100) $\xrightarrow{2°}$ (110)	Sumitomo 506216	0.0005	10^{19}	InP 27-31 InGaAs 25-30, 37-46, 48-9, 57-64, 68-9
InP:Zn (100)	Atomergic H1669	...	10^{17}	InP 1-16 InGaAs 1-2
InP:Zn (100)	Atomergic I1662	...	10^{17}	InP 35-6, 38 InGaAs 47

[a] All substrates were polished by the manufacturer.

[b] Of the first 18 InGaAs layers grown, 7 were on InP substrates and 11 were on GaAs substrates, both numbering sequences starting with "InGaAs 1". Growth numbers begining with InGaAs 20 are unique and represent layers grown on InP.

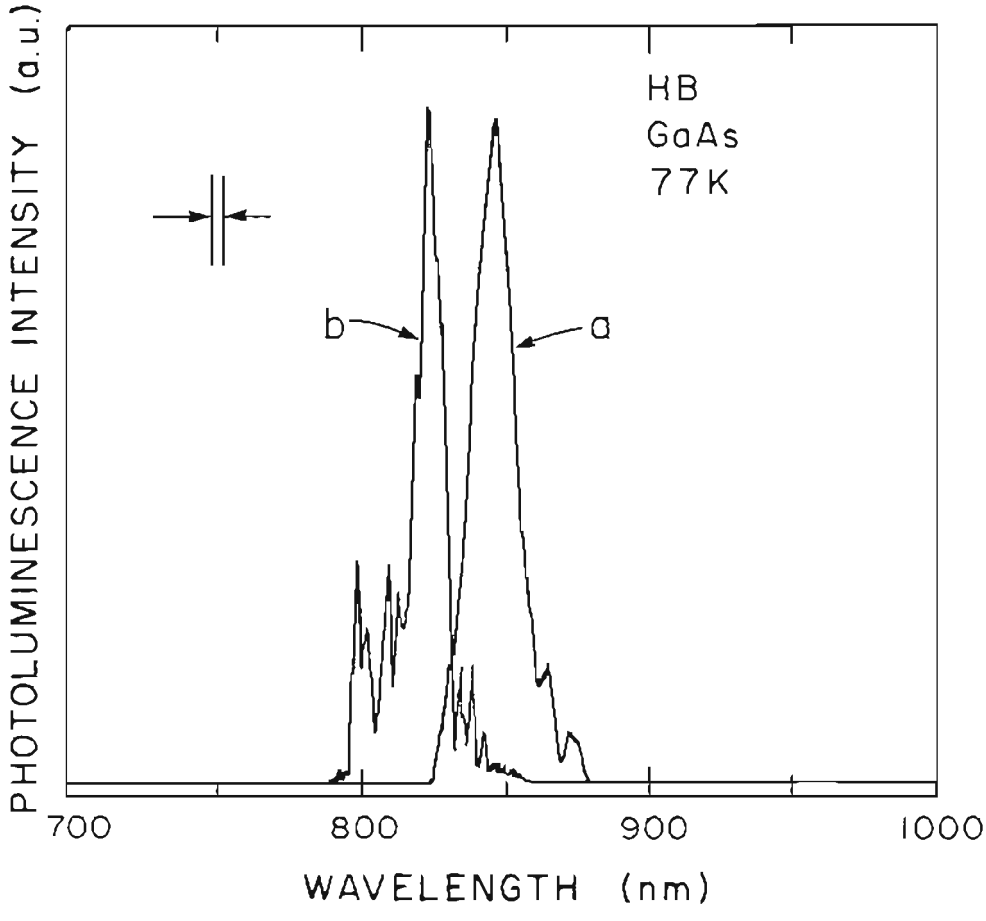

FIG. 20. PL for GaAs Substrates. a) GaAs:Zn, Crystal Specialties #E2652, b) semi-insulating GaAs, Spectrum Technology #13252.

energy of the Zn acceptor [72]. No deep-level emission was observed in these substrates.

Two peaks were observed in the n-type InP substrate #H1667 (sold as "undoped"), marked as curve (a) in Fig. 21. These were the band-to-band emission at 1.40 eV, and emission presumed to be donor-to-acceptor (or donor-to-band) at 1.37 eV. This latter emission has not been clearly identified.

With the moderately sulfur-doped substrate #H1668 (see curve (b) of Fig. 21), the emission FWHM broadened considerably (to 40 meV), and was centered at 1.39 eV. The Burstein shift is clearly seen in curve (c) of Fig. 21 for the highly doped n-type substrate #506216, with the peak now located higher in energy at 1.48 eV, and with a very broad FWHM of 150 meV. These spectra are quite similar to those reported elsewhere for n-type InP [73].

The two p-type InP:Zn substrates used in this study demonstrated the variation possible from a single manufacturer. Figure 22 does not represent high resolution data, but several peaks are seen in each substrate. Both have band-to-band emission near 1.40 eV and what is probably band-to-acceptor (Zn) emission at 1.36 eV [50]. Substrate #I1662 also has peaks resolvable at 1.33 eV and 1.29 eV. The origin of these emission lines was not investigated. Substrate #H1669 has broad emission at about 1.0 eV. Luminescence in this energy range is often attributed to phosphorus vacancies [74,75], but quite likely involves a defect complex. See Chapter V for a more detailed discussion of possible sources of this emission.

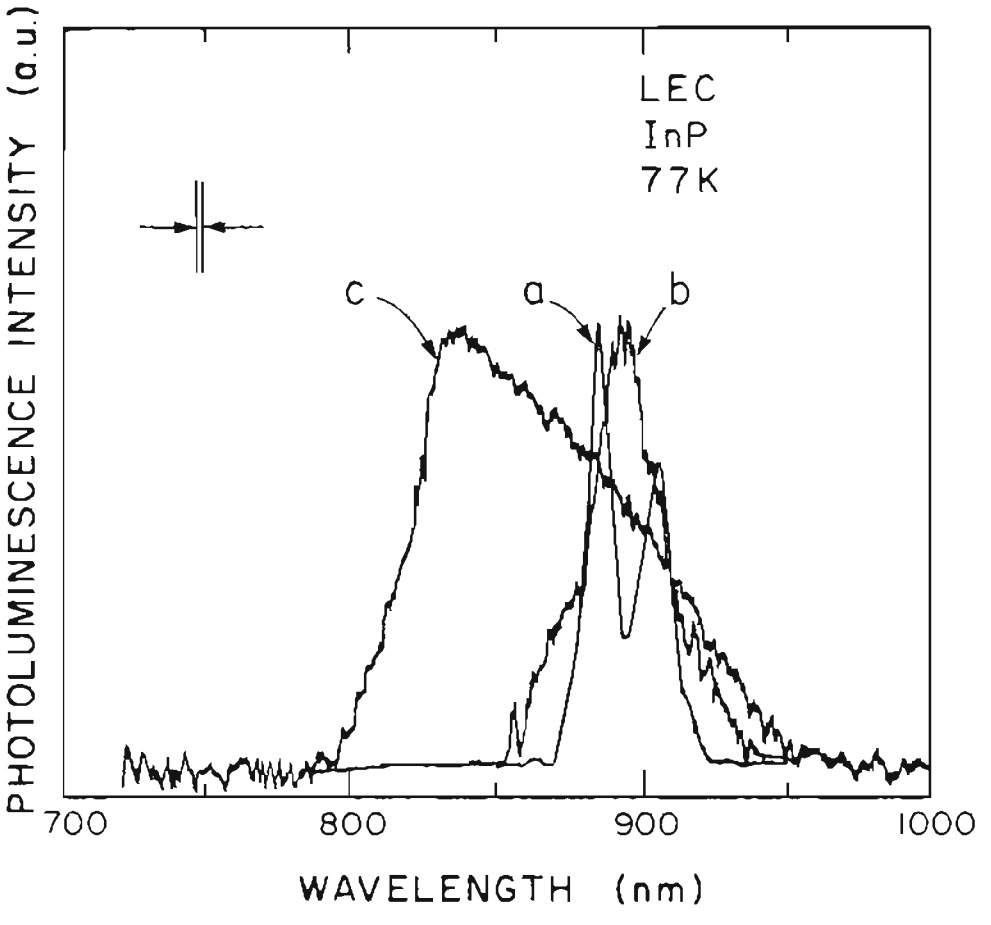

FIG. 21. PL for N-type InP Substrates. a) InP, Atomergic #H1667, b) InP:S, Atomergic #H1668, $N_D - N_A \simeq 10^{18}$ cm^{-3}, c) InP:S, Sumitomo #506216, $N_D - N_A \simeq 10^{19}$ cm^{-3}.

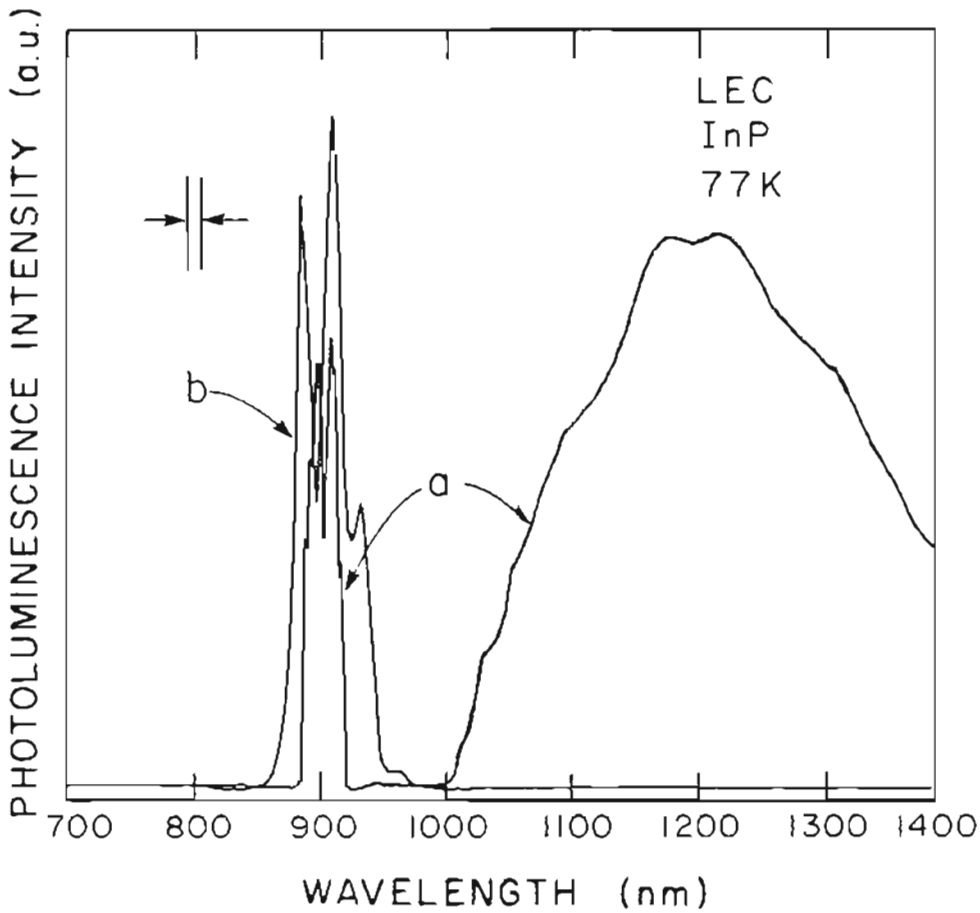

FIG. 22. PL for P-type InP Substrates. a) InP:Zn, Atomergic #H1669, b) InP:Zn, Atomergic #1662.

B. GaAs and InP Undoped Epilayers

Most of the growth parameters necessary for successful operation of the reactor were worked out by growing GaAs prior to attempting growth of In-containing compounds. Undoped InP data are also reported here. (These represent the characteristics of buffer layers used for later InGaAs epilayers.) There is a considerable body of literature regarding growth and characterization of these binary compounds, and so ample opportunity exists to evaluate the OGC reactor.

One important growth parameter was reactor geometry. As delivered, the reactor had a 55 mm diameter growth tube, which was used for all samples prior to GaAs 45, InP 26, and InGaAs 24 (i.e. through 7/21/86). A rectangular quartz insert, 2.4 x 4 cm, was used for subsequent samples. The insert provided three advantages: 1) near-laminar gas flow over the rectangular susceptor [76], 2) higher gas flow velocities for a given flow rate (more efficient gas usage), and 3) was much easier to clean than the outer tube (because disassembly of the end caps was not required). The morphology of samples grown with the rectangular insert was noticeably better than that of previous samples. Also, the data in Table VI suggest that improved crystal structure and purity result with higher gas velocity over the substrate. These InP epilayers were grown in the large round tube with H_2 flow rate as the principal variable, although the TMIn mole fraction did vary to a minor degree. Most samples grown subsequently in the rectangular insert benefited from a higher flow velocity than those in Table VI, even though the H_2 input flow rate was less.

TABLE VI. Hall Mobility and Resistivity for OMVPE InP with Various Total Gas Flow Rates.

InP sample #	[TMIn] x 10^{-5}	H_2 flow rate (l/min.)	μ_{H_2} (300 K) (cm^2/Vs)	ρ (300 K) (Ω cm)
6	2.3	5	1600	0.071
5	1.9	6	2550	0.048
13	2.8	8	4820	0.54

A second subject of concern was the gas supply purity. Hydrogen gas cylinders require frequent change, and initially were not fitted with a regulater evacuation port or N_2 purge line, as was built into the toxic gas sources. There was a suspicion, based on morphology observations and Hall mobility data, that immediately after changing the H_2 cylinder, the growth was poor due to the atmospheric gases introduced during the change (despite the presence of the H_2 purifier in-line). For example, GaAs 11 and 12 were grown under similar conditions (listed below), but the H_2 tank was changed prior to GaAs 12. Room temperature Hall mobility for GaAs 11 was 4050 cm^2/Vs but only 3300 cm^2Vs for GaAs 12. As a further example, the H_2 tank was changed just prior to growth of InP 1; the room temperature Hall mobility for this sample was 1980 cm^2/Vs. InP 2 was grown with the same parameters (T = 600 °C, $[PH_3]/[TMIn]$ = 80, 5 1/min. H_2, and [9.12 x 10^{-5}] of TMIn), but the mobility increased to 2660 cm^2/Vs.

Immediately after a vacuum exhaust port was added to the H_2 regulator line and the H_2 cylinder changed, InP 13 was grown yielding a mobility of 4820 cm^2/Vs. Sample numbers begining with GaAs 35, InP 13,

and InGaAs 12 were grown with hydrogen installed using the vacuum exhaust. That is, after installing a new cylinder, the regulator was A) evacuated, B) purged with H_2 through a separate vent, then steps A) and B) were repeated for at least three cycles before connecting the new cylinder to the reactor.

The purity of process nitrogen was also a concern. Two types are listed in Appendix E, with the relative amounts of O_2 and H_2O in each. Table VII shows the average Hall mobility and carrier concentration for three groups of GaAs samples. The middle group was grown during the time when low purity nitrogen was used for purging the reactor. Since N_2 was not used directly in the growth process, it was hoped that the

TABLE VII. Hall Mobility for OMVPE GaAs.

N_2 grade	GaAs sample #	n (cm^{-3})	Hall mobility[a] (cm^2/Vs) 300 K	77 K	PL FWHM (meV)
UPC	1 to 39	7×10^{16}	2710	6290	18
low purity	40 to 52	...	118	380	22[b]
low purity	53[c]	8×10^{14}	6480	37,700	...
UPC	54 to 62	8×10^{14}	4860	70,500	13

[a]Data shown are the averages of about half of the samples in each group and represent all data taken.

[b]No PL was measurable on GaAs 48, GaAs 50, and GaAs 51.

[c]Growth conditions were: T = 700°C, $[AsH_3]/[TMGa] = 52$, 2 l/min. H_2, and $[2.95 \times 10^{-4}]$ of TMGa.

lower purity type would be acceptable. (High purity N_2 was ten times as as expensive as the low purity type.) The data do not allow a clear decision to be made on this, because the low purity N_2 was tried during the same time period that the rectangular insert was being introduced. While cleaning the round outer tube just prior to the growth of GaAs 53, it was discovered that the O-rings which seal this tube to the end caps were not tightly sealed. This allowed atmospheric gases into the reactor during growth for samples prior to GaAs 53. While the bulk of the improvement in samples after GaAs 53 may have been due to a good reactor seal, the use of high purity N_2 was continued as a precaution.

The hydride sources were also a concern. The arsine and phosphine used initially were from Air Products. These were replaced with gas from Phoenix Research because the latter vendor was reputed in the industry to produce high purity gases. The Phoenix Research arsine was used after GaAs 34 and InGaAs 11; the new phosphine was used after InP 40 and InGaAs 66. PL at 77 K for GaAs 11 gave a FWHM of 20 meV, while that of GaAs 36 (new arsine) was 15 meV. Both samples were grown at 700 °C in 4-5 1/min. of H_2, with $[AsH_3]/[TMGa] = 20$. Regarding the phosphine, 77 K PL for InP 40 gave a FWHM of 15 meV, while that of InP 46 (new phosphine) was 10 meV. (Note that the growth conditions of these were the same--see Table I--except that 2 1/min. of UPC N_2 was used in growing InP 46.)

Because the best binary material was grown after changing to the new sources, it was concluded that Phoenix Research hydrides give the

potential of growing high purity material. They do not assure such growth; too many other parameters were varied in this study to quantify the improvement. Samples were grown over a period of a year and a half, and there were the inevitable variations in reactor cleanliness and substrate material. Also, a general improvement in gas line cleanliness is to be expected over time, and so any conclusions drawn from samples grown weeks apart must be qualified by acknowledging this.

Through the course of this work, continuing reduction in particulate contamination on or in the epilayers was sought and achieved. After GaAs 34, InP 6, and InGaAs 11, all pre-growth etching was done in a clean filtered air hood. The samples were taken to and from the reactor glove box in a covered glass dish, and were kept covered as much as possible in the glove box. Use of the rectangular insert reduced particles, mainly because during loading, the substrate was contained in the center of the newly cleaned insert. (With the round tube, particles from the tube walls fell on the substrate during loading.) A similar improvement was seen during unloading, when the entire insert was removed from the outer tube, allowing the sample to be removed from the insert without significant motion, vibration, or air movement.

The expected direct proportional relationship between growth rate and group III alkyl partial pressure [5] was observed early in the GaAs characterization phase, as can be seen in Fig. 23. The range of growth rates seen in this study was 0.01 to 0.1 μm/min. for GaAs. Growth conditions were kept relatively constant for InP layers; the typical growth

rate for this material was 0.05 μm/min. All undoped epilayers were n-type. No attempt was made to grow p-type material using low (below 10:1) [V]/[III] ratios. No extensive effort was made to optimize the [V]/[III] ratio or growth temperature for the binary compounds. The typical literature values [5,77] of [V]/[III] ≈ 20-50 and T ≈ 650-700 °C seemed to be good for GaAs growth. InP required a higher [V]/[III] ratio to compensate for P_2 evaporation (mentioned in Chapter II). See Table I for typical InP growth conditions.

Good morphology was generally obtained, as observed visually and microscopically. Morphology improved whenever the outer round growth tube was cleaned. Pinholes of varying density were observed, but the better crystals were specular. Occasionally, swirl patterns or polycrystalline areas could be seen on inferior samples, due to poor etching/rinsing or contamination in the growth tube.

With the improvements in growth procedures and gas source purity noted above, GaAs epilayers could routinely be grown with properties approaching those of very pure material. The Hall mobility versus temperature data for two OGC samples are plotted in Fig. 24, along with a well-known high purity sample for comparison. The limits of mobility due to polar scattering, deformation potential, and ionized impurity scattering are noted [78]. The upper dashed line for the ionized impurity mobility limit corresponds to an impurity concentration of 5×10^{13} cm^{-3}, while the lower one represents 5×10^{14} cm^{-3}. Typical of early samples, GaAs 7 (T = 670 °C, 4 l/min. H_2, $[AsH_3]/[TMGa] = 20$, $[1.25 \times 10^{-2}]$ of TMGa) had a low mobility ($n = 8 \times 10^{16}$ cm^{-3}). However,

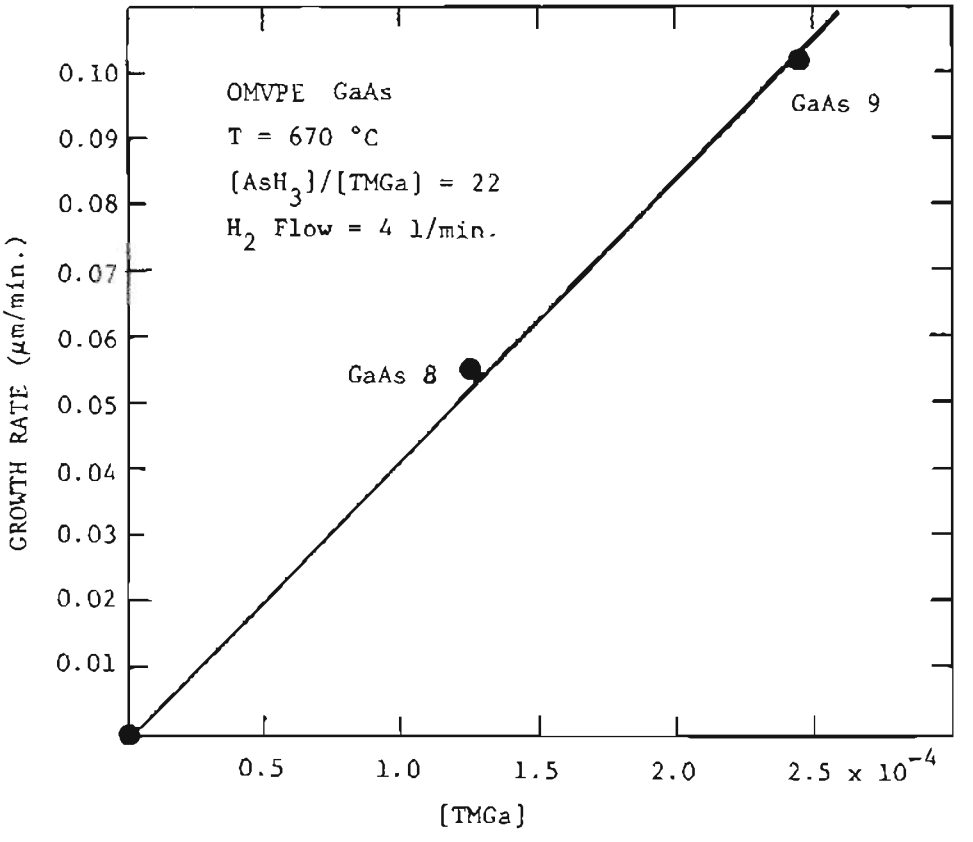

FIG. 23. OMVPE GaAs Growth Rate.

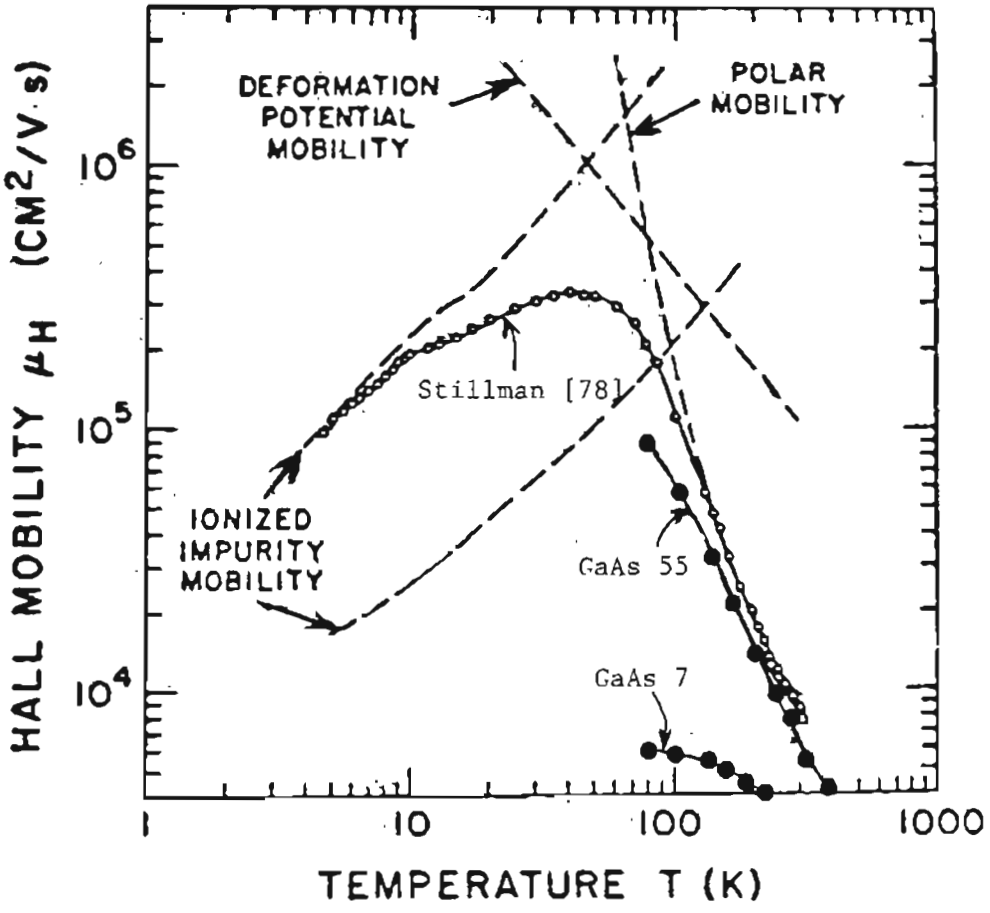

FIG. 24. Hall Mobility for GaAs at Cryogenic Temperatures.

GaAs 55 (T = 640 °C, 4 l/min. H_2, $[AsH_3]/[TMGa]$ = 20, $[1.5 \times 10^{-4}]$ of TMGa, with the benefit of a cleaner growth tube, H_2 line and arsine source) achieved a 77 K Hall mobility of nearly 10^5 cm^2/Vs. This was the typical mobility behavior for later GaAs samples, as can be seen in Table VII.

Resistivity values were calculated for 25 GaAs epilayers, the number of samples for which thickness was measured. Resistivity did not depend critically on growth conditions for the first 40 growths. The average resistivity of these samples was 0.0224 Ωcm at room temperature, ranging from 0.007 to 0.03 Ωcm. (The average at 77 K was 0.0169 Ωcm, ranging from 0.004 to 0.02 Ωcm.) GaAs 53 had 0.15 Ωcm and 0.02 Ωcm resistivities at 300 K and 77 K respectively. The best quality GaAs epilayers, GaAs 54-62, averaged 3 Ωcm at room temperature (the range was 1-6 Ωcm at 300 K, and 0.08-0.4 Ωcm at 77 K).

A comparison of Hall mobility and carrier concentration for InP epilayers grown at OGC and elsewhere is presented in Table VIII. (Resistivity data are also given for the OGC samples.) Thirty-eight undoped InP layers were intermittently grown over many months, and were of less consistent quality than GaAs layers. (InP 18-25 were p-type and are discussed in Chapter V.) The best of the early samples was InP 13. The last batch, InP 42-5, were uniform and generally an improvement over earlier samples and comparable to recent literature reports [28,31, 34,40]. (The highest reported mobilities [79,80] are often not repeatable [81].) The room temperature mobility values for InP 32-40 were the same as for later samples. However, the liquid nitrogen mobility was

TABLE VIII. Undoped OMVPE InP Electrical Characterization Results.

Sample # or reference	Hall mobility (cm^2/Vs) 300 K	77 K	Resistivity (cm^2/Vs) 300 K	77 K	n (cm^{-3})
[40]	4260	29,800	...	...	2×10^{15}
[41]	5000	70,000	...	...	8×10^{14}
[28]	3400	28,500	...	...	...
[31]	3660	...	...	...	2×10^{16}
[34]	3670	...	...	...	...
OGC:					
InP 13	4820	13,100	0.54	0.60	2×10^{15}
InP 32-40[a]	2150	5220	0.20	0.10	1×10^{16}
InP 42-5[a]	2100	10,000	0.30	0.10	7×10^{15}

[a]All data are averages of the numbered samples.

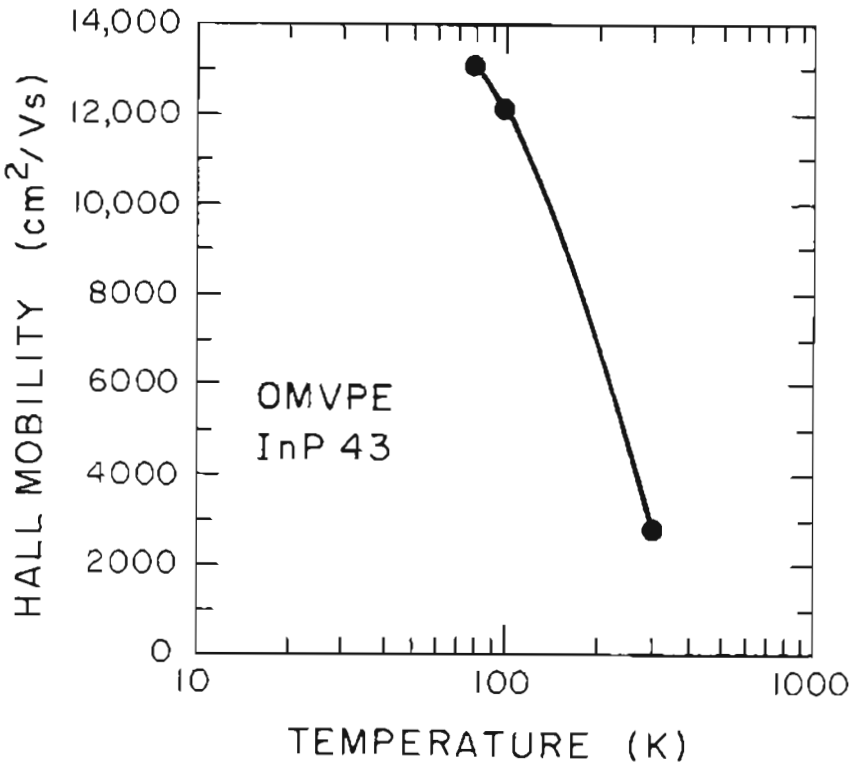

FIG. 25. Hall mobility for OMVPE InP.

about half, probably due to the inferior phosphine source.

InP 43, in Fig. 25, shows the expected Hall mobility for ionized impurity scattering with $n = 8 \times 10^{15}$ cm^{-3} [82]. The TMIn source is presumed to contribute most of the impurities [40,83]. The InP substrates etched and rinsed more slowly than GaAs substrates, and the InP substrates themselves were probably less pure than the GaAs ones. It was disappointing, yet not unexpected, that growth of high quality InP did not come as easily as it did for GaAs.

As the OGC crystal growth "learning curve" progressed, PL data showed improvements for both GaAs and InP. Shown in Fig. 26 are data from GaAs 11 and GaAs 61. These samples were grown under similar conditions, except for temperature (GaAs 11: T = 755 °C, GaAs 61: T =

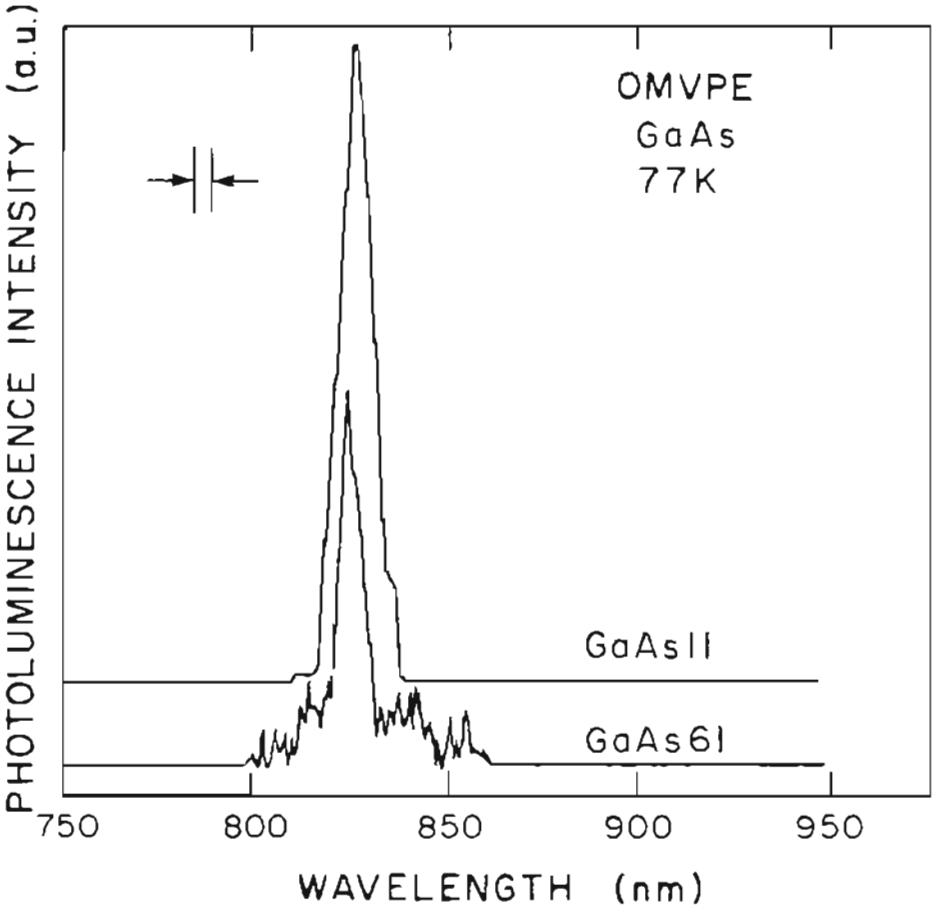

FIG. 26. PL for OMVPE GaAs.

640 °C). The emission FWHM for GaAs 61 is significantly less than that of GaAs 11. GaAs 61 also had very good Hall mobility: 5090 and corporation of carbon at lower growth temperatures should be considered in comparing these samples [84], it seems clear that the material quality is improved over early samples. The intensity of emission is comparable in these samples. The peaks are centered at 1.501 eV, which corresponds closely to the reported bandgap of GaAs at 77 K, 1.5076 [85].

Growth parameters for InP 6 and InP 46 were given in Tables VI and I respectively. Figure 27 gives the 77 K PL data for these two samples. Again, the intensity is comparable, and the FWHM difference is quite clear, 16 vs. 10 meV. The peaks are centered at 1.407 eV (InP 46) and 1.404 eV (InP 6), acceptably close to the reported liquid nitrogen temperature bandgap value of 1.4046 eV [57]. A variety of references are available which discuss the photoluminescence of InP at various temperatures. The classic references are [49,50,73,86]. More recent data from a variety of growth techniques are contained in [71,72,74-7]. The effects of heat and surface treatments are discussed in [87-90]. Recently, there has been interest in Si-implanted InP for FETs [91,92]. Good general references for the growth and characterization of InP are [93,94,95].

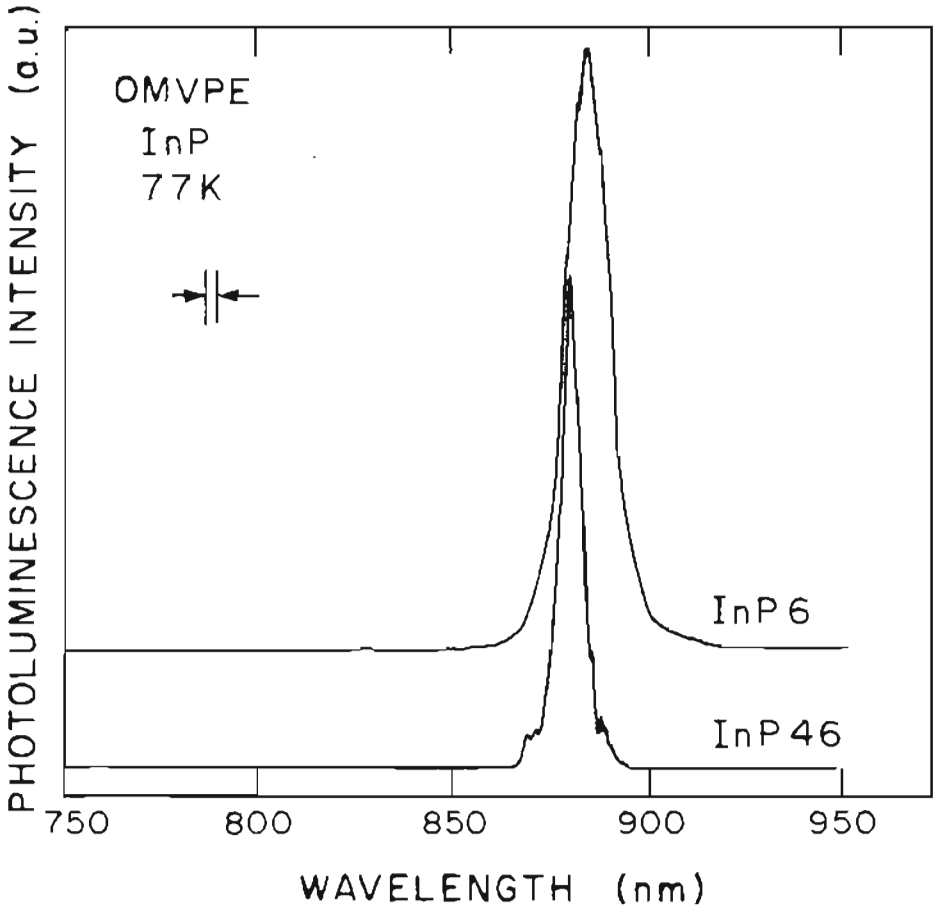

FIG. 27. PL for Undoped OMVPE InP.

CHAPTER V

InP:Mg EPILAYERS

As a prelude to the growth of the InGaAs ternary, a number of p-type layers were grown onto InP substrates. There was more than one reason for this approach. First, it was desirable to have a well-established capability for the growth of p-type buffer layers. Secondly, information about reliable procedures for p-type doping of InP epilayers is far from plentiful. That is particularly the case for the Mg-doped regime described in this chapter. Much of the material here has now been provided in published form [96].

In considering the possible elements for providing shallow acceptors as a p-type dopant in InP, it may be noted that zinc has often been used, but is undesirable in applications where its high diffusivity can adversely affect device performance. Magnesium, in the form Mg_{In}, also provides a shallow monovalent acceptor in this semiconductor, and has been reported as being much less mobile than zinc [97]. However, even the OMVPE literature on magnesium doping of GaAs is scanty [98,99]. Reported here is a photoluminescence study of OMVPE InP:Mg over a wide doping range.

This work has demonstrated that, in addition to the expected role of Mg_{In} as a shallow acceptor, magnesium at higher doping concentrations forms complexes with deep-level flaws. The data here can be compared to PL data for bulk InP:Mg [100-2], Mg-implanted InP [103], and

molecular beam epitaxial InP:Mg [100].

Table IX gives the growth parameters for five samples. Growth rates for Mg-doped samples of 3 or 6 microns per hour were achieved, depending on the TMIn mole fraction. The morphology was generally good, nearly on a par with the best GaAs grown at OGC. During PL testing, the surface was scanned to demonstrate qualitative uniformity.

Figure 28 exemplifies PL results for four of the five InP:Mg samples of Table IX, and an undoped reference sample. Net acceptor concentrations were derived from the reported correlation with PL peak width [46] (see Chapter III). Figure 29 shows a log-log plot of the net acceptor concentration achieved in these samples as a function of the Cp_2Mg input flux, and the solid line is a least squares fit to the data. The broken line reproduces data from Cp_2Mg incorporation in the adduct OMVPE technique, assuming a "typical" molar flow of 6×10^{-5} mole/min. [97]. Our power-law slope of 1.82 is similar to the slope of 1.85 in the Nelson and Westbrook work. Such a slope is indicative of a near-quadratic dependence of Mg incorporation on $[Cp_2Mg]/[TMIn]$ ratio, rather than on Cp_2Mg molar flow alone. The mechanism of incorporation from the gas phase into the crystal is not postulated here, see e.g. [97,104].

The band-to-band peak at 1.41 is observed in Fig. 26 for all but the most highly doped sample. Band-to-band transitions were the only emissions observed in undoped material, but became less significant as the Mg acceptor concentration was increased. A peak at 1.37 eV was seen in all Mg-doped samples, resulting from conduction band and/or

TABLE IX. Growth Conditions and PL FWHM for OMVPE InP:Mg.

InP:Mg Sample #	Mole Fractions TMIn	Cp_2Mg	PL FWHM (meV)
InP 19	4.1×10^{-5}	1.2×10^{-8}	15
InP 23	8.3×10^{-5}	4.6×10^{-8}	17
InP 20	4.1×10^{-5}	3.2×10^{-8}	22
InP 25	8.3×10^{-5}	2.3×10^{-7}	25
InP 24	8.3×10^{-5}	4.6×10^{-7}	72

Growth temperature 600 °C, $[PH_3]/[TMIn] = 80$, 8 l/min. H_2 in the 55 mm diameter growth tube.

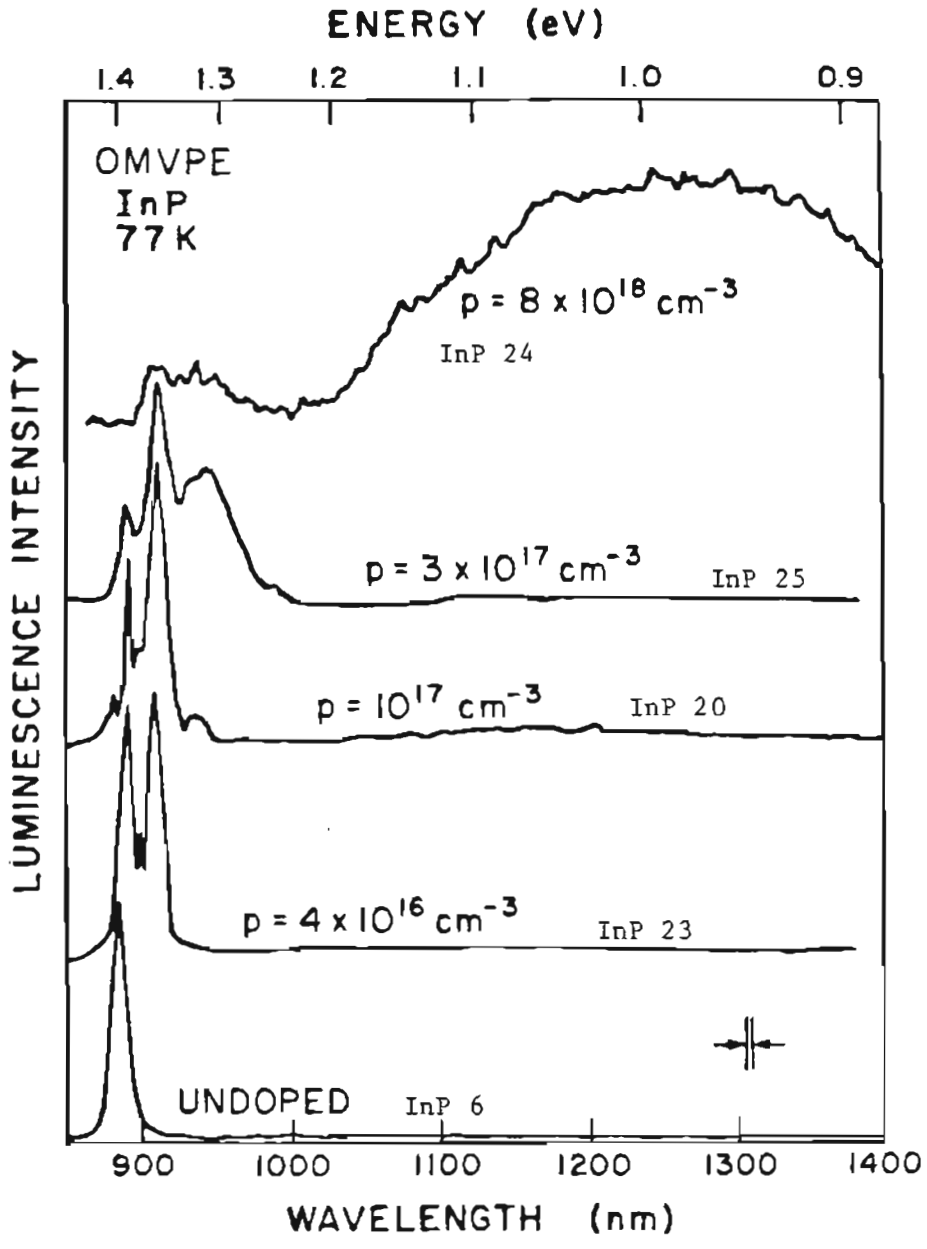

FIG. 28. PL for OMVPE InP:Mg.

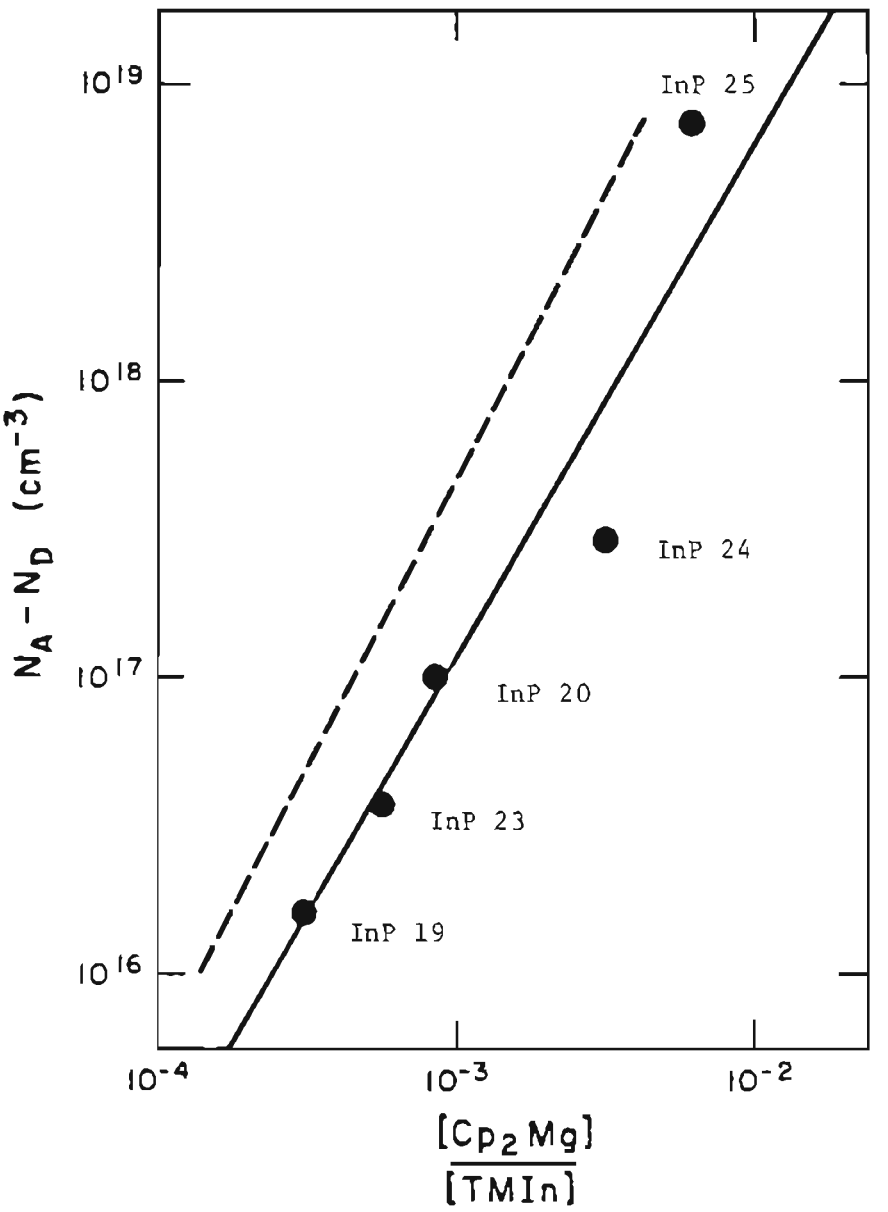

FIG. 29. Net Acceptor Concentration in InP:Mg versus $[Cp_2Mg]/[TMIn]$ Ratio. Solid line, this study; broken line, data from [97].

shallow acceptor transitions. The FWHM of this peak is given in Table IX for each sample. The Mg-doped samples were confirmed as p-type by the polarity of thermoelectric power, whereas "undoped" control samples were weakly n-type. The lowest net acceptor concentration we obtained was 2×10^{16} cm^{-3}, and no minimum p-type threshold (as reported by Nelson and Westbrook [97]) was observed.

There was a shift in the emission as acceptor concentration was increased. For Mg doping exceeding 10^{17} cm^{-3}, a peak at 1.30 eV was observed. Moreover, a broad additional PL band appeared centered near 1.0 eV, becoming dominant for the highest doped sample. An explanation for the 1.30 eV emission might be found by comparison to reports of emission at this energy (at 77 K) from ion-implanted InP:Mg [103], MBE-grown InP:Mg [100], as well as OMVPE-grown InP:Cd [105]. In the latter reference, the intensity of laser excitation was varied, and the 1.30 eV emission showed a large shift toward higher energy (50 meV per decade change in excitation). In that work, it was extensively argued that this represents a deep donor-to-acceptor transition, and that the donor complex could be $(Cd_i^{++}-Cd_{In}^{-})^{+}$. (See also [106].)

Since the 1.3 eV emission is seen consistently in ion-implanted InP:Mg and not consistently in InP:Mg grown by other techniques [97, 100], and is removed by annealing [103], I postulate that it represents the transition $(Mg_i^{++}-Mg_{In}^{-})^{+} \rightarrow Mg_{In}^{-}$. That this emission only begins to occur in the doping range 10^{17}-10^{18} cm^{-3} is consistent with the above cited reports and that the concentration of Mg_{In} must be high for it to occur.

There is more literature discussion of the 1.0 eV peak in InP [70, 74,74,100,103]. All authors attribute this emission to an impurity complex involving a phosphorus vacancy. This is seen in In-rich LPE InP with high impurity content [75]. The impurities identified with this defect have included iron [74] and copper [70]. In our case, we have no evidence to support identification of the impurity other than to assume it is Mg_{In}, with the transition being $(Mg^{-}_{In}\text{-}V_P)^{+} \rightarrow Mg^{-}_{In}$. If phosphorus vacancies are involved, then the fact that the 1.0 eV emission only appears in the highest doping levels is sensible since a phosphorus over-pressure during growth is maintained to prevent vacancies. As noted in Table V, the substrates for these samples were nominally undoped.

CHAPTER VI

$In_{1-x}Ga_xAs$

This chapter presents discussion of several aspects of the InGaAs epilayer growth and characterization undertaken at OGC. The first portion discusses early efforts at ternary growth, including InGaAs/GaAs growth results. An unexpected defect was found in InGaAs/InP samples over a wide composition range, and characterization of this defect is discussed in detail. Next, the results are presented for lattice-matched InGaAs/InP. Finally, optical absorption, Hall mobility, and resistivity data are given for $In_{1-x}Ga_xAs$/InP with various x values. These data describe those important properties for both cryogenic and room temperatures.

As mentioned in Chapter II, a loss of TMIn as compared to TMGa occurs by a parasitic reaction of TMIn with PH_3. This reaction forms a white polymer which deposits on the walls of the reactor. The extent of this reaction is the major unknown factor in the determination of proper growth conditions for lattice-matched ternary material. The first step towards finding the correct [TMIn]/[TMGa] input value was to grow ternary layers on GaAs substrates with a small percentage of In. These would not be lattice-matched to GaAs, but the mismatch would be small. InGaAs 9, 10, and 11 were all grown in the 55 mm diameter reactor tube with 5 l/min. H_2, T = 675 °C, [V]/[III] = 20, [1.80×10^{-4}] of TMGa, and [2.01×10^{-5}] of TMIn. A one micron buffer layer of GaAs

was grown prior to the InGaAs growth. These parameters would give a composition near $In_{0.1}Ga_{0.9}As$ if the parasitic reaction effects were not too large. The value of x = 0.9 was chosen so that the PL peak of the ternary would be clearly separate from the GaAs peak.

PL data from all three samples at 77 K were nearly identical. A representative sample is shown in Fig. 30. The peak is centered at 1.384 eV, with a 20 meV FWHM. Using the formula for the $In_{1-x}Ga_xAs$ bandgap variation with composition at 77 K given by Wu and Pearson [55], i.e., $x = -0.538 + 0.943(2.12E_g - 0.544)^{1/2}$, one deduces that x = 0.92. Thus to get 8% indium, the required TMIn input was equivalent to 10%, meaning that 20% of the TMIn was lost to the parasitic reaction. To grow $In_{0.53}Ga_{0.47}As$, [TMIn]/[TMGa] would be 0.53/0.47 = 1.13 assuming no parasitic reaction, but increases to 1.36 assuming a 20% loss of TMIn.

The calibration described above, that 20% of the TMIn is lost for growth purposes, is a reactor-dependent calibration, not a universal constant. A different loss factor could be expected even with the same equipment were the temperatures, flow rates, etc., to be changed radically; and that factor would certainly be different using another OMVPE facility.

In fact, the loss factor turned out to be considerably more severe than estimated above, when $In_{1-x}Ga_xAs$ layers were grown onto InP substrates with x close to 0.47. Rather than [TMIn]/[TMGa] ≈ 1.36 as deduced above, those layers nearest to lattice-matching onto InP required a ratio slightly in excess of 2:1! The best laid plans for a scientific calibration were thus frustrated--but the indium-to-gallium

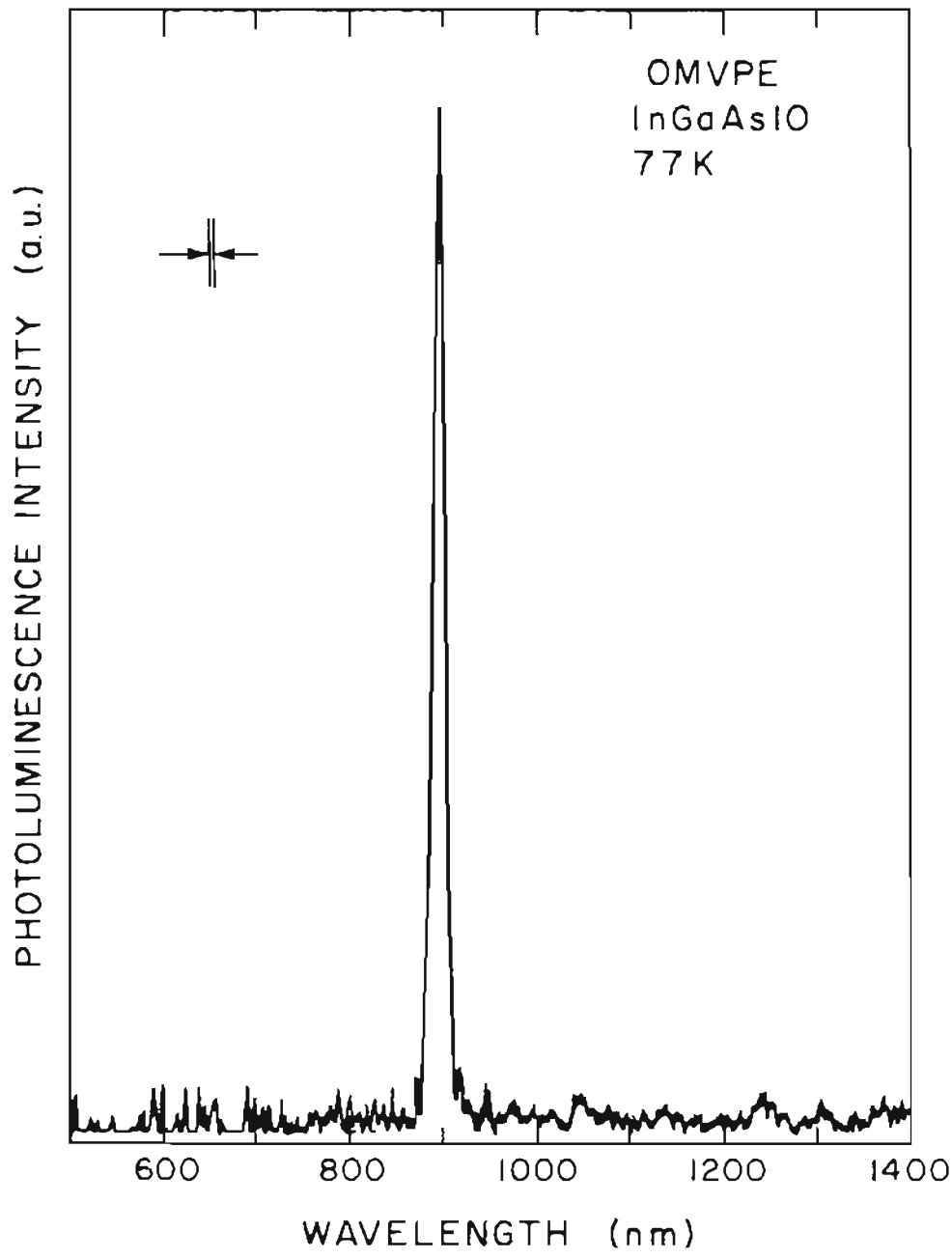

FIG. 30. PL for InGaAs 10 at 77 K. This epilayer was grown to test the extent of the TMIn + PH_3 parasitic reaction.

ratio was eventually determined on quite empirical grounds.

The morphology of the InGaAs/GaAs epilayers was good, similar in appearance to GaAs layers. Hall mobility averaged 3700 cm^2/Vs at room temperature and 2680 cm^2/Vs at liquid nitrogen temperature. The reduction at low temperatures may be explained by the significant lattice mismatch. The minimum mobility for these samples was 2500 cm^2/Vs at 100 K.

Early ternary samples on InP substrates (InGaAs 1-26) based on the the above TMIn depletion estimate employed values of [TMIn]/[TMGa] ranging from 1.1 to 1.6, but showed no PL at all. (Most, but not all, InGaAs samples were grown on an InP OMVPE buffer layer, which was later found to be important in obtaining good luminescence.) Two samples, InGaAs 27 and 28, were then grown near [TMIn]/[TMGa] = 2, but no PL was obtained from them either. An extensive series of samples were grown with [TMIn]/[TMGa] between between 1.60 and 1.77 (InGaAs 29-57). For most of these samples, PL was obtained. Typical of these was the 77 K spectrum of InGaAs 53 shown in Fig. 31. Three peaks are present. The highest energy peak (#1), which was usually the lowest in intensity, is the band-to-band transition. This emission was so broad and weak (if present at all) in most samples that it was not interpreted as the bandgap transition until optical absorption data suggested that interpretation. The two large peaks in Fig. 31 (#2 and #3) came to be seen as involving one or more deep-level defects.

As can be noted in Fig. 31, there was no variation in energy of either deep-level emission with varying laser excitation. If the tran-

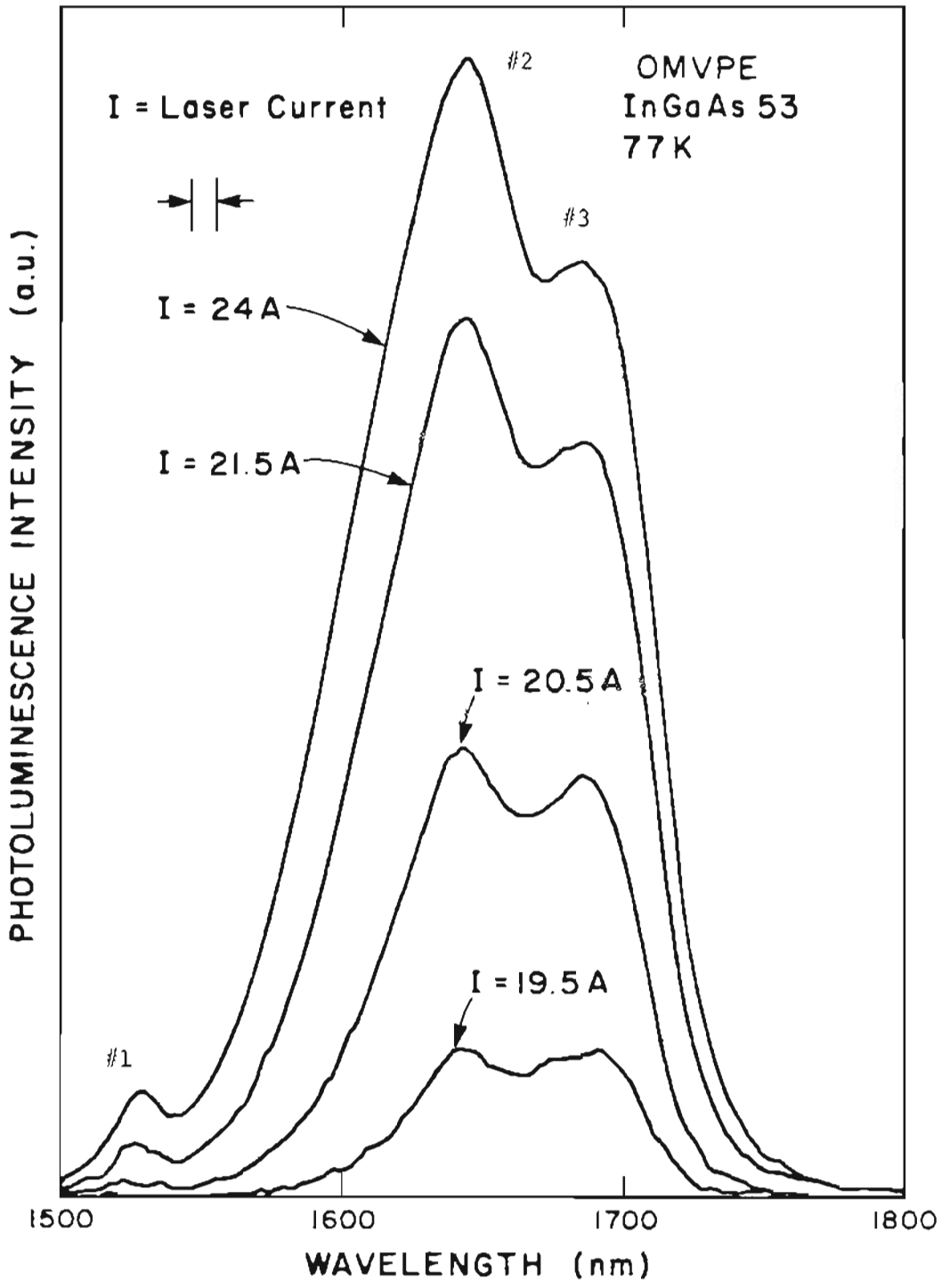

FIG. 31. Variation of InGaAs Defect PL with Excitation Light Intensity.

sitions were donor-to-acceptor, one would expect to see a measurable shift toward higher energy from the theory of Zacks and Halperin [107]. The defect PL spectrum was present for samples grown with and without buffer layers. and was present for samples grown on both the Sumitomo InP:S and InP:Fe substrates. An impurity was suspected, and a sample (InGaAs 65) was analyzed by SIMS. These data were compared to both the InP:Fe substrate and the MBE-grown sample OSU 1-29-7-86.

The elemental concentrations given by the SIMS analysis are clearly too high, but they are useful for comparison. The data are summarized in Table X. Values in this table represent graphical averages of the concentration versus depth data given in Appendix D. Measured concentrations were generally constant within the epilayer or within the substrate, while large transients were observed at the interfaces and surfaces. Within the accuracy of the SIMS analysis, which was about a factor of two, no significant differences in impurity levels were observed between InGaAs 65 and either the InP:Fe substrate or the InGaAs "standard", OSU 1-29-7-86.

No Hg-implant standard was available, so the Hg is probably totally spurious. Perhaps the "Hg" signal tracked an As-containing isotope, since it is high in both epilayers and low in both substrates. The elements listed represent the most common and expected contaminants in III-V materials, and the lack of any significant impurity concentration in InGaAs 65 as compared to its substrate or the "standard" InGaAs is interpreted as an indication that the defect is structural rather than an impurity.

TABLE X. SIMS Results for MBE and OMVPE InGaAs/InP.

Element	MBE —Epilayers— OMVPE		—Substrates—	
	OSU 1-29-7-86	InGaAs 65	InAsAs 65	OSU 1-29-7-86
C	2×10^{17}	2×10^{17}	1×10^{17}	1×10^{17}
O	3×10^{17}	3×10^{17}	5×10^{17}	3×10^{17}
Na	1×10^{15}	2×10^{15}	1×10^{15}	4×10^{15}
Mg	1×10^{16}	8×10^{15}	4×10^{15}	4×10^{15}
Al	4×10^{17}	4×10^{17}	2×10^{17}	2×10^{17}
Si	4×10^{16}	4×10^{16}	4×10^{16}	2×10^{16}
S	4×10^{15}	5×10^{15}	6×10^{16}	1×10^{19}
Cl	4×10^{16}	6×10^{15}	4×10^{15}	3×10^{15}
Cr	2×10^{16}	3×10^{14}	3×10^{14}	5×10^{15}
Fe	6×10^{16}	4×10^{16}	2×10^{17}	3×10^{16}
Ni	3×10^{16}	1×10^{15}	2×10^{15}	7×10^{15}
Cu	9×10^{17}	2×10^{18}	2×10^{18}	...
Zn	4×10^{17}	6×10^{17}	6×10^{17}	3×10^{18}
Ag	8×10^{16}	2×10^{17}	2×10^{17}	2×10^{17}
W	2×10^{18}	2×10^{18}	3×10^{17}	2×10^{18}
Hg	4×10^{21}	6×10^{21}	5×10^{19}	2×10^{18}

The defect was present in all samples from which PL data were obtainable. These samples are listed in Table XI along with the energy and intensity of each of the three PL peaks seen. A distillation of the Table XI data (with corrected PL peak intensities) is given in Fig. 32. Here, the data from two Ga-rich samples, one In-rich sample, and a nearly lattice-matched sample are reproduced to show how the PL changed with varying amounts of input [TMIn]/[TMGa]. Several features emerge from this figure: 1) the two defect peaks merge as lattice-matching is approached from the Ga-rich side, and become one peak for the In-rich sample (two peaks are sometimes resolvable in lattice-matched samples); 2) the PL intensity is highest for the lattice-matched sample, and lowest for the In-rich sample; and 3) a linear reduction of the bandgap with increasing [TMIn]/[TMGa] can be identified (variation from a linear trend is assumed to be due to variation in the amount of the parasitic reaction).

Emission at 0.69-0.70 eV has been observed in InGaAs before, described only as an "intrinsic defect" [108,109]. While the PL observed here is not as broad as in those reports, the defect may be related. Iron impurity-related defects have also been observed in InGaAs [109]. Of the 16 InGaAs samples listed in Table XI, 3 were grown on Fe doped substrates. Of these, InGaAs 65 had much larger than average emission intensity, InGaAs 53 had slightly above average emission intensity, and InGaAs 54 had very low emission intensity. The spectral distribution of the emission in each of these samples correlated with that of Fig. 32. The most that can be said regarding the Fe doped substrate as a

TABLE XI. PL Peak Energies for OMVPE $In_{1-x}Ga_xAs$.

InGaAs Sample #	[TMIn]/[TMGa]	Peak #1 Energy (eV)	Peak #1 Intensity (a)	Peak #2 Energy (eV)	Peak #2 Intensity (a)	Peak #3 Energy (eV)	Peak #3 Intensity (a)
39	1.60	0.816	63	0.775	177	0.756	115
40	1.70	0.820	25	0.731	263	0.710	300
41	1.70	0.813	50	0.732	431	0.708	269
42	1.60	0.821	53	0.794	44	0.775	28
43	1.60	0.827	13	0.719	438	0.695	363
44	1.65	0.816	44	0.754	311	0.730	255
46	1.63	0.818	59	0.786	56	...	...
48	1.72	0.820	80	0.738	55	0.718	70
49	1.72	0.816	11	0.734	24	0.718	16
53	1.72	0.810	63	0.750	313	0.735	288
54	1.74	0.810	14	0.780	18	...	...
55	1.75	...	...	0.750	119	...	...
58	2.05	0.795	56	0.737	1000	...	...
59	2.09	0.777	18	0.734	27	0.704	15
62	2.19	0.787	19	0.734	110	...	...
65	2.07	0.787	325	0.742	4350	0.729	2500

[a] Intensity values are relative to: 1.5 mm slit width, 5000 gain, 10 mV lock-in, 26.5 A laser, Si filter, 10 V full scale on X-Y. In most cases, the FWHM was not resolvable.

Growth conditions were: [9.23×10^{-5}] of TMIn, [V]/[III] = 55 except for InGaAs 39 and 40 in which 30 was used, T = 650 °C for InGaAs 41-57, T = 630 °C for InGaAs 39-40, T = 600 °C for InGaAs 58-66, no InP buffer was grown on InGaAs 47 & 49, a 2 μm buffer was grown on InGaAs 53, one micron buffers were grown on all others, 4 l/min. H_2 flow was used in the rectangular growth tube.

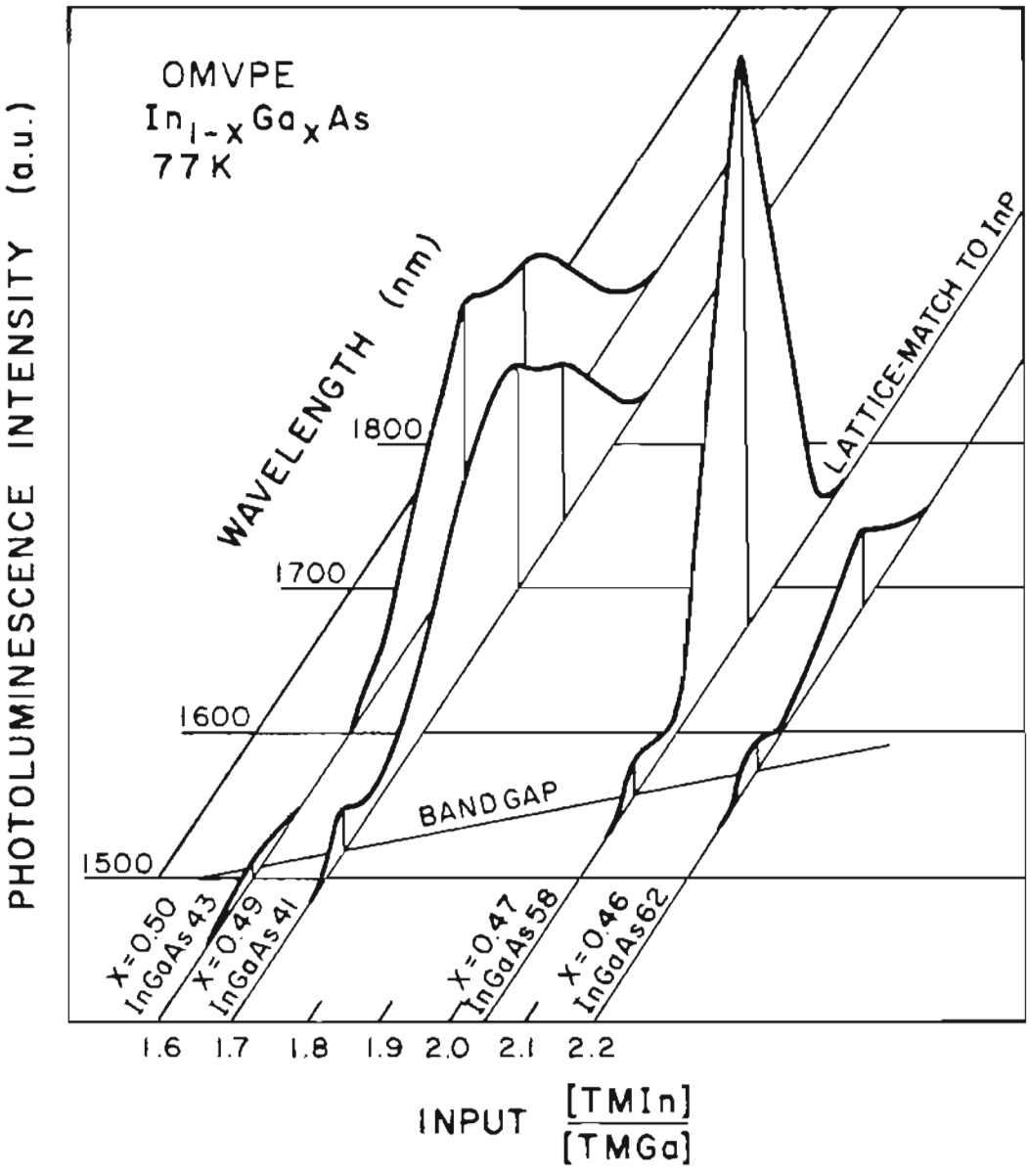

FIG. 32. Variation of $In_{1-x}Ga_xAs$ PL with x.

contributor to the deep-level PL seen in these InGaAs layers is that Fe diffusion activated an emission that was also present in samples not grown on this type of substrate.

The relative peak heights of the two defect peaks were consistent. Peak #2 was always significantly higher than #3, with the exception of InGaAs 40. This sample was grown at a slightly lower temperature (630 °C versus 650 °C) and with a somewhat lower [V]/[III] ratio (30:1 versus 55:1) than InGaAs 41, but growth conditions were otherwise the same. The higher temperature and/or [V]/[III] ratio may have caused a large increase in peak #2 intensity for InGaAs 41, or InGaAs 40 may instead be regarded as an anomaly. PL is a very surface-sensitive technique due to recombination mechanisms and the fact that most of the laser light is absorbed in less than one micron thickness. Variation in surface condition may have contributed significantly to variability in the data in Table XI. Corroborative absorption data were not available for this deep level defect because layers were not thick enough to measure α in the low energy regime.

There was some suspicion that the ternary defect was due to a deviation from lattice-matching to InP. Striking evidence that this is not the case is given by Figs. 33 and 34. Figure 33 shows 77 K PL data from two $In_{0.53}Ga_{0.47}As$ samples not grown by OMVPE. Of these, (a) denotes LPE material reported by Pearsall [56], while (b) is the "standard" MBE sample, OSU 1-29-7-86. Also, data from InGaAs65 are shown, which might be taken as indicating an In-rich composition of x = 0.41. However, the coincident 300 K PL data in Fig. 34 for the same

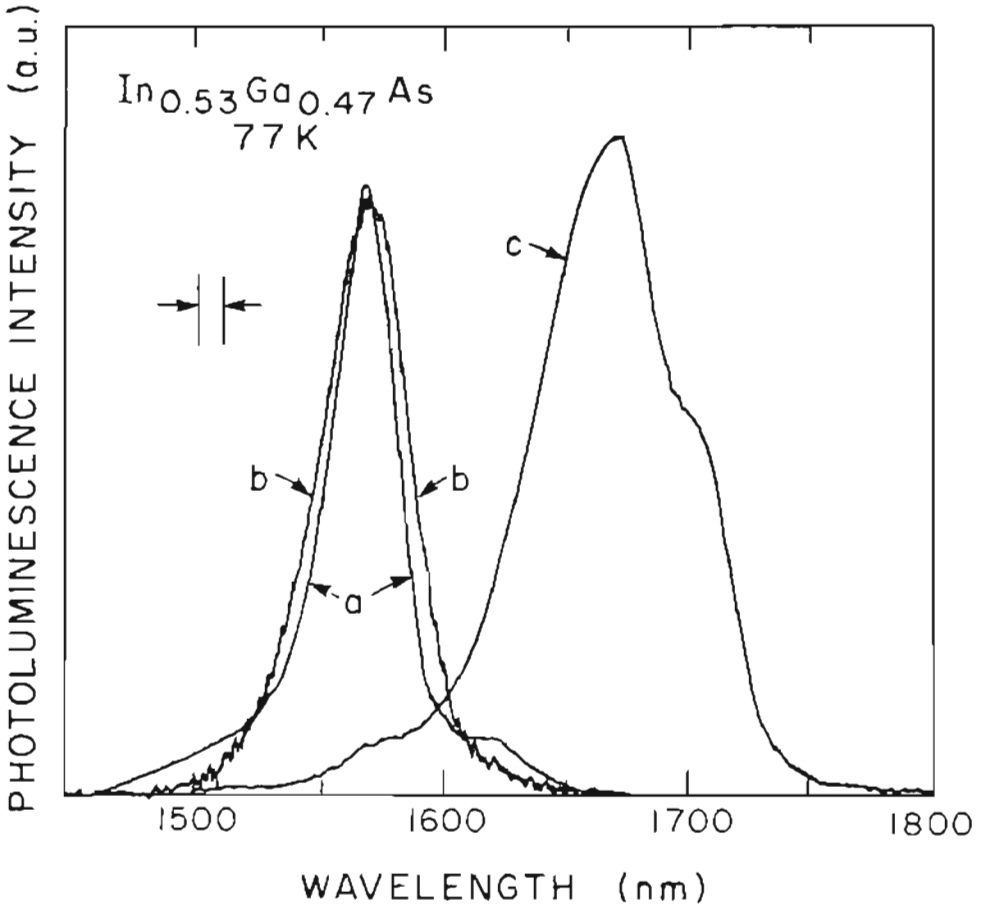

FIG. 33. PL for $In_{0.53}Ga_{0.47}As$ at 77 K. a) data from Pearsall [56], b) OSU 1-29-7-86, c) InGaAs 65.

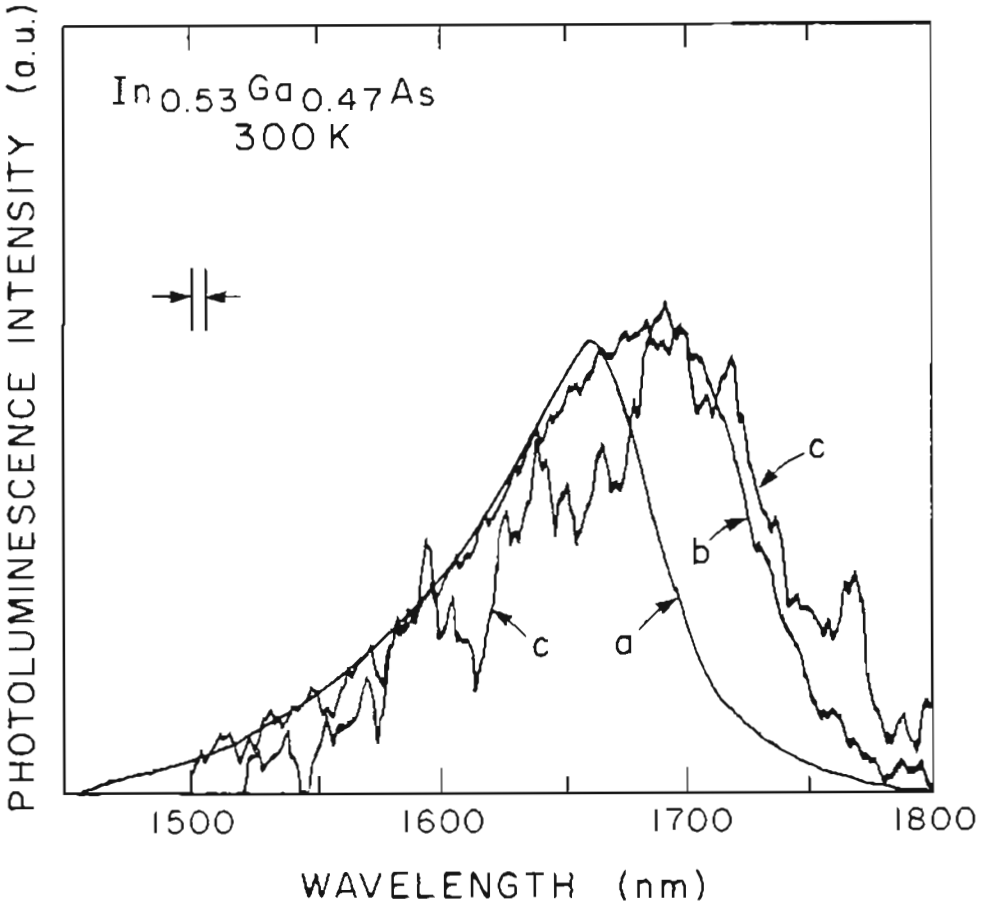

FIG. 34. PL for $In_{0.53}Ga_{0.47}As$ at 300 K. a) data from Pearsall [56], b) OSU 1-29-7-86, c) InGaAs 65.

three samples support the conclusion that all of these layers are lattice-matched.

As a further test for lattice-matching, the composition of InGaAs 65 was analyzed by AES. These results are presented in Fig. 35. Within the experimental error of the method (2%), this sample is of the same composition as OSU 1-29-7-86 (i.e. the sample that was used to derive the vertical scale in Fig. 35). The accumulated evidence thus confirms Fig. 32 for the scaling of [TMIn]/[TMGa] to x and hence to bandgap. We must then conclude that structural defects are present in the OMVPE InGaAs/InP samples which are not due to impurities or lattice mismatch alone.

Further study was made of composition through bandgap determination by optical absorption. The absorption coefficients of eleven samples were measured at 10 K. Data from four of these are presented in a log-linear plot in Fig. 36. The steepest drop in α below the bandgap was obtained for lattice-matched samples. The value of α rose to about 6000 cm^{-1} near the bandgap, regardless of composition.

The bandgaps determined by absorption at 10 K are plotted in Fig. 37, along with the bandgap found by PL (assuming the highest energy PL emission was band-to-band emission). In this figure, the PL data are shifted 20 meV higher than the actual 77 K measured value to correct for the increase in bandgap expected when InGaAs is cooled from 77 K to 10 K [56]. Five samples were tested by both methods, and these are underlined in the figure.

Absorption gave somewhat more reliable data for these samples.

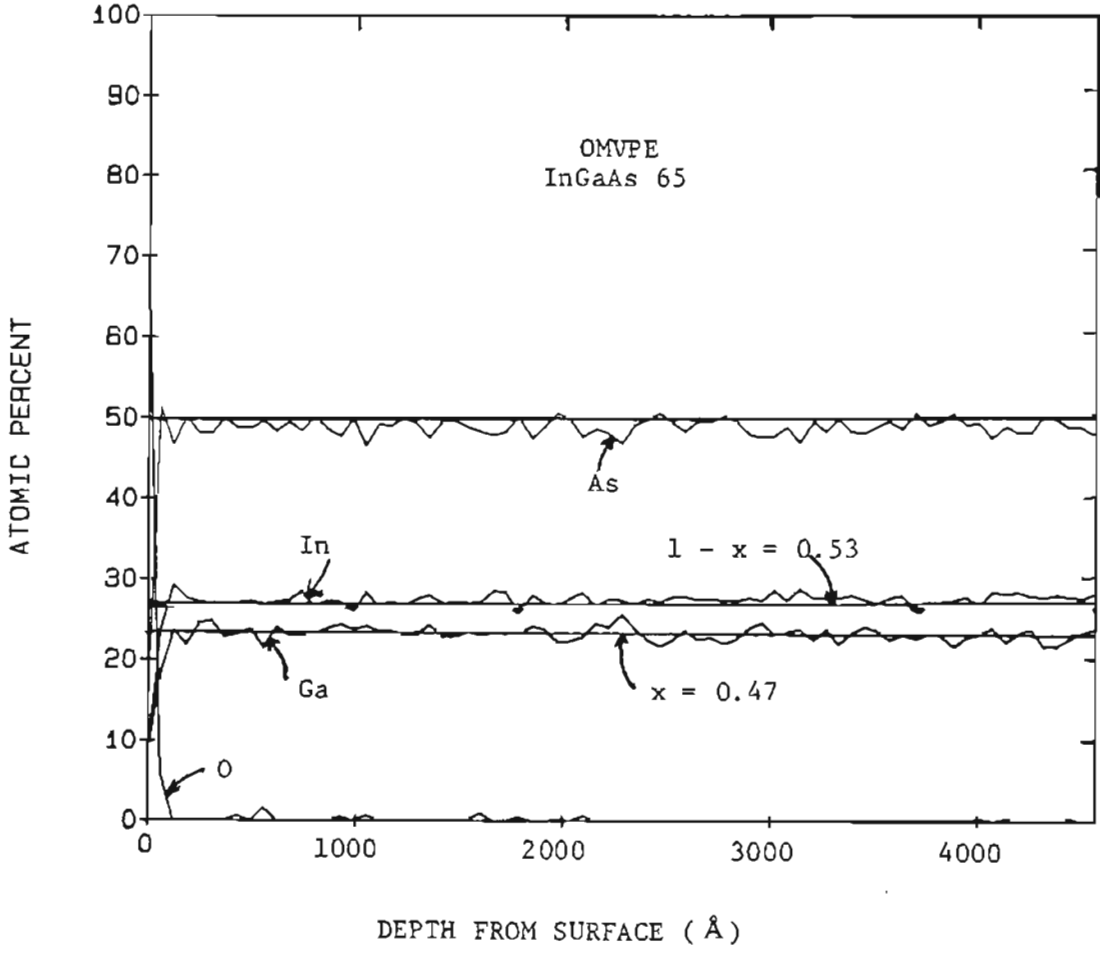

FIG. 35. AES Profile for InGaAs 65.

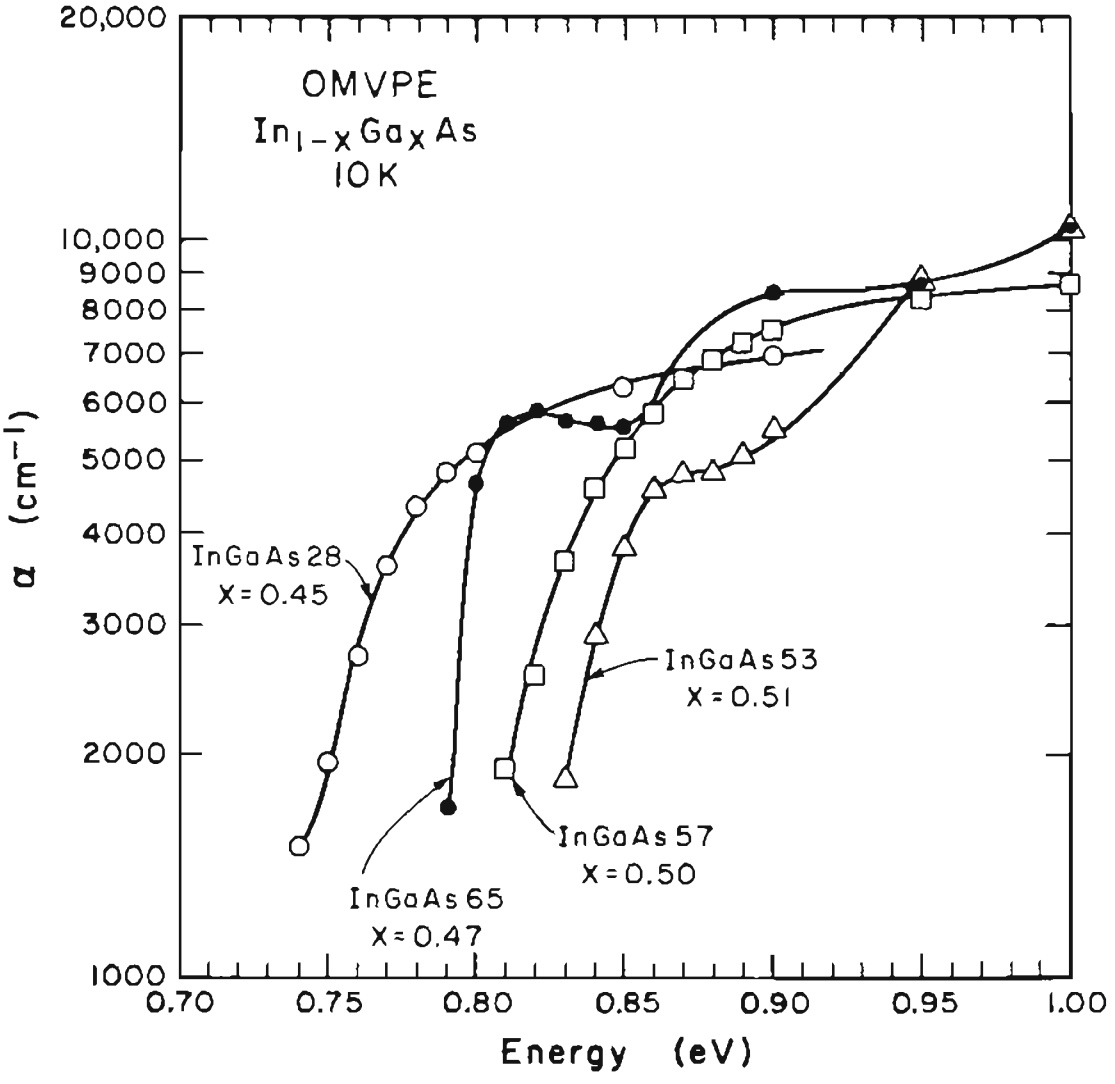

FIG. 36. Absorption Coefficient for OMVPE $In_{1-x}Ga_xAs$ at 10 K.

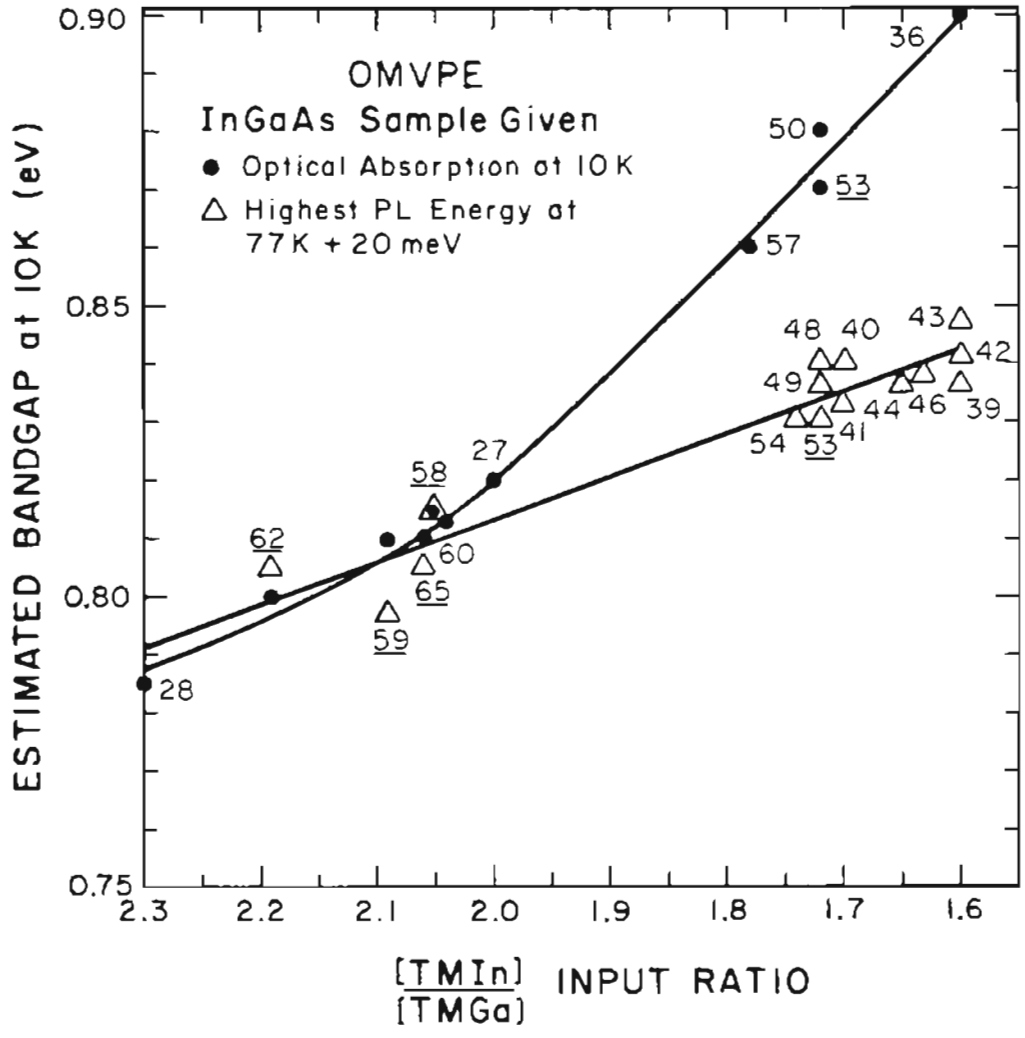

FIG. 37. Bandgap Estimates for OMVPE InGaAs vs. [TMIn]/[TMGa] Ratio.

This is particularly seen in the range $2.0 < [TMIn]/[TMGa] < 2.1$, where the α data are quite orderly, yet the PL data are scattered. A curved line of best fit is drawn through the absorption data, while a straight least-squares fit line seems adequate for the PL data ($r = -0.948$). That the two methods suggest different bandgaps for compositions that are not lattice-matched is not unreasonable. The α samples are removed from their substrates, and so have no strain due to lattice mismatch, while PL samples are still attached to their substrates. (See Kuo et al [110] for a discussion of this effect.)

Lattice-matching was obtained for samples with $E_g(10\ K) = 0.81$ eV [56,59], which corresponded to an input [TMIn]/[TMGa] ratio of 2.0 The flattening of the absorption data curve at high [TMIn]/[TMGa] values may be evidence of increased depletion of [TMIn]--an acceleration of the parasitic reaction--but there are not enough data to quantify this.

The growth conditions and PL peak energies for the samples in Fig. 37 are given in Table XI. Note that the substrate could not be fully removed from InGaAs 27 and InGaAs 50, so the absorption data for these were taken with the InP substrate, and its effect was subtracted out.

The InGaAs/InP epilayers had mostly good morphology. The lattice-matched samples, such as InGaAs 65, were highly reflective. A light grey haze was present on samples which were not lattice-matched, particularly InGaAs 28, 57, and 60. InGaAs 27 and 56 had large dark grey spots.

A comparison can be made of the 10 K absorption coefficient for InGaAs 65 and the "standard" $In_{0.53}Ga_{0.47}As$ MBE sample, OSU 1-29-7-86. As can be seen in Fig. 38, these data are quite close, again indicating lattice-matching for the OMVPE sample. Comparable low temperature InGaAs α data are given in the figure also [69]. The near-bandgap peak absorption of 5800 cm^{-1} for InGaAs 65 is the same as the Zielinski et al value. (For the sample in [69], the bandgap was estimated to be 0.82 eV rather than 0.81 eV.) At 300 K, there are two additional reports; but the data from InGaAs 65 is over a broader range than any of those. Figure 39 shows the Zielinski et al room temperature data [69], labelled (a), as well as those of Humphreys et al [111], (b), and of Burkhard et al [61], (c). The Burkhard et al data appear to be too high, perhaps the result of a thickness measurement error. Above the bandgap, α does not rise as fast in InGaAs as it does in either GaAs [112] or InP [113]. Above 1.3 eV, the curves α(300 K) and α(10 K) merge.

A step in the absorption spectrum at $(E_g + \Delta_o)$, where Δ_o denotes the spin-orbit splitting parameter (= 0.35 eV for $In_{0.53}Ga_{0.47}As$ [114]) was not observed in this study. Enhanced absorption occurred at 0.1 eV above the bandgap for both our data and those of Humphreys et al, but the cause of this absorption is not explored here. No strong exciton absorption was observed either with the monochromator slits narrowed to 0.1 mm or the temperature lowered to 7 K, perhaps because of the presence of the unknown defect.

Absorption data at 300 K for InGaAs samples of varying composition

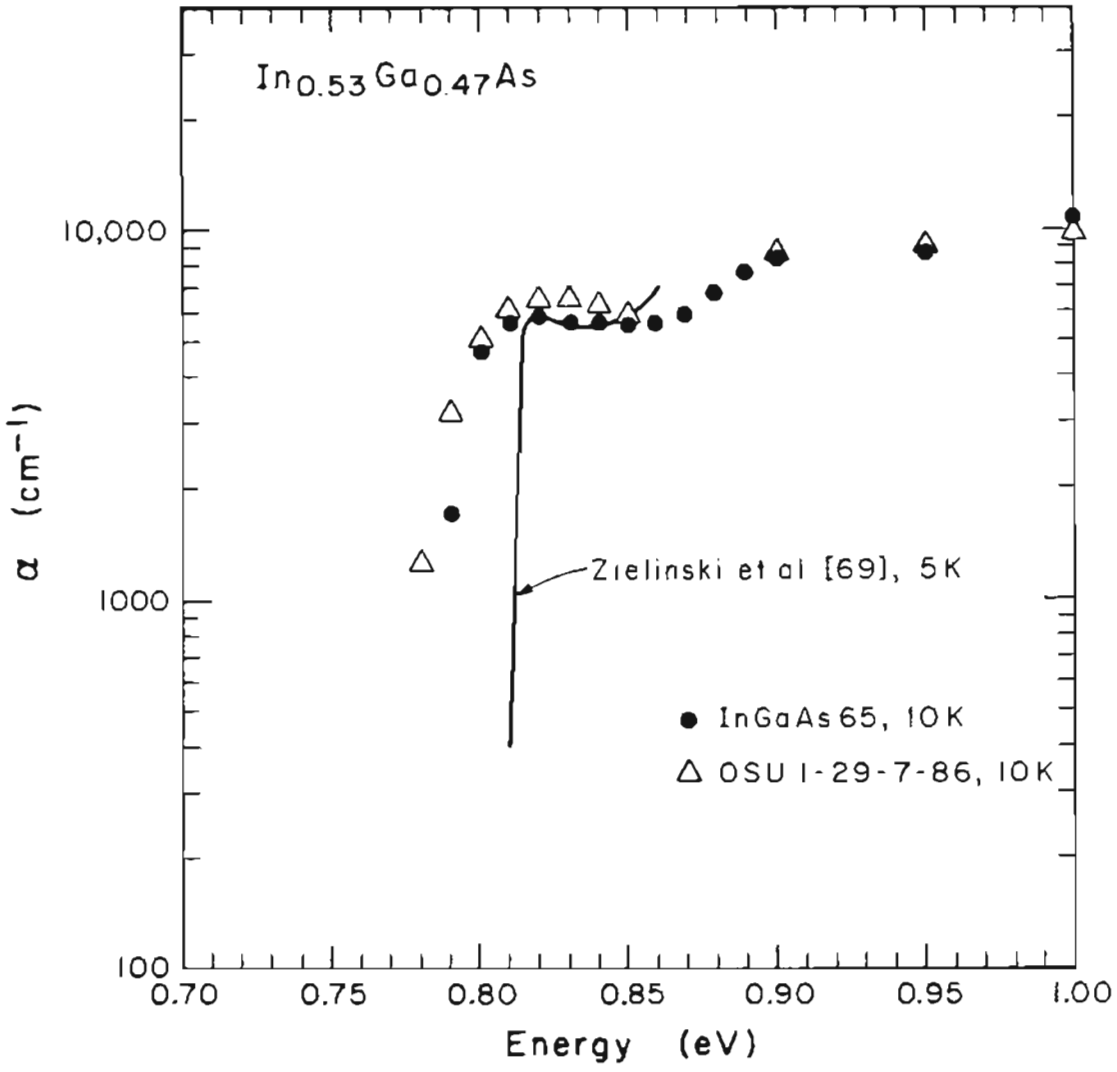

FIG. 38. Near-bandgap Absorption Coefficient for $In_{0.53}Ga_{0.47}As$.

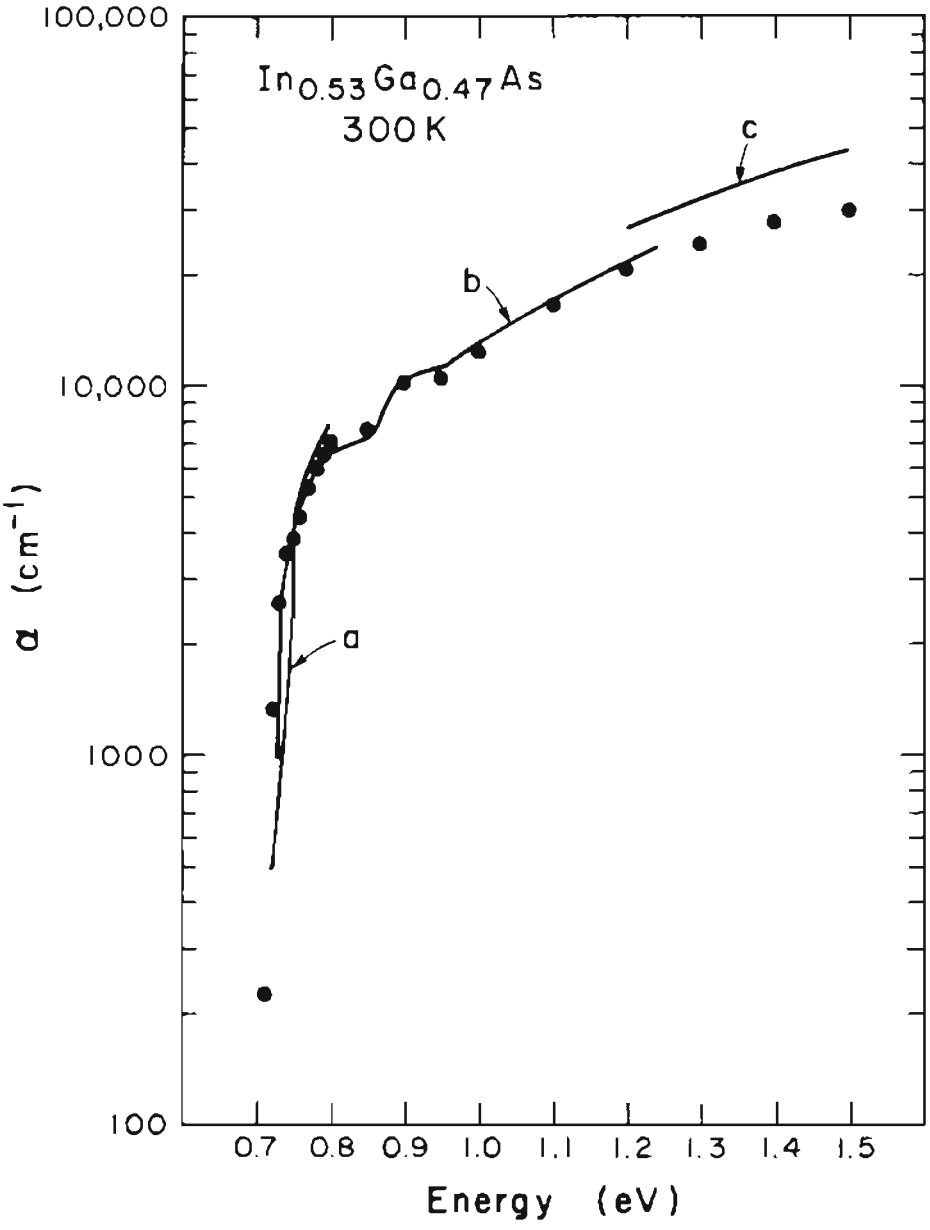

FIG. 39. Absorption Coefficient for $In_{0.53}Ga_{0.47}As$ at 300 K. a) data from Zielinski et al [69], b) data from Humphreys et al [111], c) data from Burkhard et al [61], data points are InGaAs 65 from this study.

are shown in Fig. 40. Above 1.0 eV, all samples had nearly the same α, regardless of composition. Note that the energy scale on this figure is broader than that of Fig. 36, to show the higher energy range. Since the PL data for OMVPE InGaAs/InP samples were ambiguous, it was indeed fortunate that the absorption coefficient turned out to be a parameter which could be measured reliably on samples with relatively large lattice mismatch.

Absorption data were also taken at 77 K. An example appears in Fig. 41, for sample InGaAs 59. Data at 77 K were coincident with 10 K data for all samples, except for 1) a 20 meV shift near the bandgap, and 2) less structure above the bandgap (e.g. no threshold at E_g + 0.1 eV).

The Hall mobility was measured for some of the InGaAs epilayers grown on semi-insulating InP substrates. (Poor contacts prevented measurement for all such InGaAs samples.) Table XII lists Hall mobility and carrier concentration for the best samples reported in the literature, and the OGC samples. The OGC results are encouraging in light of the brief time available (six months) to develop InGaAs growth techniques. Samples which are not lattice-matched have much reduced mobility, but still compare favorably with InP and GaAs at 300 K.

The best InGaAs sample obtained in this study was InGaAs 66. For this sample, a log-log plot of Hall mobility vs. temperature is given in Fig. 42. The growth conditions for this sample were the same as those for InGaAs 65 (as listed in Table II), except that at the end

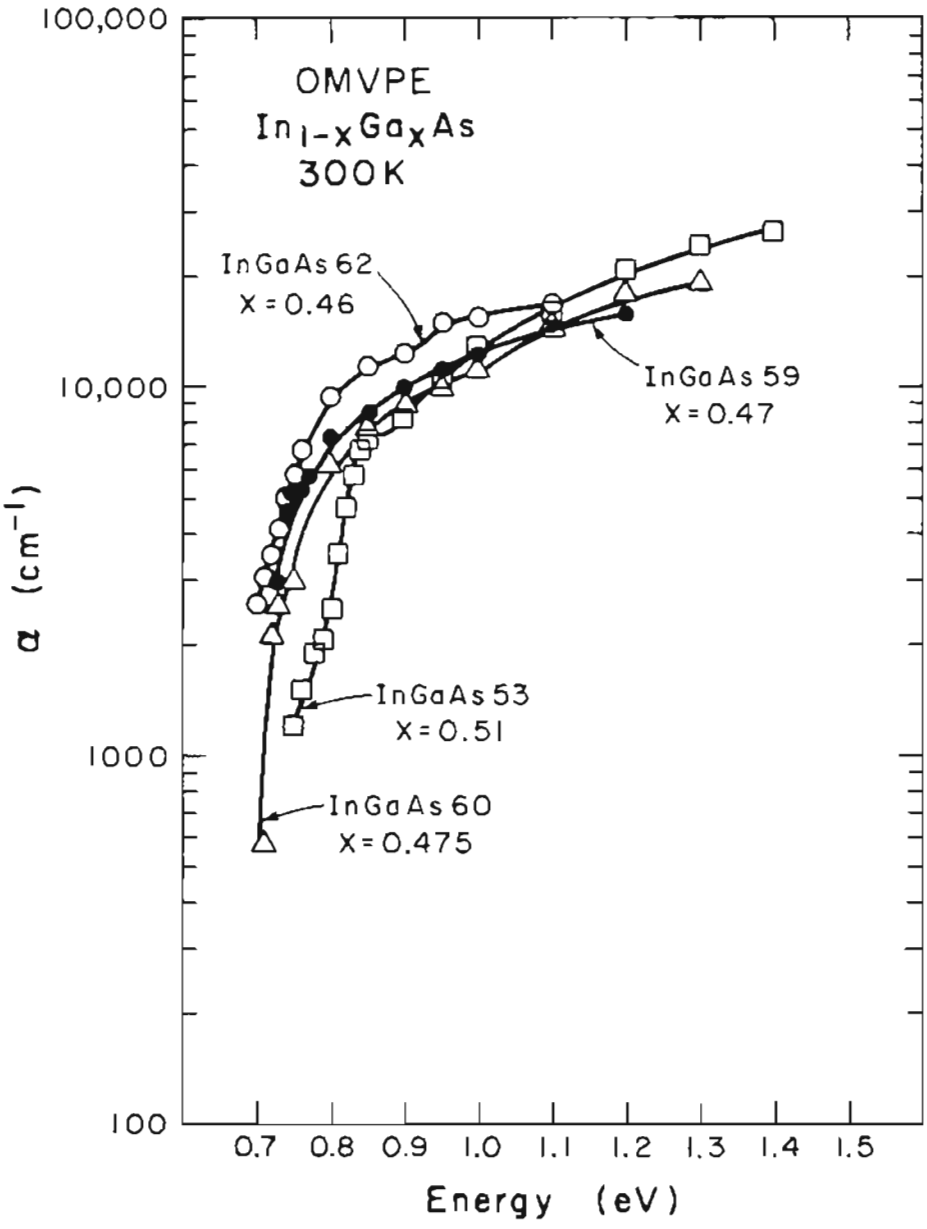

FIG. 40. Absorption Coefficient for OMVPE $In_{1-x}Ga_xAs$ at 300 K.

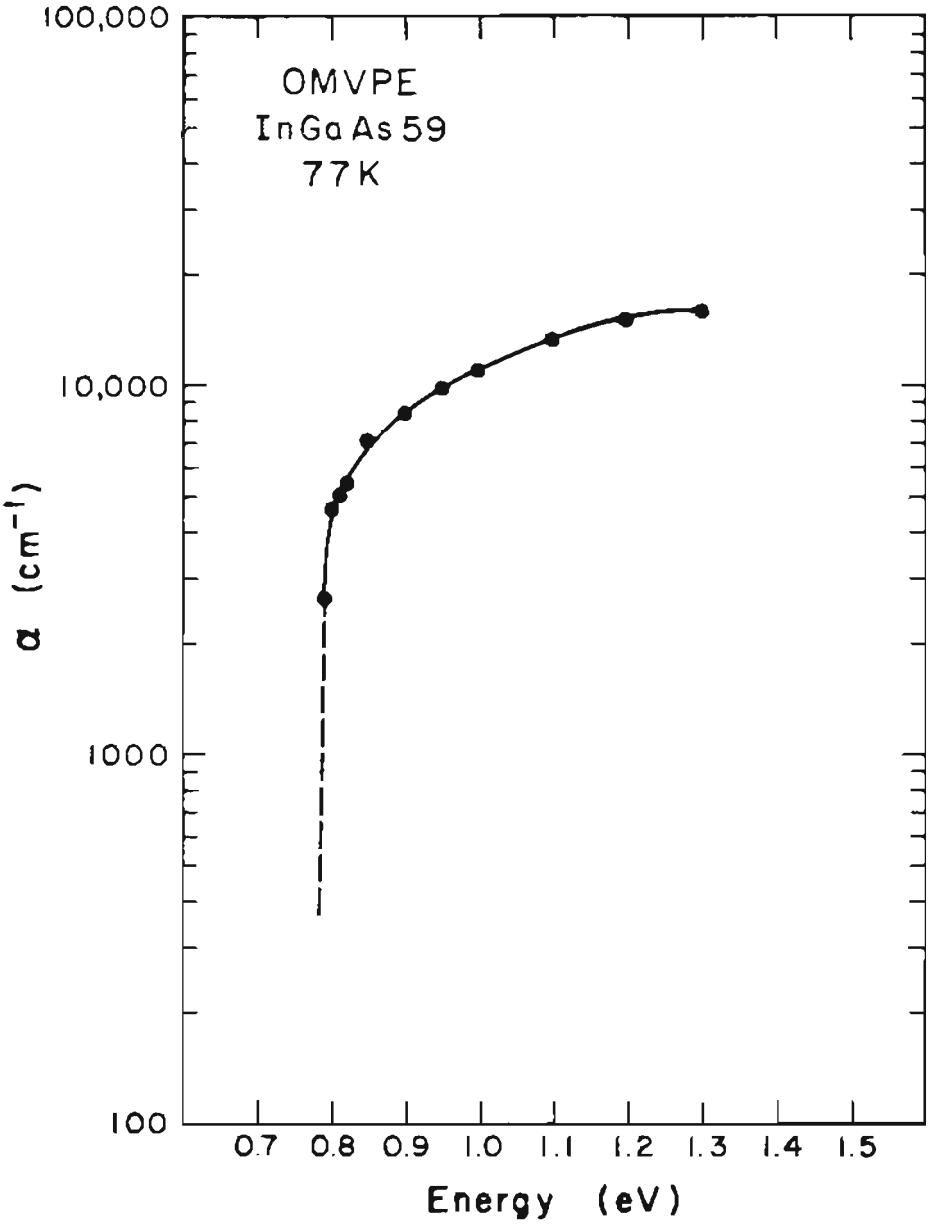

FIG. 41. Absorption Coefficient for $In_{0.53}Ga_{0.47}As$ at 77 K.

TABLE XII. Hall Mobility and Carrier Concentration for $In_{1-x}Ga_xAs/InP$.

Sample/Reference	Hall Mobility (cm^2/Vs) 300 K	77 K	n (cm^{-3})
Lattice-matched (x = 0.47):			
Pearsall *et al*, Thomson/CSF [115]	10,000	26,500	1×10^{16}
Goetz *et al*, Thomson/CSF [59]	10,400[a]	43,400[a]	4×10^{15}
Saxena *et al*, HP [116]	10,600	79,000	8×10^{14}
Carey *et al*, HP [117]	...	64,000	5×10^{14}
OGC:			
InGaAs 65	6500	7600	2×10^{15}
InGaAs 66	9000	26,500	6×10^{15}
Not lattice-matched (x = 0.49):			
OGC:			
InGaAs 47	3000	4000	1×10^{16}
InGaAs 50	5300	10,600	5×10^{15}

[a] average of four samples.

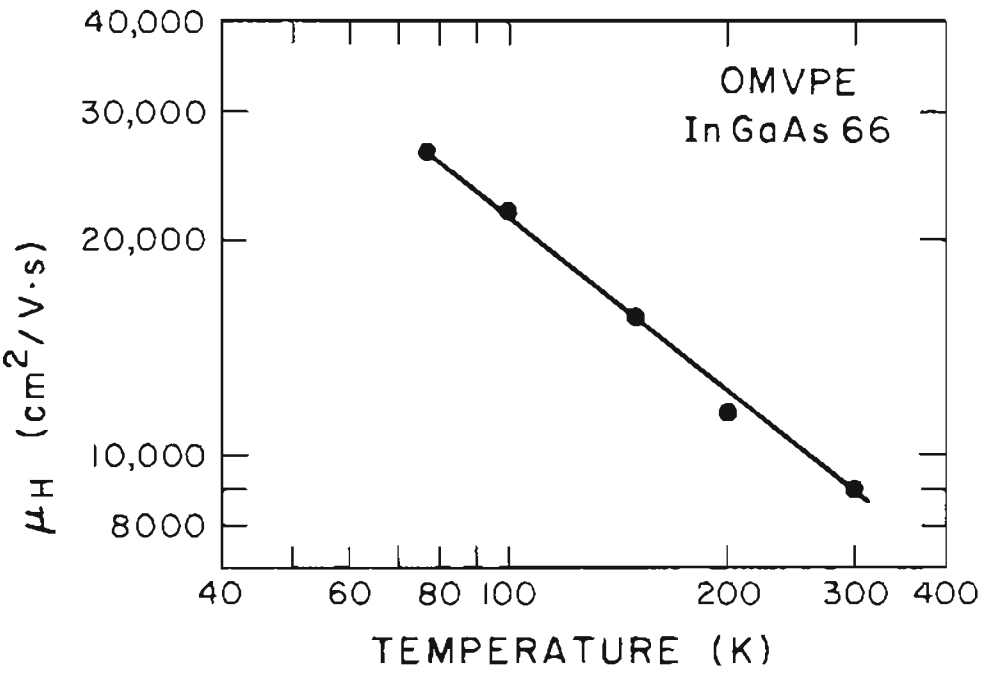

FIG. 42. Hall Mobility for OMVPE $In_{0.53}Ga_{0.47}As$.

of the buffer layer growth, the temperature was reduced to 450 °C to begin ternary growth, then raised to the final growth temperature of 600 °C within two minutes. The PH_3 flow was maintained until the temperature fell below 500 °C. The purpose of this procedure was to reduce phosphorus evaporation from the buffer layer.

Resistivity for the InGaAs/InP epilayers was typically 0.1 to 0.4 Ωcm at 300 K, similar to the resistivities obtained for InP. For InGaAs 65, ρ = 0.315 Ω cm, and for InGaAs 66, 0.113 Ω cm.

CHAPTER VII

CONCLUSIONS

Epitaxial growth of the III-V compounds InP, GaAs, and InGaAs using OMVPE has been accomplished, resulting in at least 50 samples of each. Factors influencing the growth have been discussed. With improvements in technique and source material purity, the quality of epilayers of each compound progressively improved. The final series of growths of GaAs, InP, and InGaAs approached the quality of material reported in the literature. The primary thrust of this work has been with the ternary, for which reports of OMVPE growth with trimethyl-based sources have been few.

A series of Mg doped InP crystals showed new and interesting photoluminescence which reflected several mechanisms of Mg incorporation. Magnesium formed at least two deep level defect complexes in InP in addition to the expected shallow acceptor. Mg doping was accomplished over the range 10^{16} to 10^{19} cm^{-3}.

Methods for measuring the optical absorption coefficient of InGaAs were developed. The strength of optical absorption is not a parameter which depends strongly on composition, as seen in the data here (although the absorption edge clearly shifts with composition change). Also, the absorption coefficient becomes independent of temperature for energies larger than 1.3 eV.

Optical absorption proved useful in demonstrating the growth of

lattice-matched InGaAs/InP. This was supplemented with photoluminescence and AES characterization. While the optical properties of InGaAs layers did not depend strongly on composition, the morphology and electrical properties did; Hall mobility improved dramatically for InGaAs when lattice-matching was achieved.

This study has shown that InGaAs epitaxial layers of good quality for both electrical and optical device applications can be readily grown by OMVPE. The data presented here does not indicate inherent deficiencies in the OMVPE process; favorable comparisons are made to MBE-, LPE-, and VPE-grown material. Further refinement of growth techniques should provide material of even higher perfection while retaining the economies of scale and the relative simplicity of OMVPE.

REFERENCES

[1] V. Narayanamurti, "Artificially structured thin-film materials and interfaces," Science 235, 1023 (1987).

[2] F. Capasso, K. Mohammed, and A. Y. Cho, "Tunable barrier heights and band discontinuities via doping interface dipoles: an interface engineering technique and its device applications," J. Vac. Sci. Technol. B 3, 1245 (1985).

[3] P. D. Dapkus, "Metalorganic chemical vapor deposition," Ann. Rev. Mater. Sci. 12, 243-69 (1982).

[4] Proceedings of the Third International Conference on Metalorganic Vapor Phase Epitaxy, edited by G. B. Stringfellow, J. Cryst. Growth 77 (1-3)(1986).

[5] M.J. Ludowise, "Metalorganic chemical vapor deposition of III-V semiconductors," J. Appl. Phys. 58, R31 (1985).

[6] G. B. Stringfellow, "OMVPE growth of III-V semiconductors," in Semiconductors and Semimetals, Vol. 22A, edited by W. T. Tsang (Academic, New York, 1985) pp. 209-60.

[7] S. D. Hersee and J. P. Duchemin, "Low-pressure chemical vapor deposition," Ann. Rev. Mater. Sci. 12, 65-80 (1982).

[8] G. H. Olsen and T. J. Zamerowski, "Vapor-phase growth of (In,Ga)(As,P) quaternary alloys," IEEE J. Quantum Electron. QE-17, 128 (1981).

[9] R. H. Moss and J. S. Evans, "A new approach to MOCVD of InP and GaInAs," J. Cryst. Growth 55, 129 (1981).

[10] H. M. Cox, "Vapor levitation epitaxy: a new concept in epitaxial crystal growth," J. Cryst. Growth 69, 641 (1984).

[11] R. Solanki, C. A. Moore, and G. J. Collins, "Laser-induced chemical vapor deposition," Solid State Technol. 28, 220 (1985).

[12] J. J. Yang, R. P. Ruth, and H. M. Manasevit, "Electrical properties of epitaxial indium phosphide films grown by metal-organic chemical vapor deposition," J. Appl. Phys. 52, 6279 (1981)

[13] H. M. Manasevit and W. I. Simpson, "The use of metalorganics in the preparation of semiconductor materials," J. Electrochem. Soc. 120, 135 (1973).

[14] Proceedings of the First International Conference on Metalorganic Chemical Vapor Deposition, edited by J. F. Bonfils, S. J. Irvine, and J. B. Mullin, J. Cryst. Growth 55 (1981).

[15] Proceedings of the Second International Conference on Metalorganic Vapour Phase Epitaxy, edited by J. B. Mullin, J. Cryst. Growth 68 (1)(1984).

[16] B. J. Baliga and S. K. Ghandhi, "Growth and properties of heteroepitaxial GaInAs alloys on GaAs substrates using trimethylgallium, triethylindium, and arsine," J. Electrochem. Soc. 122, 683 (1975).

[17] B. J. Baliga, R. Bhat, and S. K. Ghandhi, "Composition dependence of energy gap in InGaAs alloys," J. Appl. Phys. 46, 4608 (1975).

[18] C. B. Cooper, M. J. Ludowise, V. Aebi, and R. L. Moon, "The organometallic VPE growth of $GaAs_{1-y}Sb_y$ using trimethylantimony and $Ga_{1-x}In_xAs$ using trimethylarsenic," J. Electron. Mater. 9, 209 (1980).

[19] J. P. Noad and A. J. Springthorpe, "The preparation of $Ga_{1-x}In_xAs$ by organometallic pyrolysis for homojunction LEDs," J. Electron. Mater. 9, 601 (1980).

[20] R. Dupuis, R. Lynch, C. Thurmond, and W. Bonner, "Growth of InP by MOCVD," Proc. SPIE 323, 131 (1982).

[21] T. Fukui and Y. Horikoshi, "Properties of InP films grown by OMVPE method," Jpn. J. Appl. Phys. 19, L395 (1980).

[22] M. Ogura, K. Inoue, Y. Ban, T. Uno, M. Morisaki, and N. Hase, "InP MESFET grown by MOCVD," Jpn. J. Appl. Phys. 21, L548 (1982).

[23] M. Ogura, M. Mizuta, N. Hase, and H. Kukimoto, "Deep levels in InP grown by MOCVD," Jpn. J. Appl. Phys. 22, 658 (1983).

[24] E. P. Menu, D. Moroni, J. N. Patillon, T. Ngo, and J. P. Andre, "High mobility of two-dimensional electrons in $Ga_{1-x}In_xAs$/InP heterostructures grown by atmospheric pressure MOVPE," J. Cryst. Growth 79, 920 (1986).

[25] J. S. Whiteley and S. K. Ghandhi, "Factors influencing the growth of $Ga_{0.47}In_{0.53}As$ on InP substrates using the metalorganic process," J. Electrochem. Soc. 129, 383 (1982); "Growth and characterization of $Ga_{0.47}In_{0.53}As$ films on InP substrates using triethylgallium, triethylindium, and arsine," 130, 1191 (1983).

[26] K. Carey, "OMVPE growth and characterization of high purity GaInAs on InP," Appl. Phys. Lett. 46, 89 (1985).

[27] K. T. Chan, L. D. Zhu, and J. M. Ballantyne, "Growth of high quality GaInAs on InP buffer layers by MOCVD," Appl. Phys. Lett. 47, 44 (1985).

[28] A. Mircea, R. Azoulay, L. Dugrand, R. Mellet, K. Rao, and M. Sacilotti, "Metalorganic InP and $In_xGa_{1-x}As_yP_{1-y}$ on InP epitaxy at atmospheric pressure," J. Electron. Mater. 13, 603 (1984).

[29] B. I. Miller, E. F. Schubert, U. Koren, A. Ourmazd, A. H. Dayem, and R. J. Capik, "High quality narrow GaInAs/InP quantum wells grown by atmospheric organometallic vapor phase epitaxy," Appl. Phys. Lett. 49, 1384 (1986).

[30] M. Sacilotte, A. Mircea, and R. Azoulay, "InP growth by OMVPE," J. Cryst. Growth 63, 111 (1983).

[31] M. D. Scott, A. G. Norman, and R. R. Bradley, "The characterisation of $Ga_{1-x}In_xAs$, $Al_{1-x}In_xAs$ and InP epitaxial layers prepared by metal organic chemical vapour deposition," J. Cryst. Growth 68, 319 (1984).

[32] D. Wake, A. W. Nelson, S. Cole, S. Wong, I. D. Henning, and E. G. Scott, "InGaAs/InP junction field-effect transistors with high transconductance made using metal organic vapor phase epitaxy," IEEE Electron Device Lett. EDL-6, 626 (1985).

[33] K. Fry, C. Kuo, R. Cohen, and G. Stringfellow, "Photoluminescence of OMVPE GaInAs," Appl. Phys. Lett. 46, 955 (1985).

[34] C. Hsu, R. Cohen, and G. Stringfellow, "OMVPE growth of InP using TMI," J. Cryst. Growth 63, 8 (1983).

[35] C. Hsu, R. Cohen, and G. Stringfellow, "OMVPE growth of InP using TMI," Proc. Electrochem. Soc. 83-13, 193 (1983).

[36] C. Hsu, R. Cohen, and G. Stringfellow, "OMVPE growth of InP using TMI," J. Cryst. Growth 62, 648 (1983).

[37] C. Kuo, J. Yuan, R. Cohen, J. Dunn, and G. Stringfellow, "OMVPE growth of high-purity GaInAs using TMI," Appl. Phys. Lett. 44, 550 (1984).

[38] C. Kuo, R. Cohen, and G. Stringfellow, "OMVPE growth of GaInAs," J. Cryst. Growth 64, 461 (1983).

[39] C. P. Kuo, R. M. Cohen, K. L. Fry, and G. B. Stringfellow, "Characterization of $Ga_xIn_{1-x}As$ grown with TMIn," J. Electron. Mater. 14, 231 (1985).

[40] S. Bass, C. Pickering, and M. Young, "MOVPE of InP," J. Cryst. Growth 64, 68 (1983).

[41] S. Bass and M. Young, "High quality epitaxial InP and indium alloys grown using TMI and phosphine in an atmospheric pressure reactor," J. Cryst. Growth 68, 311 (1984).

[42] S. J. Bass, S. J. Barnett, G. T. Brown N. G. Chew, A. G. Cullis, A. D. Pitt, and M. S. Skolnick, "Effect of growth temperature on the optical, electrical and crystallographic properties of epitaxial indium gallium arsenide grown by MOCVD in an atmospheric pressure reactor," J. Cryst. Growth 79, 378 (1986).

[43] S. J. Bass, M. S. Skolnick, H. Chudzynska, and L. Smith, "MOCVD of indium phosphide and indium gallium arsenide using trimethylindium-trimethylamine adducts," J. Cryst. Growth 75 221 (1986).

[44] R. F. C. Farrow, "The evaporation of InP under Knudsen (equilibrium) and Langmuir (free) evaporation conditions," J. Phys. D: 7, 2436 (1974).

[45] T. S. Moss, Optical Properties of Semiconductors, (Academic, New York, 1959), p. 13.

[46] T. P. Pearsall, L. Eaves, and J. C. Portal, "Photoluminescence and impurity concentration in $Ga_xIn_{1-x}As_yP_{1-y}$ alloys lattice-matched to InP," J. Appl. Phys. 54, 1037 (1983).

[47] Handbook of Optics, edited by W. G. Driscoll (McGraw-Hill, New York, 1978), p. 14-40.

[48] E. D. Towe and T. J. Zamerowski, "Properties of Zn-doped p-type $In_{0.53}Ga_{0.47}As$ grown by vapor phase epitaxy (VPE) on InP substrates," J. Electron. Mater. 11, 957 (1982).

[49] B. D. Joyce and E. W. Williams, "The preparation and photoluminescent properties of high purity vapour grown indium phosphide layers," Inst. Phys. Conf. Ser. No. 9, 57 (1971).

[50] E. W. Williams, W. Elder, M. G. Astles, M. Webb, J. B. Mullin, B. Straughan, and P. J. Tufton, "Indium phosphide 1. a photoluminescence materials study," J. Electrochem. Soc. 120, 1741 (1973).

[51] C. Pickering, P.R. Tapster, P.J. Dean, L. L. Taylor, P. L. Giles, and P. Davies, "Optical characterisation of acceptors in doped and undoped VPE InP," J. Cryst. Growth 64, 142 (1983).

[52] L. J. van der Pauw, "A method of measuring specific resistivity and Hall effect of discs of arbitrary shape," Philips Res. Rep. 13, 1 (1958).

[53] G. E. Stillman, C. M. Wolfe, and J. O. Dimmock, "Hall coefficient factor for polar mode scattering in n-type GaAs," J. Phys. Chem. Solids 31, 1199 (1970).

[54] M. Benzaquen, D. Walsh, and K. Mazuruk, "Hall factor of doped n-type GaAs and n-type InP," Phys. Rev. B: 34, 8947 (1986).

[55] T. Y. Wu and G. L. Pearson, "Phase diagram, crystal growth, and band structure of $In_xGa_{1-x}As$," J. Phys. Chem. Solids 33, 409 (1972).

[56] T. P. Pearsall, "$Ga_{0.47}In_{0.53}As$: a ternary semiconductor for photodetector applications," IEEE J. Quantum Electron. QE-16, 709 (1980).

[57] H. C. Casey and M. B. Panish, Heterostructure Lasers Part B, (Academic, New York, 1978).

[58] R. E. Nahory, M. A. Pollack, W. D. Johnston, and R. L. Barns, "Band gap versus composition and demonstration of Vegard's law for $In_{1-x}Ga_xAs_yP_{1-y}$ lattice matched to InP," Appl. Phys. Lett. 33, 659 (1978).

[59] K. -H. Goetz, D. Bimberg, H. Jurgensen, J. Selders, A. V. Solomonov, G. F. Glinskii, and M. Razeghi, "Optical and crystallographic properties and impurity incorporation of $Ga_xIn_{1-x}As$ ($0.44 < x < 0.49$) grown by liquid phase epitaxy, vapor phase epitaxy, and metal organic chemical vapor deposition," J. Appl. Phys. 54, 4543 (1983).

[60] P. Chandra, L. A. Coldren, and K. E. Strege, "Refractive index data from $Ga_xIn_{1-x}As_yP_{1-y}$ films," Electron. Lett. 17, 6 (1981).

[61] H. Burkhard, H. W. Dinges, and E. Kuphal, "Optical properties of $In_{1-x}Ga_xP_{1-y}As_y$, InP, GaAs, and GaP determined by ellipsometry," J. Appl. Phys. 53 655 (1982).

[62] E. Rabinowicz, An Introduction to Experimentation, (Addison-Wesley Reading, Mass., 1970), p.32.

[63] M. Born and E. Wolf, Principles of Optics, 4th ed. (Pergamon, Oxford, 1970), p. 324.

[64] Handbook of Mathematical Functions, edited by M. Abramowitz and I. Stegun (NBS, Washington, 1972), p. 81.

[65] M. M. Tashima, L. W. Cook, and G. E. Stillman, "The application of x-ray diffraction measurements in the growth of LPE InGaAs/InP," J. Cryst. Growth 54, 132 (1981).

[66] R. E. Enstrom, P. J. Zanzucchi, and J. R. Appert, "Optical properties of vapor-grown $In_xGa_{1-x}As$ epitaxial films on GaAs and $In_xGa_{1-x}P$ substrates," J. Appl. Phys. 45, 300 (1974).

[67] Y. Takeda, A. Sasaki, Y. Imamura, and T. Takagi, "Electron mobility and energy gap of $In_{0.53}Ga_{0.47}As$ on InP substrate," J. Appl. Phys. 47, 5405 (1976).

[68] R. J. Elliott, "Intensity of optical absorption by excitons," Phys. Rev. 108, 1384 (1957).

[69] E. Zielinski, H. Schweizer, K. Streubel, H. Eisele, and G. Weimann, "Excitonic transitions and exciton damping processes in InGaAs/InP," J. Appl. Phys. 59, 2196 (1986).

[70] E. V. K. Rao, A. Sibille, and N. Duhamel, "Investigation of process-induced defects in InP," Physica (Utrecht) 116B, 449 (1983).

[71] H. C. Casey and E. Buehler, "Evidence for low surface recombination velocity on n-type InP," Appl. Phys. Lett. 30, 247 (1977).

[72] D. J. Ashen, P. J. Dean, D. T. J. Hurle, J. B. Mullin, A. M. White, and P. D. Greene, "The incorporation and characterisation of acceptors in epitaxial GaAs," J. Phys. Chem. Solids 36, 1041 (1975).

[73] O. Roder, U. Heim, and M. H. Pilkuhn, "Electron mobilities and photoluminescence of solution grown indium phosphide single crystals," J. Phys. Chem. Solids 31, 2625 (1970).

[74] P. W. Yu, "A model for the 1.10 eV emission band in InP," Solid State Commun. 34, 183 (1980).

[75] J. B. Mullin, A. Royle, B. W. Straughan, P. J. Tufton, and E. W. Williams, "Crystal growth and properties of Group IV doped indium phosphide," J. Cryst. Growth 13/14, 640 (1972).

[76] L. J. Giling, "Gas flow patterns in horizontal epitaxial reactor cells observed by interference holography," J. Electrochem. Soc. 129, 634 (1982).

[77] D. H. Reep and S. K. Ghandi, "Deposition of GaAs epitaxial layers by organometallic CVD," J. Electrochem. Soc. 130, 675 (1983).

[78] G. E. Stillman, C. M. Wolfe, and J. O. Dimmock, "Hall coefficient factor for polar mode scattering in n-type GaAs," J. Phys. Chem. Solids 31, 1199 (1970).

[79] L. D. Zhu, K. T. Chan, and J. M. Ballantyne, "Very high mobility InP grown by low pressure metalorganic vapor phase epitaxy using solid trimethylindium source," Appl. Phys. Lett. 47, 47 (1985).

[80] A. H. Moore, M. D. Scott, J. I. Davies, D. C. Bradley, M. M. Faktor, and H. Chudzynska, "High mobility InP epitaxial layers prepared by atmospheric pressure MOVPE using trimethylindium dissociated from an adduct with 1,2-bis(diphenyl phosphino) ethane," J. Cryst. Growth 77, 19 (1986).

[81] G. E. Stillman, L. W. Cook, T. J. Roth, T. S. Low, and B. J. Skromme, "High purity material," in GaInAsP Alloy Semiconductors, edited by T. P. Pearsall (John Wiley & Sons, New York, 1982), p. 147.

[82] W. Walukiewicz, J. Lagowski, L. Jastrzebski, P. Rava, H. C. Gatos, M. Lichtensteiger, and C. H. Gatos, "Electron mobility and free-carrier absorption in InP; determination of the compensation ratio," J. Appl. Phys. 51, 2659 (1980).

[83] A. C. Jones, P. R. Jacobs, R. Cafferty, M. D. Scott, A. H. Moore, and P. J. Wright, "Analysis of high purity metalorganics by ICP emission spectrometry," J. Cryst. Growth 77, 47 (1986).

[84] D. H. Reep and S. K. Ghandi, "Electrical properties of organo-metallic chemical vapor deposited GaAs epitaxial layers," J. Electrochem. Soc. 131, 2697 (1984).

[85] J. S. Blakemore, "Semiconducting and other major properties of gallium arsenide," J. Appl. Phys. 53, R123 (1982).

[86] K. Hess, N. Stath, and K. W. Benz, "Liquid phase epitaxy of InP," J. Electrochem. Soc. 121, 1208 (1974).

[87] J. C. Paris, M. Gauneau, H. L'Haridon, and G. Pelous, "Effects of annealing on unintentionally doped LEC InP," J. Cryst. Growth 64, 137 (1983).

[88] T. Kamijoh, H. Takano, and M. Sakuta, "Heat treatment of semi-insulating InP:Fe with phosphosilicate glass encapsulation," J. Appl. Phys. 55, 3756 (1984).

[89] R. E. Hollingsworth, and J. R. Sites, "Photoluminescence dead layer in p-type InP," J. Appl. Phys. 53, 5357 (1982).

[90] H. Nagai, and Y. Noguchi, "Surface-treatment effect on photoluminescence of InP," J. Appl. Phys. 50, 544 (1979).

[91] G. S. Pomrenke, "Evidence of amphoteric behavior of Si in VPE InP," J. Cryst. Growth 64, 158 (1983).

[92] N. Duhamel, E. V. K. Rao, M. Gauneau, H. Thibierge, and A. Mircea, "Silicon implantation in semi-insulating bulk InP; electrical and photoluminescence measurements," J. Cryst. Growth 64, 186 (1983).

[93] K. J. Bachmann, "Properties, preparation, and device applications of indium phosphide," Ann. Rev. Mater. Sci. 11, 441 (1981).

[94] Growth and Characterization of InP (First NATO workshop on InP), edited by J. K. Kennedy, J. Cryst. Growth 54 (1)(1981).

[95] Materials Aspects of InP (Second NATO workshop on InP), edited by B. Cackayne, J. Cryst. Growth 64 (1) (1983).

[96] F. R. Bacher and W. B. Leigh, "Photoluminescence study of magnesium doped MOVPE indium phosphide," J. Cryst. Growth 80 456 (1987).

[97] A. W. Nelson and L. D. Westbrook, "A study of p-type dopants for InP grown by adduct MOVPE," J. Cryst. Growth 68, 102 (1984).

[98] C. R. Lewis, W. T. Dietze and M. J. Ludowise, "The growth of magnesium-doped GaAs by the OM-VPE process," J. Electron. Mater. 12, 507 (1983).

[99] R. R. Bradley, R. M. Ash, N. W. Forbes, R. J. M. Griffiths, D. P. Jebb, and H. E. Shephard, "Metalorganic chemical vapour deposition of junction isolated GaAsAs/GaAs LED structures," J. Cryst. Growth 77, 629 (1986).

[100] K. J. Bachmann, E. Buehler, B. I. Miller, J. H. McFee, and F. A. Thiel, "The current status of the preparation of single crystals, bicrystals, and epitaxial layers of p-InP and of polycyrstalline p-InP films for photovoltaic applications," J. Cryst. Growth 39, 137 (1977).

[101] D. Barthruff and H. Haspeklo, "Excited states of shallow acceptors in InP," J. Lumin. 24/25, 181 (1981).

[102] E. Kubota, Y. Ohmori, and K. Sugii, "Electrical and optical properties of Mg-, Ca-, and Zn-doped InP crystals grown by the synthesis, solute diffusion technique," J. Appl. Phys. 55, 3779 (1984).

[103] G. S. Pomrenke, Y. S. Park, and R. L. Hengehold, "Photoluminescence from Mg-implanted, epitaxial, and semi-insulating InP," J. Appl. Phys. 52, 969 (1981).

[104] S. J. Bass and P. E. Oliver, "Controlled doping of gallium arsenide produced by vapour epitaxy, using trimethylgallium and arsine," Inst. Phys. Conf. Ser. No. 33b, 1 (1977).

[105] V. Swaminathan, V. M. Donnelly, and J. Long, "A photoluminescence study of Cd-related centers in InP," J. Appl. Phys. 58, 4565 (1985).

[106] H. Burkhard, E. Kuphal, F. Kuchar, and R. Meisels, "Donor-acceptor pair recombination from donor ground and first excited states in InP," Inst. Phys. Conf. Ser. No. 56, 659 (1981).

[107] E. Zacks and A. Halperin, "Dependence of the peak energy of the pair-photoluminescence band on excitation intensity," Phys. Rev. B 6, 3072 (1972).

[108] T. Yagi, Y. Fujiwara, T. Nishino, and Y. Hamakama, "Photoluminescence and lattice mismatch in InGaAs/InP," Jpn. J. Appl. Phys. 22, L467 (1983).

[109] K.-H. Goetz, D. Bimberg, K.-A. Brauchle, H. Jurgensen, J. Selders, M. Razeghi, and E. Kuphal, "Deep Fe and intrinsic defect levels in $Ga_{0.47}In_{0.53}As$/InP," Appl. Phys. Lett. 46, 277 (1985).

[110] C. P. Kuo, S. K. Vong, R. M. Cohen, and G. B. Stringfellow, "Effect of mismatch strain on band gap in III-V semiconductors," J. Appl. Phys. 57, 5428 (1985).

[111] D. A. Humphreys, R. J. King, D. Jenkins, and A. J. Moseley, "Measurement of absorption coefficients of $Ga_{0.47}In_{0.53}As$ over the wavelength range 1.0-1.7 μm," Electron. Lett. 21, 1187 (1985).

[112] D. D. Sell and H. C. Casey, "Optical absorption and photoluminescence studies of thin GaAs layers in GaAs-$Al_xGa_{1-x}As$ double heterostructures," J. Appl. Phys. 45, 800 (1974).

[113] W. J. Turner, W. E. Reese, and G. D. Pettit, "Exciton absorption and emission in InP," Phys. Rev. 136, A1467 (1964).

[114] Y. Yamazoe, T. Nishino, and Y. Hamakawa, "Electroreflectance study of InGaAsP quaternary alloys lattice matched to InP," IEEE J. Quantum Electron. QE-17, 139 (1981).

[115] T. P. Pearsall, G. Beuchet, J. P. Hirtz, N. Visentin, M. Bonnet, and A. Roizes, "Electron and hole mobilities in $Ga_{0.47}In_{0.53}As$," Inst. Phys. Conf. Ser. No. 56, 639 (1981).

[116] R. Saxena, V. Sardi, J. Oberstar, L. Hodge, M. Keever, G. Trott, K. L. Chen, and R. Moon, "OMVPE growth of InGaAsP materials for long wavelength detectors and emitters," J. Cryst. Growth 77, 591 (1986).

[117] K. W. Carey, S. Y. Wang, R. Hull, J. E. Turner, D. Oertel, R. Bauer, and D. Bimberg, "Characterization of InP/GaInAs/InP heterostructures grown by organometallic vapor phase epitaxy for high-speed p-i-n photodiodes," J. Cryst. Growth 77, 558 (1986).

APPENDIX A

OHMIC CONTACT PREPARATION

For n-type GaAs or InP samples, the method for making contacts was as follows: 1) evaporate AuGe alloy (88% Au, 12% Ge by weight), 2) anneal at 390 °C for 2 minutes in an Ar atmosphere, 3) rub In dots onto the contacts, 4) anneal in Ar at 200 °C for 30 seconds, 5) epoxy a thin Cu wire, 6) bake in air at 150 °C for 30 minutes. The contact resistance of the wire-to-indium joint thus formed was typically 2 Ohms; silver paste was occasionally used to bridge poor contacts.

If neither rigid wire connection or cryogenic operation was necessary, InGa alloy (70% In, 30% Ga by weight) was found to make good contact to GaAs.

For InGaAs, the same procedure as above was followed, except that steps 1) and 2) were omitted. For p-type samples, the above procedure was followed, except that AuZn alloy was used instead of AuGe (75% Au, 25% Zn by weight). The AuZn material was made at OGC by annealing gold and zinc together at 900 °C in a quartz ampul for 3 hours.

For evaporation, 35 mg of metal were used. The source was 4 cm from the sample, and a shutter blocked the sample until evaporation began. The sample was covered by a mask with four 0.75 mm diameter holes separated by 2.5 mm in a square pattern. The sample was allowed to cool prior to exposure to air.

All contacts were verified to have a linear current/voltage rela-

tionship continuously through positive and negative current values in the region of measurement for Hall mobility (usually less than 1 mA), using a Tektronix 576 curve tracer.

APPENDIX B

EPILAYER THICKNESS MEASUREMENT

Several methods were used to measure thickness of epitaxial layers. All methods involved selective etching of the substrate. The etchant used for GaAs and InP epilayers was ferricyanide: 12 g $K_3Fe(CN)_6$ + 8 g KOH in 100 ml H_2O. Ferricyanide etches a semi-insulating substrate at a different rate from the n-type epilayer. For InGaAs/InP, 40% HCl was used to etch InP, leaving the InGaAs layer undisturbed.

The procedure for delineating the layers was: 1) cleave the sample cleanly along a plane perpendicular to the growth surface, 2) mount the sample on a small piece of microscope slide using clay, with the freshly cleaved edge up (GE #7031 varnish was used for HCl etches), 3) etch for 60 seconds under a microscope illuminator (15 s for InGaAs), 4) rinse in H_2O, 5) mount under the Zeiss light microscope.

An eyepiece scale accompanies this microscope. The scale was calibrated with a variety of millimeter scale rules, including one with half-millimeter markings. Thus "one" on the Zeiss scale was determined to equal 0.061 mm at 128X and 0.0244 mm at 320X. The error in this measurement was estimated to be $\pm$ 0.01 "Zeiss units", or $\pm$ 0.25 microns at 320X.

The epilayer could be visually delineated by noting a dark line separating the layer from the substrate. InGaAs layers could be seen

quite easily, GaAs and InP with more difficulty. On InGaAs/InP samples, cracks or etch lines in the substrate could occasionally be seen begining at the interface and leading away at random angles.

An independent method for measuring InGaAs thickness utilized the interference of multiple coherent reflections of monochromatic light. For energies below the bandgap, InGaAs layers with the InP substrate removed functioned as Fabry-Perot etalons: minima and maxima could easily be observed in their light transmission versus wavelength plots. Then thickness = $t = m\lambda/2n_t$ for normal incidence, with m the order of successive maxima and n_t the InGaAs refractive index found in Chapter III. To find m, the wavelengths of several maxima (m, m + 1, etc.) are compared, using the appropriate value of n_t for each.

APPENDIX C

TABLE XIII. 77 K FWHM versus Net Carrier Concentration: Raw Data From the Literature.

Reference	Material	$\lvert N_D - N_A \rvert$ (cm^{-3})	PL FWHM (meV)
[46]	$In_{0.53}Ga_{0.47}As$:Zn	1×10^{16}	11
		1×10^{18}	32
[48]	$In_{0.53}Ga_{0.47}As$:Zn	4×10^{17}	19
		1.3×10^{18}	33
		2.2×10^{18}	31
		6.5×10^{18}	38
		2×10^{19}	40
		2.7×10^{19}	53
		3.7×10^{19}	62
[49]	InP:Cr	1.2×10^{16}	11
		2.5×10^{16}	16
		3×10^{16}	13
		5×10^{16}	18
		7×10^{16}	15
		1.4×10^{17}	19
[49]	InP:Sn	5×10^{17}	35
		9×10^{17}	35
		1.5×10^{18}	50
[50]	InP:Zn	1.2×10^{16}	16
		1.9×10^{16}	17
		6×10^{16}	21
		7×10^{16}	19
		1.6×10^{17}	17
		2.6×10^{17}	20
		3.7×10^{17}	25
		8×10^{17}	21, 26, 29
		1.4×10^{18}	30
		2.1×10^{18}	30
		2.4×10^{18}	33, 35
		5×10^{18}	65
		5×10^{18}	65

APPENDIX D

RAW SIMS DATA FOR InGaAs/InP LAYERS

The data from SIMS analysis performed on InGaAs 65 and OSU 1-29-7-86 are summarized in Table X of Chapter VI. Presented here in Figs. 43-6 are concentration (in atoms/cc) versus depth profiles as provided by Charles Evans & Assoc. There are two profiles for each sample, one Cs beam and one O beam. (The SIMS conditions were discussed in Chapter III.)

The horizontal scale on these figures was calibrated using the thickness determined by interference effects observed in optical absorption testing. At least two isotopes per element were monitored for S, Si, Cu, Zn, and Hg to check for possible molecular ion interference. The lower curve for each element is presumed to be the most accurate.

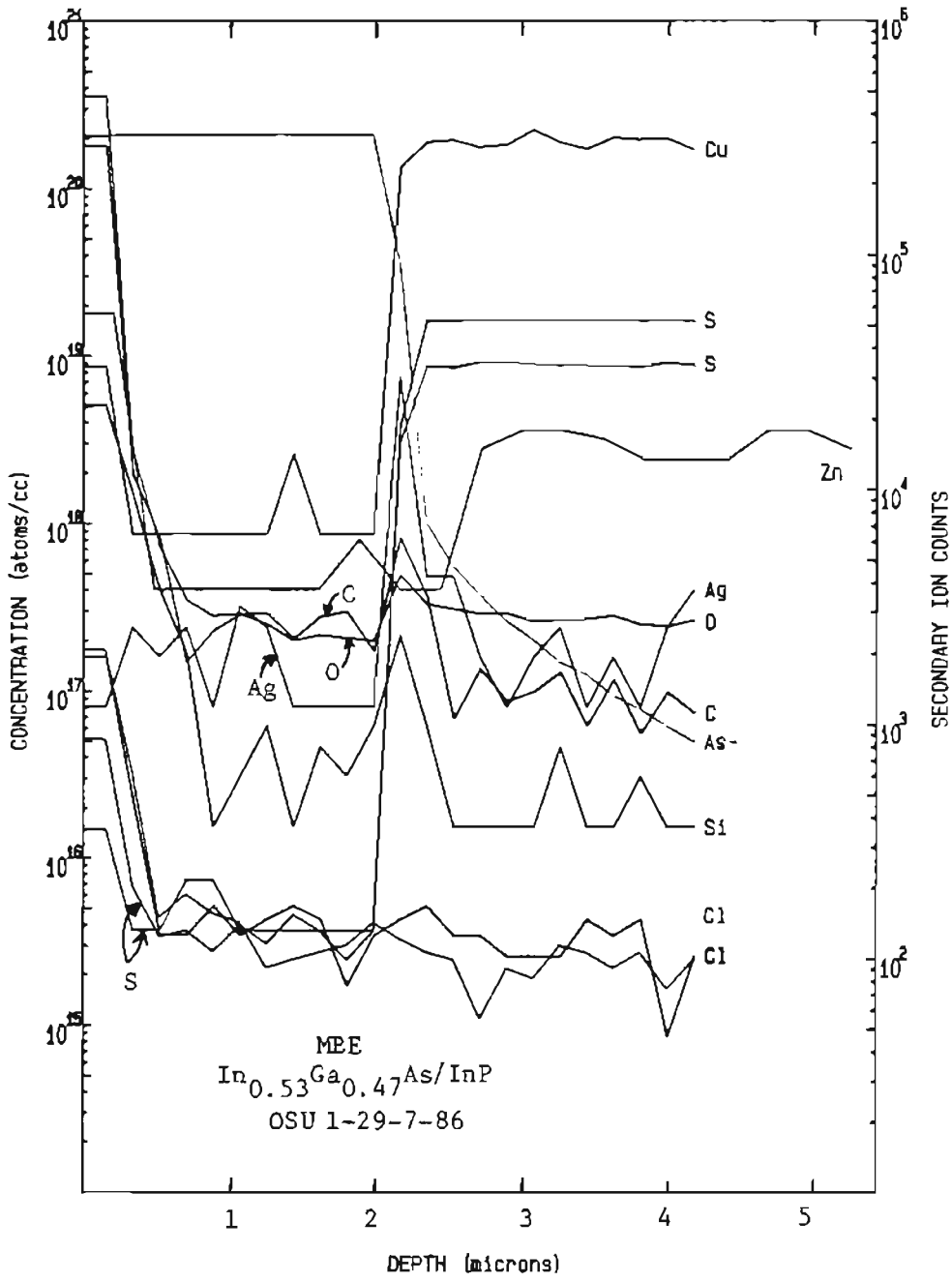

FIG. 43. Cs Beam SIMS Data for MBE $In_{0.53}Ga_{0.47}As$. Right scale applies to As only.

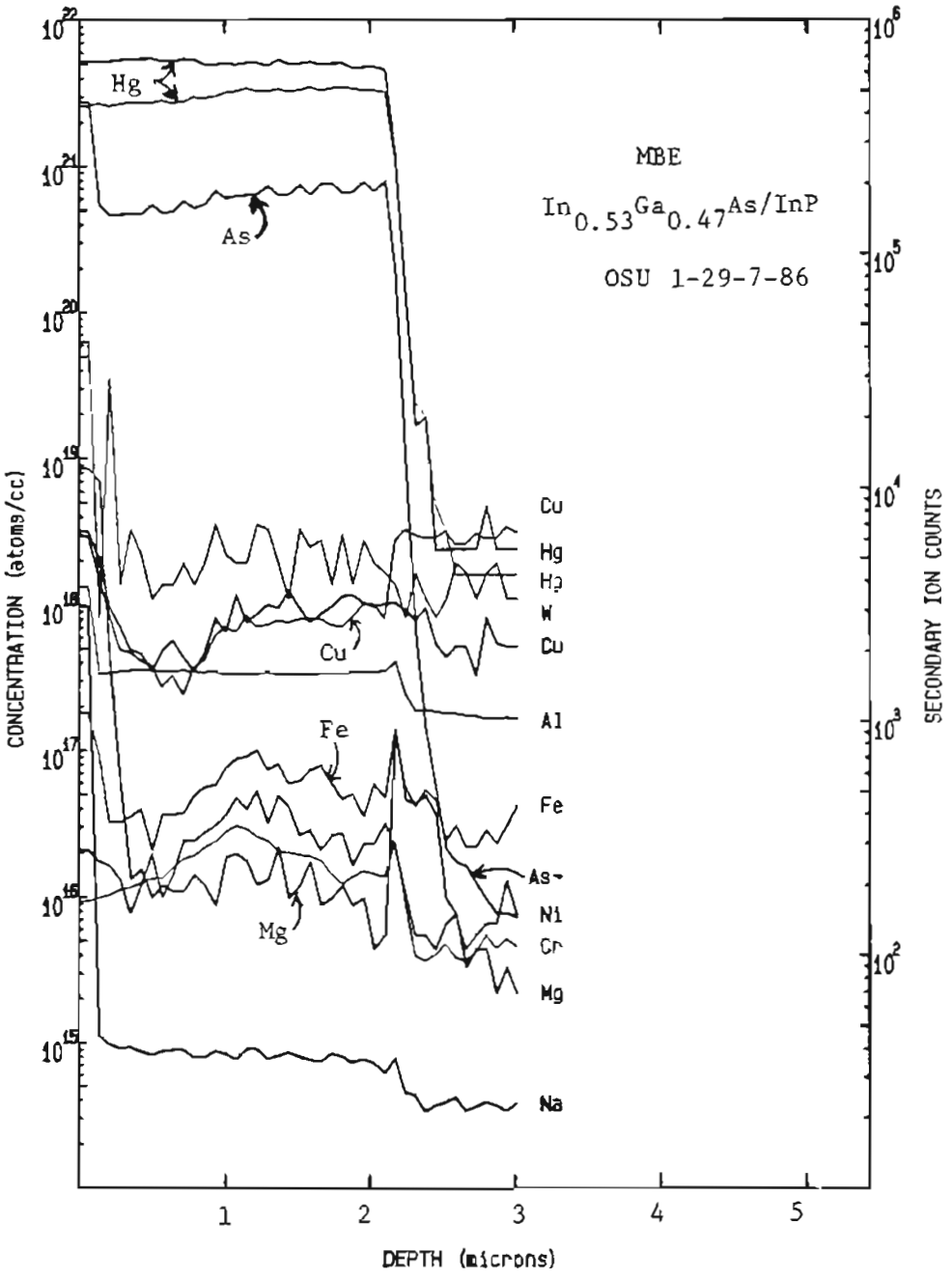

FIG. 44. O Beam SIMS Data for MBE $In_{0.53}Ga_{0.47}As$. Right scale applies to As only.

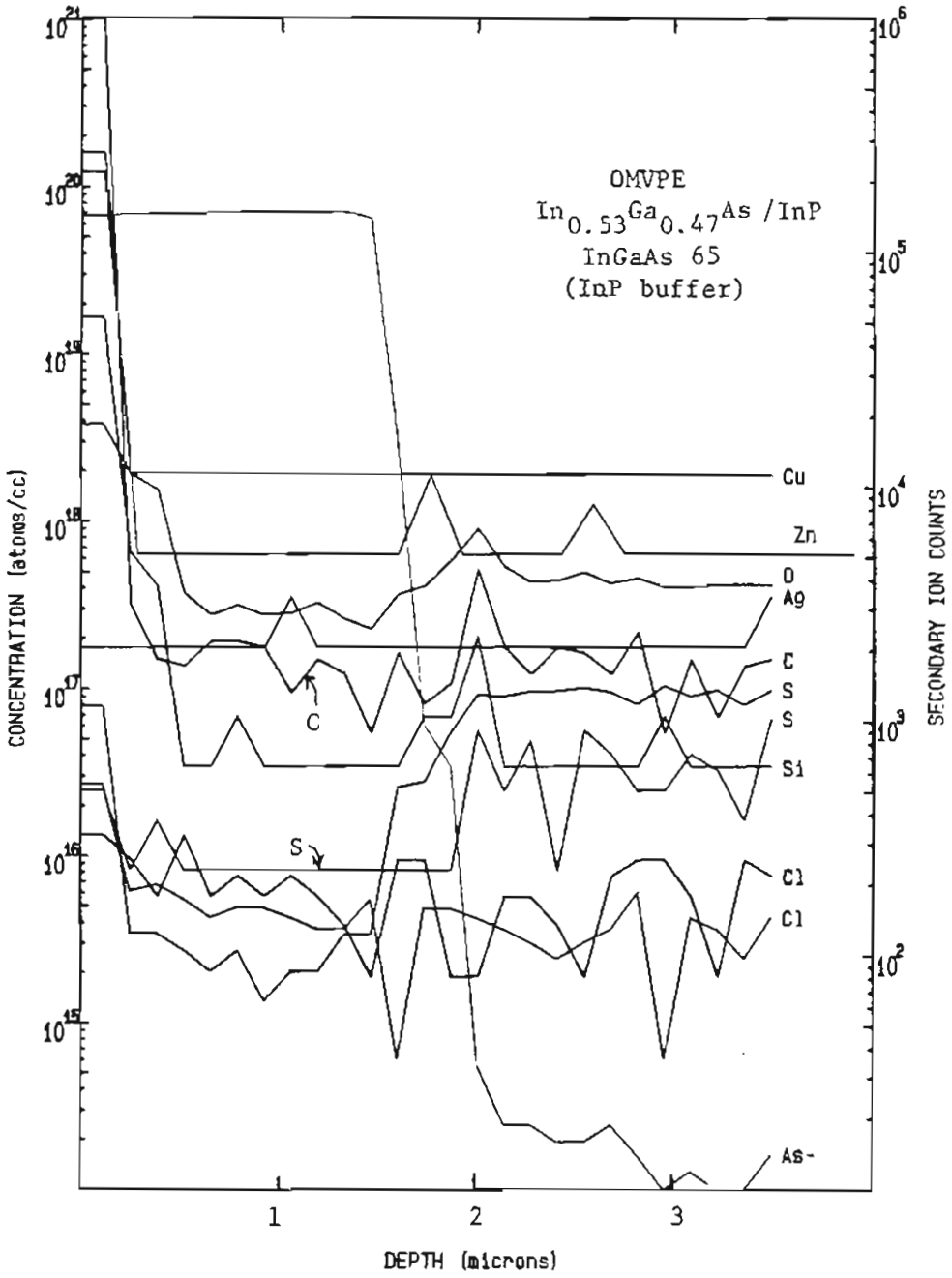

FIG. 45. Cs Beam SIMS Data for OMVPE $In_{0.53}Ga_{0.47}As$. Right scale applies to As only.

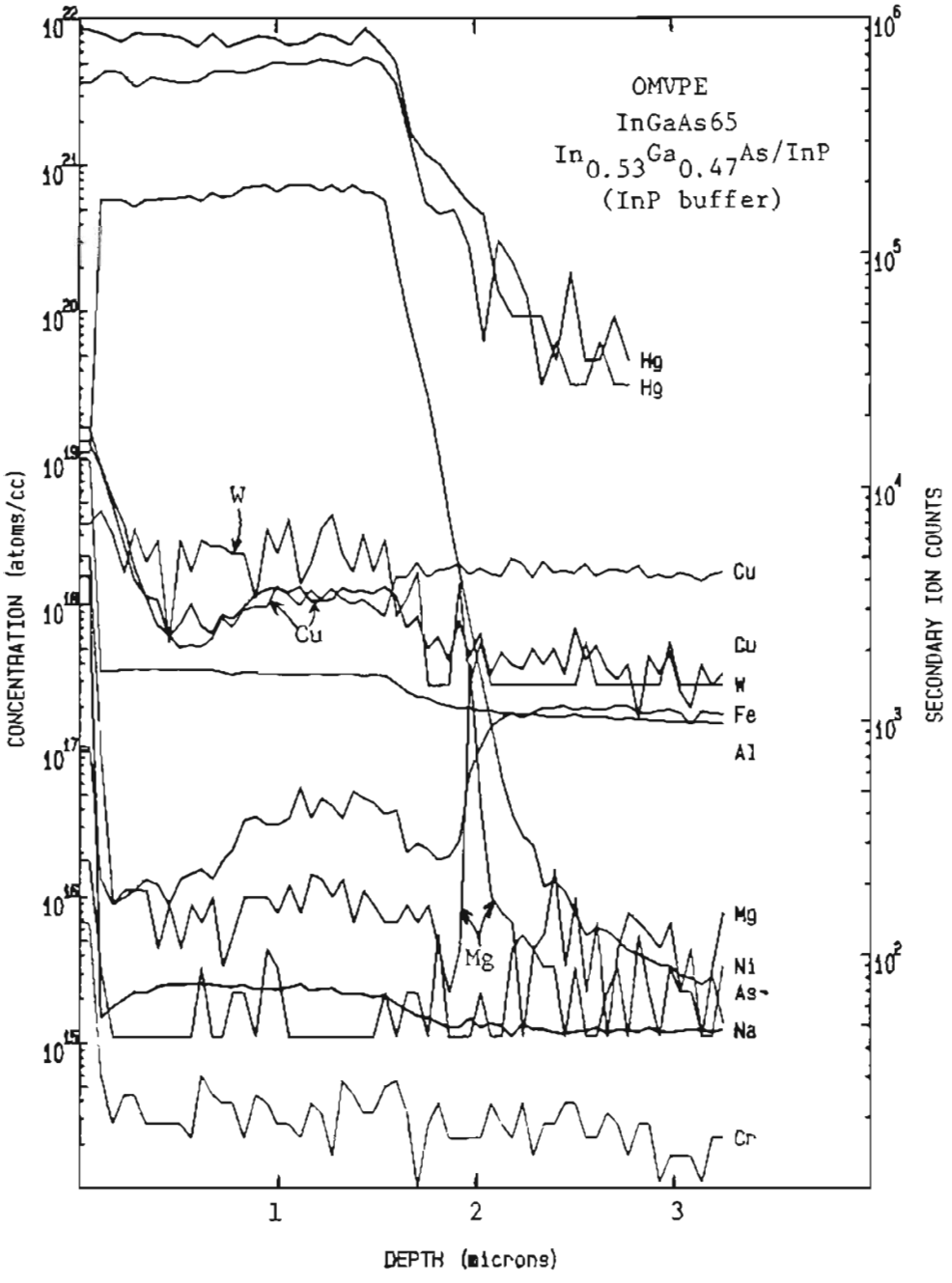

FIG. 46. O Beam SIMS Data for OMVPE $In_{0.53}Ga_{0.47}As$. Right scale applies to As only.

APPENDIX E

TABLE XIV. List of chemicals and equipment.

Item	Manufacturer & model #	Comments
PHOTOLUMINESCENCE:		
275 mm monochromator	Jarrell Ash, Mark X 82462	f/3.85, 6 nm/mm slit dispersion, 600/mm grating
PbS detector	Hammamatsu	
Ar^+ ion laser	Coherent Radiation Labs 52	514.5 nm, 150 mT
cryostat	MMR Technologies R2105	1 mm sapphire window
temperature indic.	MMR Technologies K-77	
amplifier	Tektronix AM 502	
x-y recorder	Houston Instrument 2000	
lock-in amplifier	EG&G Princeton Applied Res. 5105	810 Hz
vacuum pump	VacTorr 100	
N_2 pump	Thomas Industries 107CA18	
Si filter	262C	1.5 mm, polished
glass filter	Bausch & Lomb 780 nm	
HALL MOBILITY:		
voltmeter	Keithly 619	
current source	Keithly 220	
scanner	Keithly 705	
6" electromagnet	Alpha Scientific 6002	
temp. controller	MMR Technologies K-20	
cryostat	MMR Technologies R2105	
IEEE bus control	Apple IIe	
vacuum pump	Edwards 2 stage	
gaussmeter	Bell Inc. 615	

TABLE XIV. (cont.)

OMVPE CRYSTAL GROWTH:		
vacuum leak checker	Alcatel ASM 10	He to 10^{-8} T
H_2 purifier	Johnson Matthy HP-25	
rf generator	Lepel T-5-3-KC-A-B	7.5 kW, 100 kHz
N_2 filter (glove box)	Millipore N66	0.2 micron
heat tape	Thermolyne	
heat tape controller	YSI 72	
N_2 (glove box)	Air Products pre-purified	2-3 ppm O_2, 10-5 ppm H_2O
H_2	Air Products UHP grade	2 ppm O_2, 3.5 ppm H_2O
N_2	Air Products UPC grade	1 ppm O_2, 1 ppm H_2O
temperature baths	Neslab RTE 9DD	rated $\pm$ 0.01 °C
mass flow control	Unit Instruments UFC-1000	rated $\pm$ 0.2% of full scl.
rf/oven controller	Watlow series 859	
gas regulators	Veriflow TDR 450	
gas filters	David J. Tripp Assoc. TEM	
trimethylindium	Alfa Products 87958	6.6 ppm Si
trimethylgallium	Alfa Products	
Cp_2Mg	Strem Chemical	
arsine	Phoenix Research	10% in H_2
phosphine	Phoenix Research NA 1953	10% in H_2
valves	Nupro SS-4BK-TW	
deionized H_2O	Continental Water Sys. 3218	0.2 micron, 17 megOhm
30% H_2O_2	General Chemical 109-003502	low particle grade
96% H_2SO_4	Baker 9673-1	trace metal analysis grade
37% HCl	Van Waters & Rogers UN 1789	microprocess grade
70% HNO_3	Van Waters & Rogers UN 2031	microprocess grade
99.5% TCE	American Burdick & Jackson MS80897	VLSI grade
99.5% $[CH_3]_2CO$	Van Waters & Rogers UN1090	microprocess grade
99.9% CH_3OH	Van Waters & Rogers	microprocess grade
clean bench	Envirco	class 10 tested 3/86

TABLE XIV. (cont.)

OPTICAL ABSORPTION:		
275 mm monochromator	Jarrell Ash, Mark X 82487	
PbS detector	Hammamatsu	
lock-in amplifier	EG&G Princeton Applied Res. 5101	810 Hz
amplifier	Tektronix AM 502	
Si filter	262C	1.5 mm, polished
glass filter	Bausch & Lomb 780 nm	
cryostat	Air Products Displex	temp. cal. $\pm$ 1 °C
x-y recorder	Hewlett Packard 7045B	zeroed with detector covered
tungsten lamp	Oriel	8 V
epoxy	Hardman transparent	24 hour cure
OHMIC CONTACTS:		
Mo evaporation boat	Balzers	
diffusion pump	CVC CVE-15	
Ag paste	DuPont 7941	
conductive epoxy	Epoxy Technology H31D	one-part
curve tracer	Tektronix 576	
THICKNESS MEASUREMENT:		
microscope	Zeiss 64702	
(see optical absorption apparatus)		

APPENDIX F

COMPUTER PROGRAMS

Two programs were used to speed the characterization effort. Table XV gives the full program for resistivity and Hall mobility measurement. This apparatus was controlled by the computer, except for N_2 cooling and the electromagnet, which were manually operated. The program is to be run once without any magnetic field, then Hall voltages are remeasured with the field on. The output is a printout of sample ID, set temperature, actual temperature, assumed thickness and magnetic field, sample/contact uniformity (F), resistivity, Hall mobility, carrier concentration, and conductivity type. The Hall factor is easily incorporated if desired. Figure 47 gives the flowchart for this program.

A second program was used to calculate optical absorption coefficients for InGaAs. The refractive index of InGaAs as a function of wavelength and temperature are written into the program. Figure 48 shows the flowchart, and Table XVI gives the program lines. When interference effects are included, the operator inputs absorption coefficient estimates which the computer uses to calculate a predicted transmission. The operator can then compare the measured transmission to this value and re-enter estimates until the best value of the absorption coefficient is obtained.

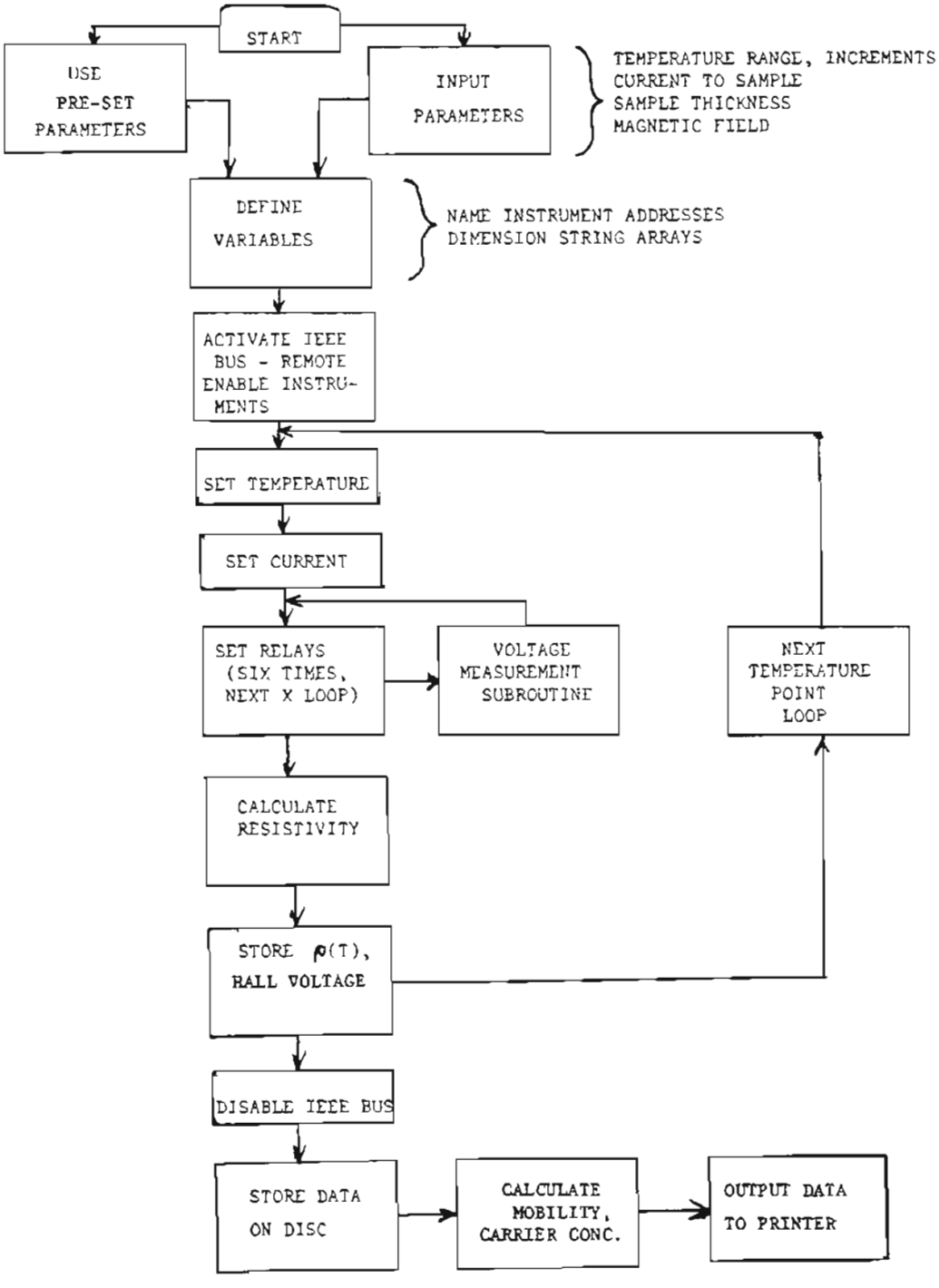

FIG. 47. Flowchart for Hall Mobility Measurement Program.

TABLE XV. Hall Mobility Measurement and Calculation Program.

Line # BASIC (DOS 3.3) Program Statement

```
10  CALL 1002
20 D$ =  CHR$ (4)
30  PRINT D$;"PR#3"
40  PRINT D$;"IN#0"
50  PRINT "      van der Pauw Resistivity/Hall Mobility measurement..."
60  PRINT "NOW' With SAMPLEFIX'      (Rev. 3/26/87)"
70  PRINT " "
80  PRINT "Enter sample identification (up to 20 characters, no commas).
    "
90  INPUT I$
100  IF I$ = "TEMPCONT" THEN  GOTO 210
110  PRINT "Enter thickness  (in microns)."
120  INPUT T
122  PRINT "Enter settle time (1000 = 1 sec.)"
124  INPUT TT
130  PRINT "Use Preset (PR) or Manual (MA) current  and temperature valu
    es?"
135  PRINT " "
140  PRINT "Presets:  I = .0005A, starting temp. is 78K, and 7 data poin
    ts are taken             30K apart up to 258K, assuming a 5000 Gauss
     magnetic field."
145  PRINT " "
150  PRINT "Type PR or MA."
160  INPUT T$
170  IF T$ = "PR" THEN  GOTO 1890
180  IF T$ = "MA" THEN  GOTO 1780
190  PRINT "TRY AGAIN"
200  GOTO 130
205  PRINT D$;"DELETE PATCH"
210 Z$ =  CHR$ (26)
220 A$ =  CHR$ (38)
230 B$ =  CHR$ (44)
240 C$ =  CHR$ (49)
250 P$ =  CHR$ (97)
260 Q$ =  CHR$ (42)
270 J$ =  CHR$ (74)
280 E$ =  CHR$ (98)
290 F$ =  CHR$ (70)
300  IF I$ = "TEMPCONT" THEN  GOTO 2620
310  PRINT "Is the magnet on?  (Type Y or N; if yes, only Hall data will
     be taken.)"
320  IF T$ = "PR" THEN  PRINT "MAGNETIC FIELD ASSUMED TO BE 5000 GAUSS."

330  INPUT S$
340  IF S$ = "N" THEN  GOTO 400
350  IF T$ = "PR" THEN  GOTO 380
360  PRINT "Enter magnetic field (in Gauss)."
370  INPUT C
375  IF  LEFT$ (I$,3) = "INP" THEN  GOTO 394
380  PRINT "Use Hall Factor correction? Type Y or N (for N, Hall Factor
    = 1.0)"
390  INPUT ZZ$
392  GOTO 400
394 ZZ$ = "N"
400  PRINT "Use temperature controller? (Type Y or N)"
410  INPUT U$
420  IF U$ = "N" THEN  GOTO 440
430  GOTO 2620
440  FOR Y = 1 TO J
450  CALL 1002
```

TABLE XV. (cont.)

```
460  PRINT D$;"PR#1"
470  PRINT D$;"IN#1"
480  PRINT "LF1"
490  IF U$ = "N" THEN  GOTO 710
500  ONERR  GOTO 520
510  PRINT "WT";Q$;Z$;"SK ";K
520  PRINT "RD";J$;Z$;
530  INPUT TA$
540  PRINT D$;"PR#3"
550  HOME
560  PRINT TA$
570  PRINT "Set temperature is ";K;", and this is measurement number ";Y
    ;" of ";J;"."
580  PRINT D$;"PR#1"
590  PRINT D$;"IN#1"
600  PRINT "LF1"
610  FOR B = 1 TO 30000: NEXT B
620  ONERR  GOTO 640
630  PRINT "WT";Q$;Z$;"TE"
640  PRINT "RD";J$;Z$;
650  INPUT TE$
660  PRINT D$;"PR#3"
670  PRINT "Actual temperature is ";TE$;" (set point ";K;", data point "
    ;Y;" of ";J;")."
680  PRINT D$;"PR#1"
690  PRINT D$;"IN#1"
700  PRINT "LF1"
710  PRINT "RM";B$;Z$
720  PRINT "RM";C$;Z$
730  PRINT "RM";A$;P$;Z$
740  PRINT "LL"
750  PRINT "WT";A$;P$;Z$;"F0R1T4P1C1Z0X"
760  PRINT "WT";A$;P$;Z$;"Z1X"
770  FOR B = 1 TO 1000: NEXT B
780  IF S$ = "Y" THEN  GOTO 1200
790  FOR X = 1 TO 2
800  PRINT "CL";C$;Z$
810  IF X = 1 THEN  PRINT "WT";C$;Z$;"B1C2C5C10C13C18X"
820  IF X = 2 THEN  PRINT "WT";C$;Z$;"B3C3C6C10C14C15X"
830  PRINT "WT";B$;Z$;"F1B1L1D0V100X";"I";I;"X"
840 R = 0
850  GOTO 1000
860  PRINT "WT";A$;P$;Z$;"F0R1T4C0Z0X"
870  FOR B = 1 TO TT: NEXT B
880  PRINT "RD";F$;P$;Z$;
890  INPUT " ";M$
900  FOR B = 1 TO 400: NEXT B
910  PRINT "UT"
920  FOR B = 1 TO 400: NEXT B
930  PRINT "WT";B$;Z$;"F0X"
940 M =  VAL ( MID$ (M$,5,16))
950 M =  ABS (M)
960 R = M / I + R
970  PRINT "WT";A$;P$;Z$;"F0R1C1X"
980  FOR B = 1 TO 500: NEXT B
990  RETURN
1000  GOSUB 2360
1010  PRINT "WT";B$;Z$;"F1X";"I-";I;"X"
1020  GOSUB 2360
1030  PRINT "CL";C$;Z$
1040  IF X = 1 THEN  PRINT "WT";C$;Z$;"B2C4C7C10C11C16X"
1050  IF X = 2 THEN  PRINT "WT";C$;Z$;"B4C1C8C10C12C17X"
```

```
1060  PRINT "WT";B$;Z$;"F1X"
1070  GOSUB 2360
1080  PRINT "WT";B$;Z$;"F1X";"I";I;"X"
1090  GOSUB 2360
1100  IF X = 1 THEN S = R / 4
1110  IF X = 2 THEN R = R / 4
1120  NEXT X
1130 F = 1 - .34657 * ((R - S) / (R + S)) ^ 2 - .092358 * ((R - S) / (R +
    S)) ^ 4
1140 R = .000226622 * F * (R + S) * T
1200  PRINT "CL";C$;Z$
1210  PRINT "WT";C$;Z$;"B5C3C5C10C12C18X"
1220  PRINT "WT";B$;Z$;"F1B1L1D0V100X";"I";I;"X"
1230  GOSUB 2440
1240 ZA$ = W$
1250  PRINT "WT";B$;Z$;"F1X";"I-";I;"X"
1260  GOSUB 2440
1270 ZB$ = W$
1280  PRINT "CL";C$;Z$
1290  PRINT "WT";C$;Z$;"B6C4C6C10C11C17X"
1300  PRINT "WT";B$;Z$;"F1X"
1310  GOSUB 2440
1320 ZC$ = W$
1330  PRINT "WT";B$;Z$;"F1X";"I";I;"X"
1340  GOSUB 2440
1350 ZD$ = W$
1370  ONERR  GOTO 1390
1380  IF Y = J THEN  PRINT "WT";Q$;Z$;"SR 000.00"
1390  PRINT "RD";J$;Z$;
1400  INPUT TA$
1415 YY = 100 + Y
1420  PRINT "WT";C$;Z$;"R0X"
1430  IF Y = J THEN  PRINT "LA"
1440  PRINT D$;"PR#3"
1450  PRINT D$;"IN#0"
1460  CALL 1002
1470  PRINT D$;"OPEN PATCH,L100"
1480  IF S$ = "Y" THEN  GOTO 1710
1490  PRINT D$;"WRITE PATCH,R";Y
1500  PRINT K
1510  PRINT A
1520  PRINT ZA$
1530  PRINT ZB$
1540  PRINT ZC$
1550  PRINT ZD$
1560  PRINT D$;"CLOSE PATCH"
1570  IF U$ = "N" THEN  GOTO 1605
1580  PRINT D$;"PR#4"
1591  IF Y > 1 THEN  GOTO 1600
1592  IF S$ = "N" THEN  PRINT "With magnet off, actual temps were:"
1594  IF S$ = "Y" THEN  PRINT "Magnet on:"
1600  PRINT TE$
1605 K = K + A
1610  NEXT Y
1620  PRINT D$;"PR#3"
1630  PRINT "Measurement complete."
1640  PRINT "To rerun type RE, to calculate type CA, to end type EN."
1650  INPUT O$
```

TABLE XV. (cont.)

```
1660  IF O$ = "RE" THEN  GOTO 2370
1670  IF O$ = "CA" THEN  GOTO 1950
1680  IF O$ = "EN" THEN  END
1690  PRINT "TRY AGAIN"
1700  GOTO 1630
1710  PRINT D$;"WRITE PATCH,R";YY
1720  PRINT ZA$
1730  PRINT ZB$
1740  PRINT ZC$
1750  PRINT ZD$
1760  PRINT D$;"CLOSE PATCH"
1770  GOTO 1570
1780  PRINT "Enter current (in Amps, 0.1 A max)."
1790  INPUT I
1800  PRINT "Enter starting temperature (in Kelvins)."
1810  INPUT K
1830  PRINT "Enter number of data points desired."
1840  INPUT J
1850  IF J = 1 THEN  GOTO 205
1860  PRINT "Enter temperature increments (in Kelvins, XX.XX < 50.00K)."

1870  INPUT A
1880  GOTO 205
1890 I = .0005
1900 K = 78.01
1910 A = 30.00
1920 C = 5000
1930 J = 7
1940  GOTO 205
1950  FOR P = 1 TO J
1955 PP = 100 + P
1960  ONERR  GOTO 2390
1970  CALL 1002
1980  PRINT D$;"OPEN PATCH,L100"
1990  PRINT D$;"READ PATCH,R";P
2000  INPUT AA,AB,AC,AD,AE,AF
2002  PRINT D$;"READ PATCH,R";PP
2004  INPUT AG,AH,AI,AJ
2010  PRINT D$;"CLOSE PATCH"
2016  IF AG > AC AND AI > AE AND AH < AD AND AJ < AF THEN ZN$ = "p-type
    sample"
2018  IF AH > AD AND AJ > AF AND AG < AC AND AI < AE THEN ZN$ = "n-type
    sample"
2019  IF ZN$ <  > "n-type sample" AND ZN$ <  > "p-type sample" THEN ZN$ =
    "Indeterminate"
2030 V = ( ABS (AC - AG) +  ABS (AD - AH) +  ABS (AE - AI) +  ABS (AF -
    AJ)) / 4
2040 V = (T * 10000 * V) / (C * AB)
2050 ZA = (1.6022E - 19 * V * AB) ^  - 1
2055 AZ = 1.0
2060  IF ZZ$ = "N" THEN  GOTO 2190
2065  IF AA > 250 THEN AZ = AZ * (.9 + (60.4 / AA))
2070  IF AA <  = 250 AND AA >  = 150 THEN AZ = AZ * 1.155
2075  IF AA < 150 THEN AZ = AZ * (1.265 - (18.61 / AA))
2077 ZA = ZA * AZ
2190  PRINT D$;"PR#3"
2200  PRINT D$;"PR#4"
```

TABLE XV. (cont.)

```
2210  IF P = 1 THEN  PRINT "SAMPLE ";I$;"   ";"Field was  ";C;" Gauss, t
    hickness ";T;" microns."
2212  IF P = 1 THEN  PRINT " "
2213  IF P = 1 THEN  PRINT "I = ";I
2214  IF P = 1 THEN  PRINT "For the last data point:"
2215  IF P = 1 THEN  PRINT "F = ";F;"      ";"Hall Factor = ";AZ
2220  IF P = 1 THEN  PRINT " "
2230  IF P = 1 THEN  PRINT "TEMP";"      ";"RESISTIVITY";"    ";"MOBILITY"
    ;"    ";"CARRIER CONCENTRATION"
2240  IF P = 1 THEN  PRINT " K          Ohmcm        cm^2/Vs          cm^-3
    "
2250  IF P = 1 THEN  PRINT " "
2260  PRINT AA;"    ";AB;"     ";V;"     ";ZA;"    ";ZN$
2270  IF P = 5 THEN  PRINT " "
2280  IF P = 10 THEN  PRINT " "
2290  IF P = 15 THEN  PRINT " "
2300  IF P = 20 THEN  PRINT " "
2310  NEXT P
2312  PRINT " "
2313  PRINT " "
2314  PRINT " "
2315  PRINT " "
2316  PRINT " "
2320  PRINT D$;"PR#3"
2330  PRINT " "
2340  PRINT "end."
2350  END
2360  GOTO 860
2370 K = K - (A * J)
2380  GOTO 310
2390  PRINT D$;"PR#3"
2400  PRINT "END OF DATA...CHECK DISC"
2410  CALL 1002
2420  PRINT D$;"CLOSE PATCH"
2430  GOTO 2350
2440  PRINT "WT";A$;P$;Z$;"F0R1T4C0Z0X"
2450  FOR B = 1 TO TT: NEXT B
2460  PRINT "RD";F$;P$;Z$;
2470  INPUT " ";M$
2480  FOR B = 1 TO 400: NEXT B
2490  PRINT "UT"
2500  FOR B = 1 TO 400: NEXT B
2510  PRINT "WT";B$;Z$;"F0X"
2520 M =  VAL ( MID$ (M$,5,16))
2530 W = M / I
2540 W$ =  STR$ (W)
2550  IF  LEN (W$) = 1 THEN W$ = W$ + ".000"
2590  PRINT "WT";A$;P$;Z$;"F0R1C1X"
2600  FOR B = 1 TO 500: NEXT B
2610  RETURN
2620  HOME
2630  CALL 1002
2635  PRINT " "
2640  PRINT "     Temperature controller subroutine"
2650  PRINT " "
2660  PRINT "Enter Command:"
2670  PRINT "         TE = Current temperature?"
2680  PRINT "         WK = Current set temperature?"
2690  PRINT " SK NNN.NN = Sets temp. to NNN.NN"
2700  PRINT "         VA = Current vacuum?"
```

TABLE XV. (cont.)

```
2710  PRINT "         EX = Exits from subroutine"
2720  PRINT "         EN = Ends program"
2730  INPUT CO$
2740  IF CO$ = "EN" THEN  END
2750  IF CO$ = "EX" THEN  GOTO 440
2760  ONERR  GOTO 2810
2770  PRINT D$;"PR#1"
2780  PRINT D$;"IN#1"
2790  PRINT "LF1"
2800  PRINT "WT";O$;Z$;CO$
2810  PRINT "RD";J$;Z$;
2820  INPUT CI$
2830  PRINT D$;"PR#3"
2840  PRINT D$;"IN#0"
2850  PRINT CI$
2860  GOTO 2635
```

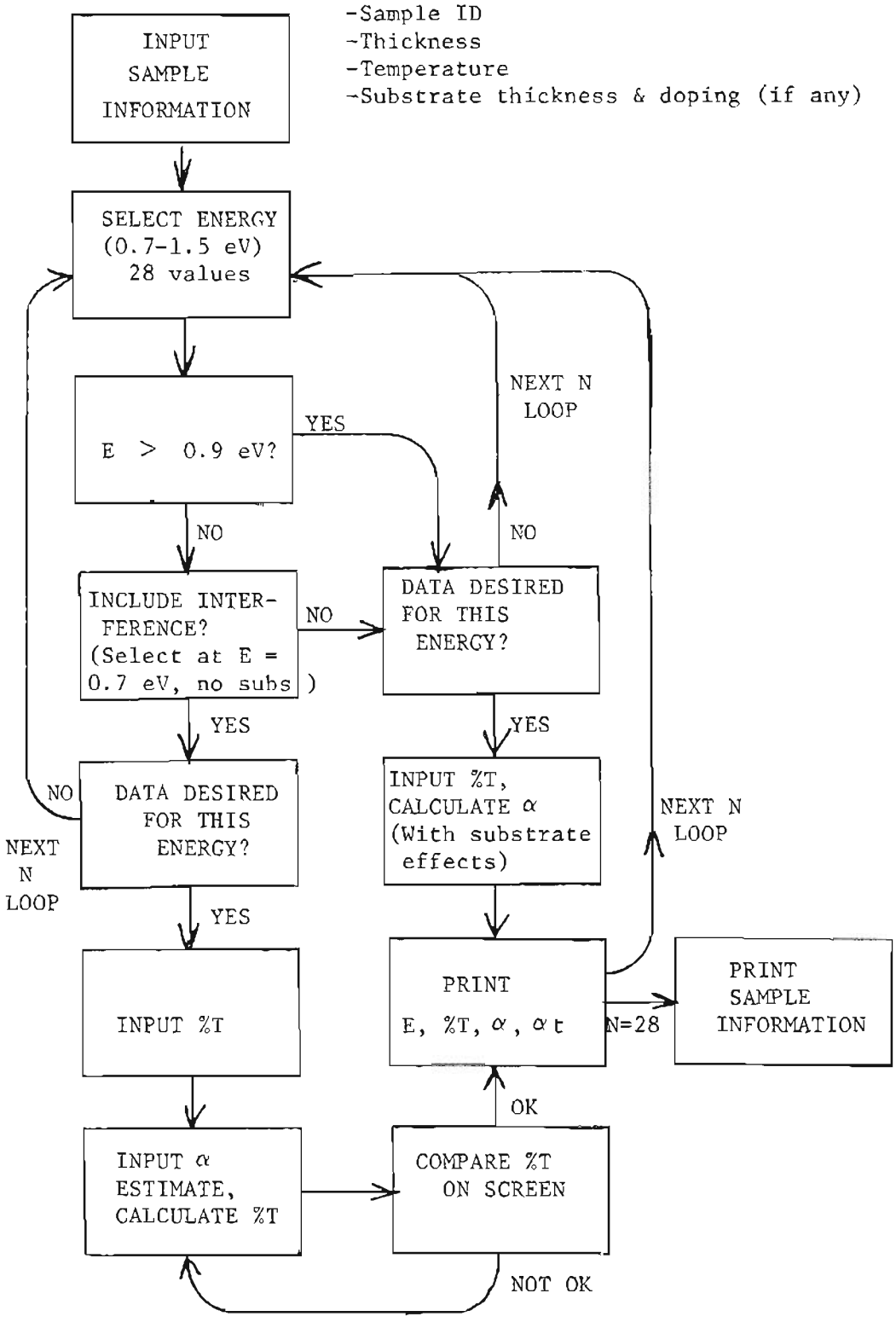

FIG. 48. Flowchart for Absorption Coefficient Calculation Program.

TABLE XVI. Optical Absorption Coefficient Calculation Program.

Line # BASIC (DOS 3.3) Program Statement

```
10  PR# 3
20  IN# 0
30  PRINT "Enter sample ID for absorption coefficient calculation (progr
    am rev. 2/5/87)."
40  INPUT I$
50  PRINT "Enter measurement temperature in Kelvins (10, 77, or 300 only
    )."
60  INPUT K
70  PRINT "Was there an InP substrate for this sample? (Y or N)"
80  INPUT S$
85  IF S$ = "N" THEN  GOTO 130
90  IF S$ = "Y" THEN  PRINT "Enter InP substrate thickness in microns."
100  INPUT TT
110  PRINT "Enter substrate type (N or P)."
120  INPUT T$
130  PRINT "Was the front surface InP (I) or InGaAs (G)?  (Input M for d
    ifferential sample       calculation; implies R = 0.)"
140  INPUT R$
144  PRINT "Enter %T scaling factor--enter 1 if no scaling is desired."
145  INPUT S
160  PRINT "Enter sample thickness in microns."
170  INPUT T
180  PR# 4
190  PRINT "SAMPLE ";I$;"      Temperature:  ";K;" K"
200  PRINT " "
210  PRINT "Energy(eV)   Trans.      a (1/cm)                at"
220  PR# 3
230  FOR N = 1 TO 28
240  IF  LEFT$ (I$,3) = "INP" THEN  GOTO 3000
250  IF N = 1 AND K = 10 THEN E = .7:RA = .574:RB = .0632:NA = 3.47
260  IF N = 1 AND K = 77 THEN E = .7:RA = .572:RB = .064:NA = 3.485
264  IF N = 1 AND K = 300 THEN E = .7:RA = .567:RB = .0657:NA = 3.515
270  IF N = 2 AND K = 10 THEN E = .71:RA = .573:RB = .0635:NA = 3.475
272  IF N = 2 AND K = 77 THEN E = .71:RA = .571:RB = .0643:NA = 3.49
274  IF N = 2 AND K = 300 THEN E = .71:RA = .566:RB = .0659:NA = 3.52
280  IF N = 3 AND K = 10 THEN E = .72:RA = .572:RB = .064:NA = 3.485
282  IF N = 3 AND K = 77 THEN E = .72:RA = .569:RB = .0648:NA = 3.5
284  IF N = 3 AND K = 300 THEN E = .72:RA = .563:RB = .0668:NA = 3.535
290  IF N = 4 AND K = 10 THEN E = .73:RA = .571:RB = .0643:NA = 3.49
292  IF N = 4 AND K = 77 THEN E = .73:RA = .567:RB = .0654:NA = 3.51
294  IF N = 4 AND K = 300 THEN E = .73:RA = .561:RB = .0676:NA = 3.55
300  IF N = 5 AND K = 10 THEN E = .74:RA = .569:RB = .0648:NA = 3.5
302  IF N = 5 AND K = 77 THEN E = .74:RA = .566:RB = .0659:NA = 3.52
304  IF N = 5 AND K = 300 THEN E = .74:RA = .559:RB = .0682:NA = 3.56
310  IF N = 6 AND K = 10 THEN E = .75:RA = .568:RB = .0651:NA = 3.505
312  IF N = 6 AND K = 77 THEN E = .75:RA = .564:RB = .0665:NA = 3.53
314  IF N = 6 AND K = 300 THEN E = .75:RA = .558:RB = .0684:NA = 3.565
320  IF N = 7 AND K = 10 THEN E = .76:RA = .567:RB = .0657:NA = 3.515
322  IF N = 7 AND K = 77 THEN E = .76:RA = .563:RB = .067:NA = 3.54
324  IF N = 7 AND K = 300 THEN E = .76:RA = .558:RB = .0684:NA = 3.565
330  IF N = 8 AND K = 10 THEN E = .77:RA = .565:RB = .0662:NA = 3.525
332  IF N = 8 AND K = 77 THEN E = .77:RA = .561:RB = .0676:NA = 3.55
334  IF N = 8 AND K = 300 THEN E = .77:RA = .559:RB = .0682:NA = 3.56
340  IF N = 9 AND K = 10 THEN E = .78:RA = .563:RB = .067:NA = 3.54
342  IF N = 9 AND K = 77 THEN E = .78:RA = .559:RB = .0682:NA = 3.56
344  IF N = 9 AND K = 300 THEN E = .78:RA = .561:RB = .0676:NA = 3.55
350  IF N = 10 AND K = 10 THEN E = .79:RA = .561:RB = .0676:NA = 3.55
352  IF N = 10 AND K = 77 THEN E = .79:RA = .558:RB = .0684:NA = 3.565
354  IF N = 10 AND K = 300 THEN E = .79:RA = .562:RB = .0673:NA = 3.545
360  IF N = 11 AND K = 10 THEN E = .8:RA = .558:RB = .0684:NA = 3.565
```

TABLE XVI. (cont.)

```
352  IF N = 11 AND K = 77 THEN E = .8:RA = .558:RB = .0684:NA = 3.565
354  IF N = 11 AND K = 300 THEN E = .8:RA = .562:RB = .0673:NA = 3.545
360  IF N = 12 AND K = 10 THEN E = .81:RA = .558:RB = .0684:NA = 3.565
362  IF N = 12 AND K = 77 THEN E = .81:RA = .558:RB = .0684:NA = 3.565
364  IF N = 12 AND K = 300 THEN E = .81:RA = .562:RB = .0673:NA = 3.545
370  IF N = 13 AND K = 10 THEN E = .82:RA = .558:RB = .0684:NA = 3.565
372  IF N = 13 AND K = 77 THEN E = .82:RA = .559:RB = .0682:NA = 3.56
374  IF N = 13 AND K = 300 THEN E = .82:RA = .562:RB = .0673:NA = 3.545
380  IF N = 14 AND K = 10 THEN E = .83:RA = .558:RB = .0684:NA = 3.565
382  IF N = 14 AND K = 77 THEN E = .83:RA = .561:RB = .0676:NA = 3.55
384  IF N = 14 AND K = 300 THEN E = .83:RA = .561:RB = .0676:NA = 3.55
390  IF N = 15 AND K = 10 THEN E = .84:RA = .561:RB = .0676:NA = 3.55
392  IF N = 15 AND K = 77 THEN E = .84:RA = .562:RB = .0673:NA = 3.545
394  IF N = 15 AND K = 300 THEN E = .84:RA = .561:RB = .0676:NA = 3.55
400  IF N = 16 AND K = 10 THEN E = .85:RA = .562:RB = .0673:NA = 3.545
402  IF N = 16 AND K = 77 THEN E = .85:RA = .562:RB = .0673:NA = 3.545
404  IF N = 16 AND K = 300 THEN E = .85:RA = .56:RB = .0679:NA = 3.555
410  IF N = 17 AND K = 10 THEN E = .86:RA = .562:RB = .0673:NA = 3.545
412  IF N = 17 AND K = 77 THEN E = .86:RA = .562:RB = .0673:NA = 3.545
414  IF N = 17 AND K = 300 THEN E = .86:RA = .559:RB = .0682:NA = 3.56
420  IF N = 18 AND K = 10 THEN E = .87:RA = .562:RB = .0673:NA = 3.545
422  IF N = 18 AND K = 77 THEN E = .87:RA = .561:RB = .0676:NA = 3.55
424  IF N = 18 AND K = 300 THEN E = .87:RA = .558:RB = .0684:NA = 3.565
430  IF N = 19 AND K = 10 THEN E = .88:RA = .561:RB = .0676:NA = 3.55
432  IF N = 19 AND K = 77 THEN E = .88:RA = .56:RB = .0679:NA = 3.555
434  IF N = 19 AND K = 300 THEN E = .88:RA = .558:RB = .0687:NA = 3.57
440  IF N = 20 AND K = 10 THEN E = .89:RA = .561:RB = .0676:NA = 3.55
442  IF N = 20 AND K = 77 THEN E = .89:RA = .559:RB = .0682:NA = 3.56
444  IF N = 20 AND K = 300 THEN E = .89:RA = .558:RB = .0687:NA = 3.57
450  IF N = 21 AND K = 10 THEN E = .9:RA = .561:RB = .0676:NA = 3.55
452  IF N = 21 AND K = 77 THEN E = .9:RA = .559:RB = .0682:NA = 3.56
454  IF N = 21 AND K = 300 THEN E = .9:RA = .557:RB = .069:NA = 3.575
460  IF N = 22 AND K = 10 THEN E = .95:RA = .558:RB = .0687:NA = 3.57
462  IF N = 22 AND K = 77 THEN E = .95:RA = .556:RB = .0693:NA = 3.58
464  IF N = 22 AND K = 300 THEN E = .95:RA = .554:RB = .0701:NA = 3.595
470  IF N = 23 AND K = 10 THEN E = 1:RA = .554:RB = .0701:NA = 3.595
472  IF N = 23 AND K = 77 THEN E = 1:RA = .553:RB = .0704:NA = 3.6
474  IF N = 23 AND K = 300 THEN E = 1:RA = .551:RB = .0712:NA = 3.615
480  IF N = 24 AND K = 10 THEN E = 1.1:RA = .549:RB = .0718:NA = 3.625
482  IF N = 24 AND K = 77 THEN E = 1.1:RA = .548:RB = .0721:NA = 3.63
484  IF N = 24 AND K = 300 THEN E = 1.1:RA = .547:RB = .0724:NA = 3.635
490  IF N = 25 AND K = 10 THEN E = 1.2:RA = .546:RB = .0729:NA = 3.645
492  IF N = 25 AND K = 77 THEN E = 1.2:RA = .546:RB = .0729:NA = 3.645
494  IF N = 25 AND K = 300 THEN E = 1.2:RA = .545:RB = .0732:NA = 3.65
500  IF N = 26 AND K = 10 THEN E = 1.3:RA = .545:RB = .0732:NA = 3.65
502  IF N = 26 AND K = 77 THEN E = 1.3:RA = .545:RB = .0732:NA = 3.65
504  IF N = 26 AND K = 300 THEN E = 1.3:RA = .543:RB = .0738:NA = 3.66
510  IF N = 27 AND K = 10 THEN E = 1.4:RA = .543:RB = .074:NA = 3.665
512  IF N = 27 AND K = 77 THEN E = 1.4:RA = .542:RB = .0743:NA = 3.67
514  IF N = 27 AND K = 300 THEN E = 1.4:RA = .54:RB = .0749:NA = 3.68
520  IF N = 28 AND K = 10 THEN E = 1.5:RA = .538:RB = .0758:NA = 3.695
522  IF N = 28 AND K = 77 THEN E = 1.5:RA = .537:RB = .076:NA = 3.7
524  IF N = 28 AND K = 300 THEN E = 1.5:RA = .535:RB = .0769:NA = 3.715
530  PRINT "For ";E;" eV energy, enter %T (if no data for this energy, e
    nter 0; for special              value, enter 1, noting that InGaAs r
    eflectance will be for T < 77 K)."
540  INPUT PT
545  IF N = 28 AND PT = 0 THEN  GOTO 770
550  IF PT = 0 THEN  NEXT N
```

TABLE XVI. (cont.)

```
557  IF PT = 1 THEN  GOTO 1300
560  IF S$ = "N" THEN  GOTO 620
570  IF E <  = .8 THEN AA = ( - 10 * E) + 13.25
580  IF E > .8 THEN AA = (10 * E) - 3
590  IF K > 100 THEN AA = 2 * AA
600  IF T$ = "P" THEN AA = AA / 10
610  GOTO 640
620 AA = 0
630 TT = 0
635  IF R$ = "M" THEN  GOTO 664
640  IF R$ = "G" THEN  GOTO 693
650  IF E <  = .9 THEN NN = 3.17
660  IF E > .9 THEN NN = (.591 * E) + 2.625
662  GOTO 670
664 NN = 1
670 R = (NN - 1) ^ 2 / (NN + 1) ^ 2
680 RI = (1 - R) ^  - 2
685 PT = PT * S
690 L = RI * PT
692  GOTO 700
693 PT = PT * S
694  IF E <  = .9 THEN  GOTO 1010
695 L = (RA / (2 * PT)) + ((RA ^ 2 / (4 * PT ^ 2)) + RB) ^ .5
700 B =  LOG (L)
710  IF R$ = "I" THEN C =  - B
715  IF R$ = "G" THEN C = B - (AA * TT * .0001)
720 F = C * (10000 / T)
730  PR# 4
740  PRINT E TAB( 10)PT TAB( 24)F;"          ";C
742  IF N = 5 THEN  PRINT " "
744  IF N = 10 THEN  PRINT " "
745  IF N = 15 THEN  PRINT " "
746  IF N = 20 THEN  PRINT " "
748  IF N = 25 THEN  PRINT " "
750  PR# 3
760  NEXT N
770  PR# 4
780  PRINT " "
790  PRINT "Sample thickness of ";T;" microns used."
800  IF S$ = "Y" THEN  PRINT "InP ";T$;"-type substrate ";TT;" microns t
    hick correction included."
810  IF R$ = "G" THEN  PRINT "Reflectance for InGaAs used."
820  IF R$ = "I" THEN  PRINT "Reflectance for InP used."
825  PRINT "%T scaling factor = ";S;"."
830  FOR X = 1 TO 10
840  PRINT " "
850  NEXT X
860  PR# 3
870  PRINT " "
880  PRINT "end"
890  END
1010  IF N = 1 THEN  PRINT "Include interference effects? (Type Y or N)"

1020  IF N = 1 THEN  INPUT G$
1030  IF G$ = "N" THEN  GOTO 695
1040 LA = E / 1.23977
1050  PRINT "Input absorption coefficient estimate, in cm^-1 (Type 0 if
    ready for next energy)"
```

TABLE XVI. (cont.)

```
1060  INPUT A
1065  IF A = 0 THEN  GOTO 730
1070 XX = (12.5664 * NA * T * LA) + (A / (LA * 3.1416 * (NA ^ 2 - 1) * 1
    0000))
1080 C = A * T * .0001
1090 TB =  EXP (C) + (RB /  EXP (C)) - (2 * RB ^ .5 *  COS (XX))
1095  GOTO 2000
1100  IF N = 11 THEN E = 1.29
1110  IF N = 12 THEN E = 1.3
1120  IF N = 13 THEN E = 1.31
1130  IF N = 14 THEN E = 1.32
1140  IF N = 15 THEN E = 1.33
1150  IF N = 16 THEN E = 1.34
1160  IF N = 17 THEN E = 1.35
1170  IF N = 18 THEN E = 1.36
1180  IF N = 19 THEN E = 1.37
1190  IF N = 20 THEN E = 1.38
1200  IF N = 21 THEN E = 1.39
1210  IF N = 22 THEN E = 1.4
1220  IF N = 23 THEN E = 1.41
1230  IF N = 24 THEN E = 1.42
1240  IF N = 25 THEN E = 1.43
1250  IF N = 26 THEN E = 1.44
1260  IF N = 27 THEN E = 1.45
1270  IF N = 28 THEN E = 1.5
1280  GOTO 530
1300  PRINT "Enter energy (in eV)."
1310  INPUT E
1320  PRINT "Enter %T."
1330  INPUT PT
1332  IF E < .8 THEN RA = .668 - (.136 * E):RB = .0285 + (.05 * E)
1334  IF E >  = .8 AND E <  = .86 THEN RA = .477 + (.1 * E):RB = .0818 -
    (.0167 * E)
1336  IF E > .86 AND E <  = 1.1 THEN RA = .606 - (.052 * E):RB = .0514 +
    (.0188 * E)
1338  IF E > 1.1 THEN RA = .571 - (.02 * E):RB = .0647 + (.00667 * E)
1340  GOTO 560
1350  IF E <  = .78 THEN NN = 3.56
1360  IF E > .78 THEN NN = (.222 * E) + 3.375
1370  GOTO 670
2000 Z = RA / TB
2010  PRINT PT
2020  PRINT Z
2030 P = A
2060  GOTO 1050
3000  IF N = 1 THEN E = .7
3010  IF N = 2 THEN E = .8
3020  IF N = 3 THEN E = .9
3030  IF N = 4 THEN E = 1
3040  IF N = 5 THEN E = 1.1
3050  IF N = 6 THEN E = 1.2
3060  IF N = 7 THEN E = 1.25
3070  IF N = 8 THEN E = 1.26
3080  IF N = 9 THEN E = 1.27
3090  IF N = 10 THEN E = 1.28
3100  GOTO 1100
```

VITA

The author is a third generation Oregonian, born on May 23, 1955. After graduating from Beaverton High School in 1973, he travelled to Massachusetts for his undergraduate education. A strong interest in music, particularly for the baroque organ, nearly led to a conservatory; however, science prevailed and he received his B.S. Physics from Worcester Polytechnic Institute in 1977. Subsequently, he worked at Galileo Electro-Optics in Sturbridge, Massachusetts, as a research engineer. In 1979, the magnetic attraction of his home state proved overpowering, and he returned to begin a career as a CRT manufacturing engineer at Tektronix, Inc.

He began studying at the Oregon Graduate Center in September of 1980, on a part-time basis. While still at Tektronix, he completed the Master of Electronic Science degree at OGC in April, 1984. The present study began at OGC in January, 1985. This time was also significant because of the author's marriage to Corinne A. Abel, in May of that year.